1-1-2004

Photonic RF signal processors

Rong Zheng
Edith Cowan University

Edith Cowan University

Copyright Warning

PHOTONIC RF SIGNAL PROCESSORS

By

Rong Zheng

A thesis submitted for the degree of

Doctor of Philosophy

at

School of Engineering and Mathematics

Edith Cowan University

Principal Supervisor : A/Prof. Kamal Alameh

Co-Supervisor : Prof. Kamran Eshraghian

December 2004

USE OF THESIS

The Use of Thesis statement is not included in this version of the thesis.

DECLARATION

I certify that this thesis does not, to the best of my knowledge and belief:

(i) incorporate without acknowledgement any material previously submitted for a degree or diploma in any institution of higher education;

(ii) contain any material previously published or written by another person except where due reference is made in the text; or

(iii) contain any defamatory material.

Signature [redacted] *Date* 21 Dec 2004

Dedication to my parents

Contents

List of Figures

Publications

Refereed Journal Articles

- **R.Zheng**, Z.Wang, K.Alameh and William A. Crossland, *An Opto-VLSI Reconfigurable Broadband Optical Splitter,* To appear in IEEE Photonic Technology Letter, Feb., 2005.

- Z.Wang, **R.Zheng,** K.Alameh, R. Robertson, U. Muller, and L. Bloom,*Dynamic optical power splitter using Opto-VLSI processor,* IEE Electronics Letters, Nov,2004

- K. Alamh, **R.Zheng,** S. Ahderom, M. Raisi,K.Eshraghian,*MicroPhotonic Reconfigurable RF Signal Processor,* Microwave and Optical Technology Letters, July 5,2004.

Refereed Conference Papers

- **R.Zheng,** Z.Wang , K. Alameh,and S. Ahderom, *Optical Interference Suppression in Using MicroPhotonic RF Filter Structure,* COMMAD2004. 8-10, Dec. 2004, Brisbane, Queensland, Australia.

- **R.Zheng**, Z.Wang and K.Alameh, *Adaptive high-Q bandpass photonic RF filter,* SPIE Photonic Asia conference on Adaptive Optics and Applications III, Beijing, China, 10-12,November, 2004.

- Z. Wang, K. Alamel, and **R.Zheng**, *High efficiency stable 213nm generation for*

LASIK application, SPIE Photonics Asia conference on Adaptive Optics and Applications III, 10-12, Nov,2004, Beijing, China.

- Z. Wang, K. Alamel, and **R.Zheng**, *Dynamic Opto-VLSI lens and lens-let generation with programmable focal length,* SPIE Photonics Asia conference on Adaptive Optics and Applications III, 10-12, Nov, 2004, Beijing, China.

- K.Alameh, **R.Zheng,** S.Ahderom, M.Raisi, and K.Eshraghian,*Adaptive Processing of Broadband RF Signals using MicroPhotonics*, In proceedings, 10th International Conf. on Information Systems Analysis and Synthesis, CITSA2004, July 21-25, 2004, Orlando, Florida, USA, pp. 39-44.

- K.Alameh,A.Bouzerdoum, **R.Zheng,** S.Ahderom, M.Raisi,K.Eshraghian, X.Zhao, and Z.Wang, *MicroPhotonic-based Multi-band RF Interference Mitigation Filtering*, In proceedings, 10th International Conf. on Information Systems Analysis and Synthesis, CITSA2004, July 21-25, 2004, Orlando, Florida, USA, pp. 45-47.

- Z.Wang, K.Alameh, S. Ahderom, **R.Zheng**, M.Raisi, and K.Eshraghian, *Integrated Optical Routing Topology for MicroPhotonic Switches*, 7th IEEE International Conference on High Speed Networks and Multimedia Communications (HSNMC'04), Toulouse, France, July, pp. 849-854, 2004.

- K.Alameh, **R.Zheng,** S.Ahderom, M. Raisi, K.Eshraghian, and M.Lee,*Adaptive processing of broadband RF signals using MicroPhotonics*, 2004 Korea-Australia International Joint Seminar Program (KOALA'04), Jeju, Korea, May 23-27, pp. 31-41, 2004.

- K.Kamal, A.Bouzerdoum, S.Ahderom, M.Raisi, K.Eshraghian, X.Zhao, **R.Zheng** and Z.wang. *Integrated MicroPhotonic Wideband RF Interference Mitigation Filter,*

Proceedings of the IEEE International Workshop on Electronic Design, Test and Applications DELTA 2004,Australia,January 2004.

- Z.Wang, K.Kamal, S.Ahderom, **R.Zheng,** M.Raisi, and K.Eshraghian. *Novel Integrated Optical Router for MicroPhotonic Switching,* Proceedings of the IEEE International Workshop on Electronic Design, Test and Applications DELTA 2004,Australia,January 2004.

- K.Kamal, S.Ahderom, M.Raisi, **R.Zheng** and K.Eshraghian, *MicroPhotonic Reconfigurable RF Signal Processor,* Proceedings of the IEEE International Workshop on Electronic Design, Test and Applications DELTA 2004,Australia,January 2004.

- K.Alameh, A.Bouzerdoum, **R.Zheng,** S.Ahderom, M.Raisi, K.Eshraghian, X.Zhao, Z.Wang. *MicroPhotonic Interference Mitigation Filter for Radio Telescope,* SPIE International Symposium Microelectronics, MEMS, and Nanotechnology. 10-12 Dec. 2003, Peth, WA. Australia.

- **R.Zheng,** D.Habibi and K.Eshraghian. *Adaptive power distribution in optical access network,* SPIE International Symposium Microelectronics, MEMS, and Nanotechnology. 10-12 Dec. 2003, Peth, WA. Australia.

- **R.Zheng** and D.Habibi. *Emerging Architectures for Optical Broadband Access Networks,* Australia Telecommunication,Networks and Applicationsc Conference(ANTAC),7-9 Dec.2003, Melbourne,Vic. Australia.

- **R.Zheng** and D.Habibi. *Scalable Optical Access Network Design using Variable Optical Splitters,* Australia Telecommunication,Networks and Applicationsc Conference(ANTAC) 7-9 Dec.2003, Melbourne,Vic. Australia.

- **R.Zheng,** Robert Minasian, *Optical Source coherence control for noise suppression in photonic signal Processors,* OECC/IOOC 2001, Sydney. Technical report. P245-247. 2001

To be published

- K.Alameh, A.Bouzerdoum, Z.Wang, **R.Zheng**, R.Jeffery, and X.Zhao, *MicroPhotonic Topology for Multi-band RF Interference Mitigation,* To appear in EURASIP Journal, France, 2004

- **R.Zheng**, Kamal E. Alameh and Zhenglin Wang, *A Microphotonic Transversal RF Signal Processor with no Laser Coherence Noise*, Submitted to Microwave and Optical Technology Letters

Acknowledgements

Acknowledgement

This work has been carried out in two phases: during 1998-2000 and 2002–2004, started at Photonics Research Laboratory, University of Sydney and finished at Electron Science Research Institute, Edith Cowan University. I wish to express my gratitude to many persons who have given their help and contributed to the work.

I am most deeply indebted to my supervisor, Associate Professor Kamal E.Alameh, for the opportunity to finish my thesis, for his support and commitment, and for his experience in scientific research which helped me greatly during the work. I also wish to express my warm thanks to Professor Kamaran Esharagian for his continuous encouragement during the research in its various phases and for his important contribution to the work.

While working at ECU, I had the pleasure to share office with postgraduate students, S.Adherom, S.Esharagian, M.Raisi, Ryan Luo et al., who made the work enjoyable. I want to express my gratitude to the entire MicroPhotonics research group at ECU for giving a lot of useful advice.

I also sincerely acknowledge the partly support for this work from Australian Research Council.

With much love, I would like to thank my parents, for their unconditional love and

encouragement.

Finally, I wish to thank my husband Zhenglin Wang and my son Jonathan Yuxin Zheng for their love, patience, encouragement and support.

Abstract

The purpose of this thesis is to explore the emerging possibilities of processing radio-frequency (RF) or microwave signals in optical domain, which will be a key technology to implement next-generation mobile communication systems and future optical networks. Research activities include design and modelling of novel photonic architectures for processing and filtering of RF, microwave and millimeter wave signals of the above mentioned applications. Investigations especially focus on two basic functions and critical requirements in advanced RF systems, namely:

- Interference mitigation and high Q tunable filters.
- Arbitrary filter transfer function generation.

The thesis begins with a review on several state-of-the-art architectures of in-fiber RF signal processing and related key optical technologies. The unique capabilities offered by in-fiber RF signal processors for processing ultra wide-band, high-frequency signals directly in optical domain make them attractive options for applications in optical networks and wide-band microwave signal processing. However, the principal drawbacks which have been demonstrated so far in the in-fiber RF signal processors are their inflexible or expensive schemes to set tap weights and time delay. Laser coherence effects also limit sampling frequency and introduce additional phase-induced intensity noise.

A novel MicroPhotonic based RF signal processing architecture is firstly proposed, in which fibre collimator arrays, Opto-VLSI processors, and a WDM combiner are integrated within an optical substrate. Opto-VLSI processors are used to dynamically split the input and pump signals, and accurately couple them into various active fiber Bragg grating - EDFA cavities, hence the gains and weights of numerous active fiber Bragg grating cavities are controlled. The new structure features high frequency resolution, arbitrary transfer characteristics and reconfigurable signal processing ability. However, its sampling frequency and weight tuning range are defined by the maximum length of EDFA in the cavity which is limited by laser coherency

To understand optical coherence effects on in-fiber RF signal processing, theoretical analysis of RF spectral responses for different photonic RF filters are conducted. The combination effects of optical interference and interference of RF signals are examined for two types of photonic RF filters, namely, optical fiber finite impulse response(FIR) filter and fiber infinite impulse response(IIR) filter. Common expression of RF spectral responses under coherence illumination is obtained and applied to analyze the spectral responses of a 4-tap fiber transversal RF filter, a fiber Fabry-Perot(FP) cavity RF filter and a fiber recirculating delay line(RDL) filter specifically. It is shown that the frequency responses of all the three types of filters are sensitive to the coherence length of laser source. In order to generate robust transfer functions, it is necessary that the coherence length of laser be much shorter than the minimum unit delay line, which limits the photonic signal processing to very low RF frequency.

A new laser coherence control scheme for photonic signal processing is proposed where an external phase modulator is employed following the laser source. By applying a pseudo random binary sequence(PRBS) to the phase modulator, the linewidth of laser can be

tailored to the requirements of photonic RF signal processing. Experimental verification of this technique has been presented, and results for a photonic notch filter have demonstrated that the PRBS phase modulation technique enables DFB laser to be used as an optical source for photonic RF signal processor, with a response that is highly stable.

We also investigate an architecture of reconfigurable RF signal processor which is free of coherence effects. A new integrated Micro-Photonic architecture is designed which integrates a Vertical Cavity Surface Emitting Laser (VCSEL) array, a 2D photo-receiver array and a multi-cavity optical substrate that generates a large number of optical true-time delays to achieve arbitrary, high-resolution RF filter transfer characteristics with no phase-induced intensity noise(PIIN). Each optical cavity can realize an adaptive FIR filter at specific center frequency. By tuning responses of the different optical cavities, a broadband adaptive FIR filter can be realized which include multi-band interference mitigation notch filter and high-Q bandpass filter.

Finally, integration technologies and feasibility of the integrated MicroPhotonic RF signal processing architectures are generally discussed and some future works are also addressed.

Chapter 1

Introduction

1.1 Background

With recent advances in high speed optical network, there is more demand for bandwidth. The conventional electrical signal processing used in the optical communication systems becomes a bottleneck [1, 2]. A great interest has been stimulated to apply optical signal processing in optical networks where optical router and header recognition are highly needed. Moreover, interests in radio-frequency (RF) communications, antenna remoting, optical interconnect and security systems have driven the use of photonics in RF signal processing.

MicroPhotonics, the marriage of micro-electronics and photonics, is an emerging technology during the last few years as a strategic technology for implementation of multiple tasks related to efficient and high-speed information processing. Devices and subsystems have been developed to provide fundamental techniques for the currently high speed WDM optical communication systems. More applications of MicroPhotonics can be found in new areas where its combined potential capacities from the best characteristics provided by optics and electronics will bring more values. The two main areas that can benefit from

photonic RF signal processing are categorized as:

- Applications where processing RF signals emitted or received within RF systems in optical domain can be advantageous in comparison to more traditional RF approaches relying on circuits, waveguides and coaxial cables. These include cable television, remote antennas, mobile communications, imaging systems and millimeter wave systems.

- Applications where direct optical processing or filtering of RF signals conveyed together with baseband information using optical carriers are required. These include, for example, Subcarrier Multiplexed (SCM) label swapping and Multi-Protocol Label Switching (MPLS) in packet switched optical networks and the management of optical networks employing SCM control pilot tones.

The unique capabilities offered by photonics for processing ultra wide-band, high-frequency RF signals at optical domain make it a key technology for implementing next-generation mobile communications systems and future optical networks. We are now at the dawn of a new era in which photonics will be deployed to provide ultra high-speed information processing capabilities.

1.2 Different approaches to photonic RF signal processing

The basic operations of photonic RF signal processing are weight control, time delay control, phase delay control, space summation and time summation. To realize these operations, different approaches have been developed:

- **In-Fiber technology**: In-fiber RF signal processing uses optical amplifier or attenuator to control the tap weights [3, 4], and dispersive fiber to generate tunable

delay line. Wavelength-division-multiplexing combined with fiber-Bragg Grating is used to generate required sampling rate and delay [5, 6]. The general drawbacks of this technology include the use of multiple optical components(expensive and lossy), broadcasting the light over all possible paths at one time(enormous insertion losses), and wavelength multiplexing (complex tunable lasers).

- **Silica Waveguide technology**: A coherent optical transversal filter using silica-based single mode waveguides was proposed by Sasayama and co-workers [7]. The filter can express arbitrary complex coefficients by utilizing phase information of optical signal, it can realize arbitrary frequency characteristics. However, its frequency response is sensitive to slightly change in propagation characteristics of any part of optical path(length, refractive index, etc) since optical phase information is used to synthesize the transfer function, making it a very sensitive, non-stable and impractical structure.

- **Free-space optics technology**: In free-space optics systems [8], optical delay lines are realized either through beam diffraction which requires physically large components or multiple spatial light modulators (SLMs) which are expensive and bulky.

1.3 Demand for reconfigurable photonic RF signal processing

The increasing demand of high quality performance for adaptive photonic RF signal processing that can be used in recent and future access network have introduced great interests in this area. Adaptive and agile photonic RF signal processors can assist in realizing all optical processing such as optical header recognition [9], optical logic and optical buffering/memory [10]. They also find applications in signal post detecting, shaping and equalizing which are important functions for the next generation optical network.

Several new application scenarios such as broadband millimeter-wave band fixed wireless access networks, wireless local area networks (WLANs) and radio-astronomy arrays have emerged, and paved the way to great opportunities for exploiting the optical beamforming concept. Adaptive photonic RF signal processing technologies will provide solutions to obtain the beam agility of array systems with wide bandwidth, making multifunction arrays possible with simultaneous multi-band operations.

1.4 Objectives of this thesis

In this work, novel architectures of adaptive photonic RF signal processors with high performance characteristics are investigated, enabling new capabilities for mobile communications and future optical networks. These new architectures have the two basic functions:

- Interference mitigation tunable notch filter and high Q tunable bandpass filters.
- Arbitrary filter transfer function generation.

1.5 Contributions of this thesis

The state-of-the-art photonic technologies are explored in this thesis to design adaptive photonic RF signal processors. Several new architectures are proposed, achieving characteristics of reconfigurable, multi-band, high-Q bandpass filters and interference mitigation notch filters. Within these new architectures, arbitrary filter transfer functions can be synthesized. The main contributions of this thesis are:

- Propose a MicroPhotonic reconfigurable RF signal processor. Opto-VLSI processors are used to control the gain and weights of fiber-Bragg grating - EDFA cavities. A high-Q and tunable bandpass filter can be realized. Notch filter can also be synthesized through the same topology.

- Theoretical analysis of optical coherence effects on photonic RF signal processing is conducted and transfer functions of RF signal processors under coherent illumination are obtained. The interaction between two interferences caused by optical carrier and modulating RF signal is examined.

- Propose an interference suppression method for photonic RF signal processing, experimentally demonstrating that the pseudo random binary sequence(PRBS) phase modulation technique can be used to transform laser coherence to the requirements of photonic RF signal processor.

- Investigate an integrated MicroPhotonic reconfigurable RF signal processor. Design the architecture with state-of-the-art integrated optical components. Some technical design issues are examined. The transfer function of the new architecture is fully reconfigurable and free of optical coherence effects.

1.6 Thesis outline

This thesis is placed in a particular context. The objective of realizing fully reconfigurable RF signal processing free of optical coherence effects makes the skeleton of this work.

- Chapter 2 reviews in-fiber RF signal processing technology, the current status of adaptive RF filter design and the state-of-the-art related optical technologies.

- Chapter 3 discusses a MicroPhotonic reconfigurable RF signal processor in which Opto-VLSI processor is proposed to dynamically distribute the optical power in the multi-fiber-Bragg grating-EDFA cavities, hence the weighting of each cavity can be individually tuned. The new architecture is discussed and simulation results show that transfer function of the filter can be arbitrary synthesized.

- In chapter 4, theoretical analysis of optical coherence effects on photonic RF signal processing is undertaken, and RF frequency responses of FIR and IIR photonic RF filters under coherent light illumination are studied. A 4-tap transversal filter, fiber Fabry-Perot filter and fiber recirculating delay line filter are examined in details under coherent illumination.

- Chapter 5 demonstrates a new method to suppress coherence effects by using a PRBS driven external phase modulator scheme. Experimental results are presented to prove that this method can be used to tailor the coherence of laser to requirements of photonic RF signal processor.

- Chapter 6 proposes a new integrated MicroPhotonic wideband adaptive RF filter. The new architecture is demonstrated and theoretical analysis shows that it can be fully reconfigured and is free of optical coherence effects. Interference mitigation notch RF filter can be realized, multi- band tunable bandpass or notch filters can

also be synthesized. Issues which relate to beam propagation in optical substrate are also investigated.

- In chapter 7, some technical feasibilities of new architectures for photonic RF signal processing are assessed. We also briefly discuss future directions motivated and initiated by this thesis.

Part of this work has been published and listed in **Publications**.

Chapter 2

In-Fiber RF signal processing

In this chapter, the state-of-the-art technologies of in-fiber RF signal processing are reviewed and different architectures of adaptive in-fiber RF signal processing are demonstrated. Some recent developments of key optical components for photonic RF signal processing are also presented.

2.1 Introduction

The possibility of processing RF and microwave signals directly in optical domain by means of fiber-optic based structures has attracted a lot of attentions around the world [11–14]. The main advantages of using photonics are associated with its extremely high carrier frequency (in the order of 200 THz) and extremely wide frequency band (in the order of several THz) available to accommodate a large number of communication channels. Small physical size, low transmission loss, immunity from electromagnetic interference and manageable dispersion characteristics are further advantages.

Photonic RF signal processors are studied intensively in telecommunication systems

for microwave signals generation, distribution and processing [13,15,16], in fibre-radio picocellular communication systems [17–19] and in phased array radar [12,20–22]. There are emerging applications in phased-array antennas, electronic warfare, ultra-fast noninvasive measurements and radio astronomy [23,24].

With more optical fiber systems deployed in both long-distance terrestrial communication and local access networks, photonic RF signal processors will be utilized in most future optical communication systems.

In this Chapter, the research field of in-fiber RF signal processing is reviewed. Section 2.2 discusses some basic concepts of in-fiber RF signal processing. In Section 2.3, architectures of high-Q bandpass filter are discussed. Section 2.4 reviews different techniques to realize adaptive RF signal processing. In Section 2.5 techniques to realize adaptive and coherent insensitive photonic RF filter are discussed and finally, some key optical technologies for photonic RF signal processing are reviewed.

2.2 Basic concepts of in-fiber RF signal processors

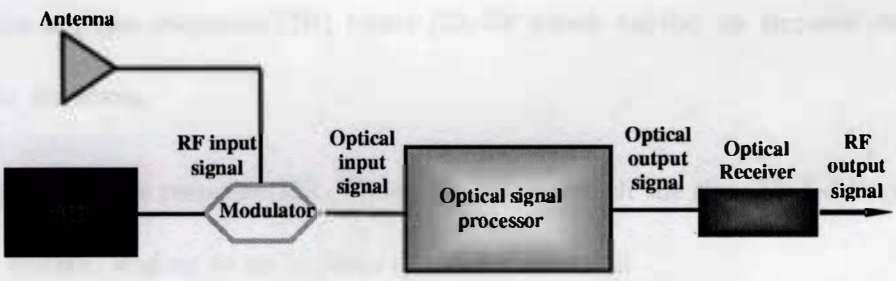

Figure 2.1: General architecture of a photonic RF signal processor

Figure 2.1 shows general architecture of an in-fiber RF signal processing system. The system includes an optical source, an external intensity modulator, an optical signal processor and a square-law photodetector.

The laser source is firstly intensity modulated by the external modulator which is driven

by RF information signal. The modulated optical signal is then launched into optical signal processor which performs a variety of linear functions on the signal. The processed signal can then be detected by a square-law detector, p-i-n photodiode for further processing.

During information transmission and processing, input optical signal is processed linearly and the output signal is detected by the photo-detector whose photocurrent is linearly proportional to the optical intensity striking on its sensitive surface. The photonic RF signal processing system is assumed to be a linear, time-invariant system in which the output signal is the convolution of input signal with the impulse response of the device, hence, principles of classical digital signal processing can be applied.

2.2.1 Transfer function of in-fiber RF processor

Since principles of photonics RF filter design bear a close relationship [25–28] with classical digital filter design, its transfer function can be synthesized in the similar fashion as for a discrete digital filter.

According to impulse responses of photonic RF filers, they can be categorized into:

- Finite impulse response(FIR) filters [29, 30] which exhibit an impulse response of finite duration.
- Infinite impulse response(IIR) filters [31–33], in which the signal is fed back through the system, leading to an impulse of infinite duration.

Finite Impulse Response (FIR) in-fiber RF Filters

The fundamental discrete FIR signal processor as shown in Figure 2.2 has a structure in which successive samples of signal are delayed, weighted and summed. For an input signal

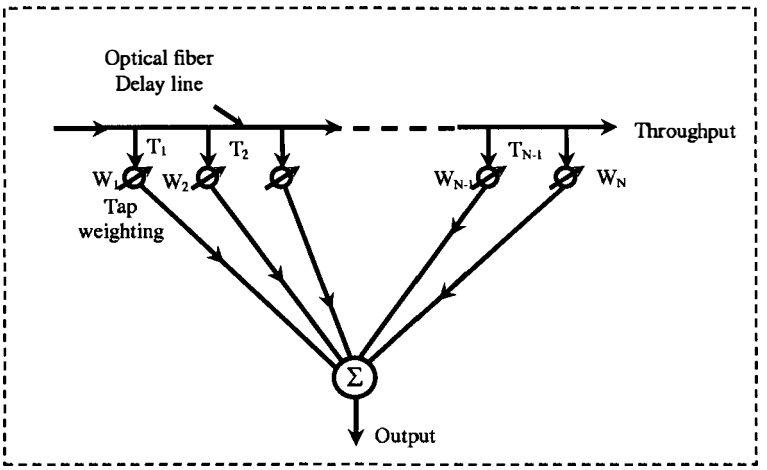

Figure 2.2: Tapped delay line with tap intervals T_m(m=1,2,.....N-1) and weighting elements W_m(m=1,2,.....N)

denoted by x(t), the output y(t) is given by:

$$y(t) = \sum_{n=1}^{N-1} b(n)x(t - n \cdot T) \tag{2.1}$$

where $b(n)$ is the n^{th} tap weight, N is the number of taps and T is the sampling period. Taking Z-transform of both sides of Equation 2.1, we can have:

$$Y(Z) = H(Z)X(Z) = (b(1) + b(2)Z^{-1} + \cdots b(n+1)Z^{-N})X(Z) \tag{2.2}$$

where H(Z) is filter's transfer function, constant $b(i)$ are filter coefficients and N is filter's order.

The tapped delay line can be high dispersion fibre [34], unbalanced Mach-Zehnder structures [35], arrayed waveguide grating(AWG) [36] and fiber Bragg grating [37]. When RF modulated optical signals are transmit in the delay line structures, they must be able to be successively sampled, weighted, and then summed either in optical domain before photo detection or by electronic summation after detection.

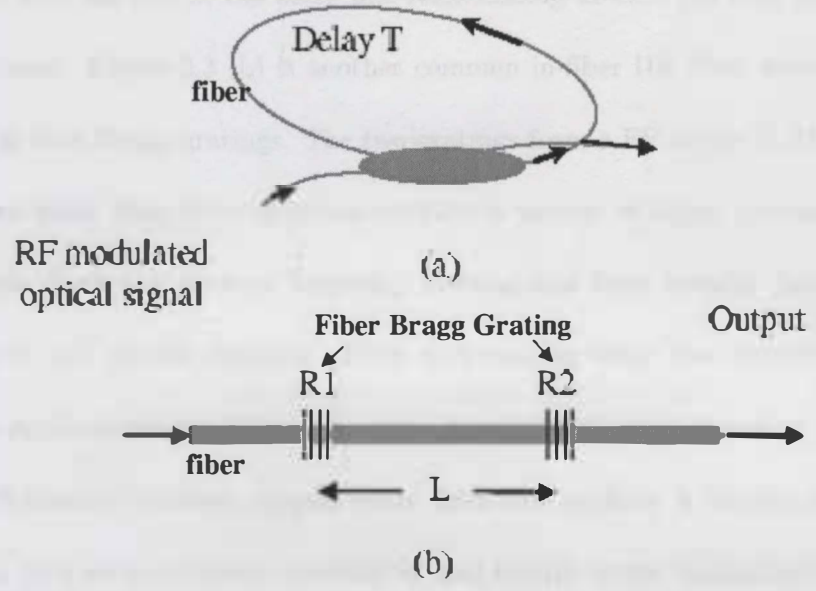

Figure 2.3: IIR in-fiber RF filter configuration. (a) Fiber recirculating delay line with delay time T (b) Fiber Bragg grating Fabry-Perot Cavity filter with delay length L

Infinity Impulse Response(IIR) in-fiber RF filters

For an infinite impulse response (IIR) filter, the P previous samples of y(t) are weighted and added in as well. In other words, an IIR filter uses feedback. This is expressed mathematically by:

$$y(t) = \sum_{n=1}^{P} a(n)y(t - n \cdot T) + \sum_{m=1}^{Q} b(m)x(t - m \cdot T) \tag{2.3}$$

where $a(n)$ is the n^{th} tap weight, Q is the number of taps and T is sampling period. Z transformation of Equation 2.3 is:

$$Y(Z) = H(Z)X(Z) = \frac{b(1)Z^{-1} + \cdots b(Q)Z^{-Q}}{a(1)Z^{-1} + \cdots a(P)Z^{-P}}X(Z) \tag{2.4}$$

where H(Z) is filter's transfer function, constant $a(n), b(m)$ are filter coefficients and the order of filter is the bigger number of P and Q.

Figure 2.3 shows two basic configurations of IIR in-fiber RF filter. Figure 2.3 (a) shows a fiber recirculating delay line filter, consisting of a loop of fiber and optical coupler. Signals

introduced into one end of the delay line recirculating around the loop produce outputs on each transit. Figure 2.3 (b) is another common in-fiber IIR filter which is configured by a pair of fiber Bragg gratings. The two gratings form a FP cavity [5,37,38].

The two basic filter structures can perform a variety of signal processing functions. For example, both can perform frequency filtering and their transfer function is the Z-transform of unit sample response. Fiber recirculating delay line structures are also of interest in applications requiring short-term storage of discrete or analog signals. In addition to frequency filtering, tapped delay lines can perform a variety of time-domain operations, such as convolution, correlation, and matrix-vector multiplication [29,31].

Using these two basic structures, more complex structures can be built, performing a wide range of frequency domain filtering [29, 39]. According to their frequency responses, they can be categorized as: low-pass filter(LPF), band-pass filter(BPF) and band-stop(BSF) or notch filter.

2.2.2 Q factor and S factor

Q factor

A typical transversal filter's spectral response is shown in Figure 2.4. The Q factor, or quality factor, is defined as:

$$Q = \frac{FSR}{\Delta f_{FWHM}} \tag{2.5}$$

where Δf_{FWHM} is the frequency width at half maximum power of the passband and FSR is the free spectral range on which the filter exhibits periodical behavior. It is related by the sampling frequency f_c by: $FSR = 1/f_c$.

It is important to obtain high Q factor in some applications where information channels to be selected or filtered are very closely distributed or RF spectrum might be shared with

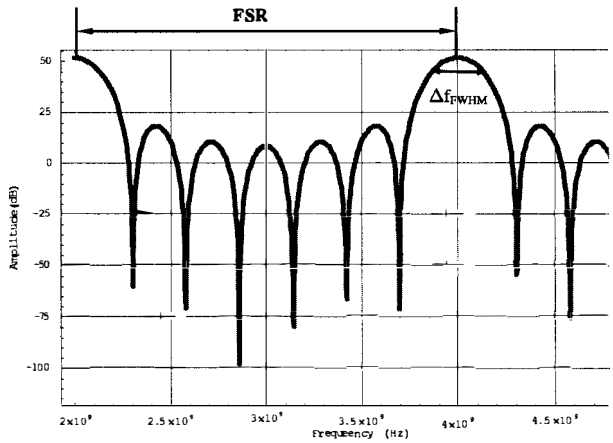

Figure 2.4: Quality factor Q definition of a bandpass filter

other applications and systems. For example, in the Universal Mobile Telecommunication Systems(UMTS), the channels center around 2 GHz with bandwidths of only 5 MHz. In other cases, this requirement can be more relaxed and the periodical pass band of the transversal filter does not represent additional problems because no RF signals must be specifically rejected or avoided in such spectral locations.

S factor

Shape factor S is a term used to quantify the steepness of a filter's roll-off. The filter can be either bandpass or notch filter. It is normally defined as:

$$S = \frac{BW_{-60dB}}{BW_{-3dB}} \tag{2.6}$$

. With reference to the general frequency response shape of a bandpass filter centered at frequency f_0, shown in Figure 2.5. The smaller the shape factor, the steeper the filter's roll-off. For an ideal filter, the shape factor is unity.

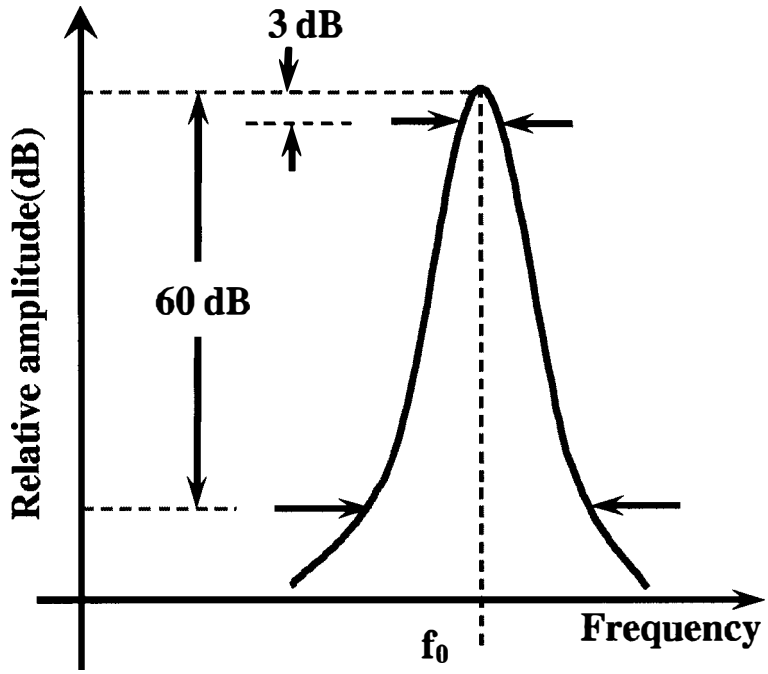

Figure 2.5: Shape factor S definition of a bandpass filter

2.3 High Q factor in-fiber RF signal processor

Since the first single-mode fiber-optic RF filter was demonstrated by Bowers et al [32] where single and two fiber optical couplers were used in the ring configuration to realize narrow bandpass filtering characteristic, extensive research has been focused on demonstrating the ability of photonic RF signal processor to process or filter RF signals with various transfer characteristics and high bandwidth [33, 40].

Reports on optical amplifier application in photonic RF filters were demonstrated in works [4, 40–42] where different topologies were proposed and analyzed. Figure 2.6 shows the first processor [40] which employed an optical amplifier to enable photonic RF signal processing with greater processing power than conventional approaches [43]. An optical amplifier(OA) was inserted in the fiber loop within the device, which not only compensated optical loss but also provided an extra degree of freedom to realize all types of fiber filters. The transfer function of amplified fiber recirculating delay line(RDL) filter can be given

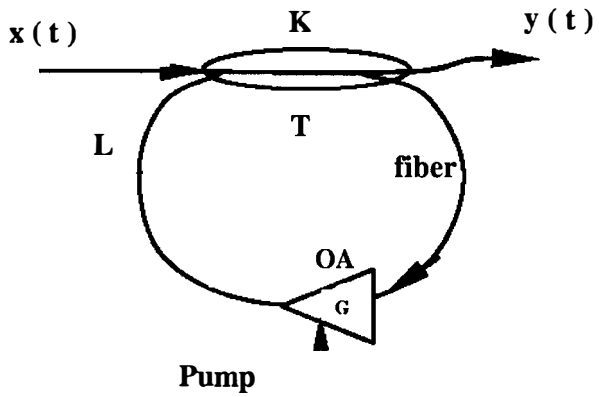

Figure 2.6: Amplified fiber recirculating delay line. T: loop delay time, L: loss of the loop, k: coupler's coupling ratio, x(t): input intensity , y(t): output intensity, OA: optical amplifier [40]

by:

$$H(Z) = \frac{Z - LG(2K-1)/K}{Z - LGK} \tag{2.7}$$

where H(Z) is Z transformation of the filter's transfer function. Net gain of the device can be defined as KLG. Since gain of optical amplifier can be tuned, different types of fiber filter can be dynamically constructed. Figure 2.7 shows the spectral responses of filter under different net gains of fiber loop.

Although dynamically tunable transfer function of the photonic RF filter was realized, its tuning range is very limited because it is very hard to precisely control tap weights and time delay within the fixed fiber delay line. For applications like photonic reconfigurable RF signal processing where more precisely controlled frequency response is necessary, different topologies were proposed [37, 44, 45].

Figure 2.8 shows one of them [37] where a pair of fiber Bragg gratings and optical amplifier constructed a fiber Fabry-Perot filter. Within this architecture, a high-Q microwave bandpass response was achieved. The filter response demonstrates high resolution, having a narrow-band response with Q of 325 at center frequency of about 1 GHz by properly setting the pump power.

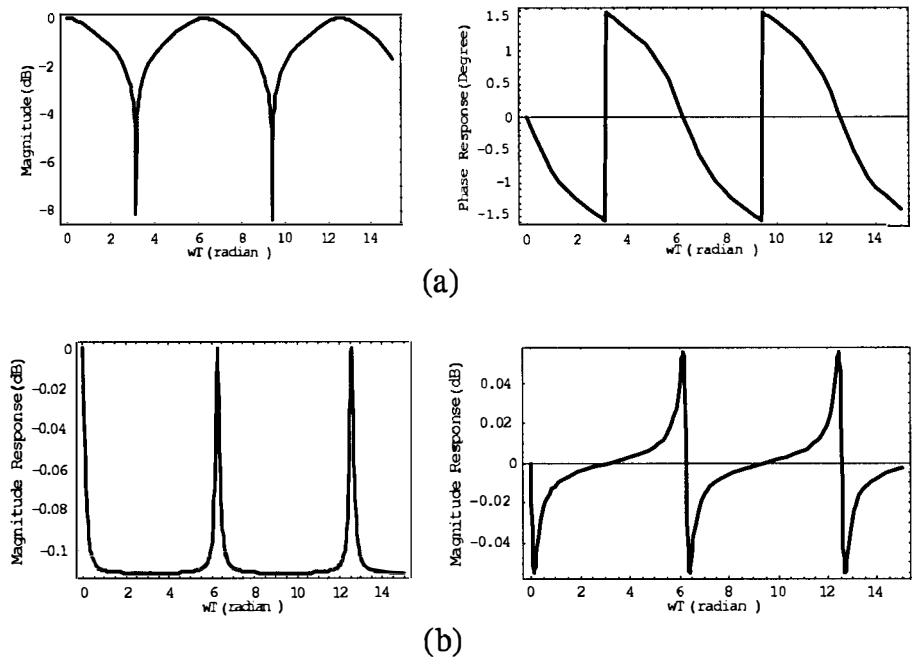

Figure 2.7: Spectral responses of amplified fiber RDL filter (a) Notch filter (b) Bandpass filter [43]

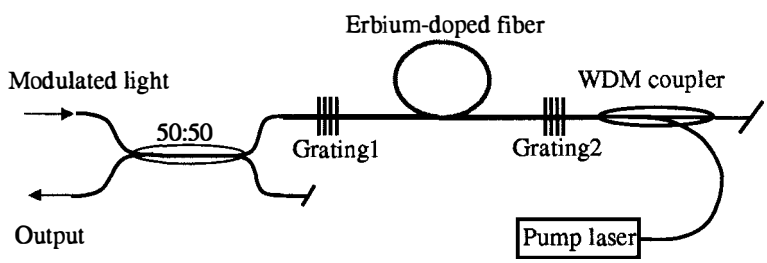

Figure 2.8: Amplified fiber Bragg grating Fabry-Perot filter [37]

The spectral responses of in-fiber RF filters we discussed so far can be shaped more flexible by introducing feedback where losses can be compensated by an optical amplifier and they are capable of performing a variety signal processing tasks both in frequency and time domains, but their tunability is limited by the requirement that they can only operate closely to the lasing threshold. Moreover, the requirements of a minimum active section length within fiber loop or F-P cavity to obtain the requisite gain limits the processor's working frequency, hence it is clear that they are inherently inflexible since tap weight and basic delay time tuning are not possible within these structures. Extensive works [44,46,47] have been undertaken to overcome those limitations.

With more advances in photonic technologies, more photonic RF signal processors are expected to be deployed in optical fiber networks, where the processing and distribution of wide band RF signals directly in optical domain become more attractive. Dynamic and adaptive photonic RF filtering provides a powerful tool.

2.4 Adaptive RF filter

The development of novel components makes adaptive photonic RF filters possible. The application of optical amplifier [4] and electro-optic or electro-absorption [48] modulator allows for easy filter reconfiguration. The combination of tunable laser, fiber grating and high dispersion fibers has opened a novel approach to solve the problem of filter tunability. To tune tap weights and delay times dynamically, WDM components combined with fiber dispersive components were applied in photonic RF filters [6, 49, 50].

The possibility of fast tuning pass band or rejection band position in either a step by step or continuous way is a key feature required for transversal RF filter. In order to tune the RF spectral response and ensure enough **Q** factor or shape factor **S**, either the unit

time delay or windowing and weighting of transversal filter has to be tuned.

In this section we review architectures and techniques of adaptive in-fiber RF signal processing.

2.4.1 Tunable in-fiber RF filter

In order to obtain high resolution in frequency domain of a RF filter, a large number of taps is required. Moreover a short sampling time is necessary in order to achieve high resolution in time domain. The processor's sampling frequency is determined by its unit time delay τ and given by:

$$f_s = \frac{1}{\tau} \tag{2.8}$$

To obtain tunable photonic RF filter with extremely high sampling frequency, several techniques have been proposed, which include the use of high dispersion fibers [34], arrayed waveguides grating [36], unbalanced Mach-Zehnder structures [35] and fiber grating devices [51].

Extensive researches have been carried on realizing tunability of photonic RF filter [34,48,51–53]. Among various implementations, some works have been reported by using constant unit time delays, while in most cases the photonic RF filter requires a plurality of control signals and complicated computation algorithms to set tap weights [7, 33]. A few other implementations use time delays that are adjustable over several discrete values [37,54,55]. Continuously tunable filter will be more demanded for applications in optical networking.

2.4.2 High dispersive fiber based tunable RF filter

Frankel et al [34] firstly proposed a continuously tunable bandpass photonic RF filter. Their configuration is shown in Figure 2.9 where a fiber optic prism was used as variable

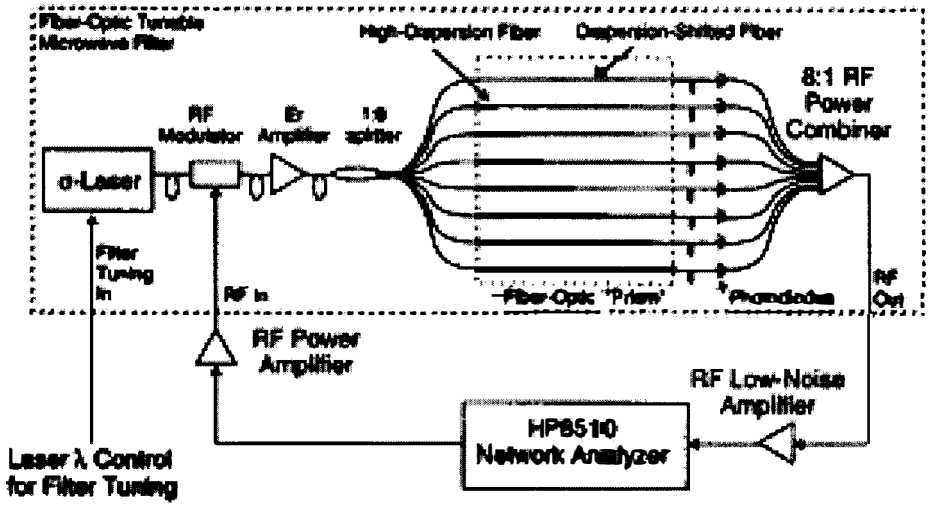

Figure 2.9: Tunable photonic RF filter with fiber optic prism [34]

time delay. The time-delay tuning relies on the use of a single wavelength-tunable laser source, external modulation and a dispersive single-mode fiber. This FIR filter is simple since it utilizes several taps with varying net chromatic dispersion coefficient. Tuning of the source wavelength alters the light velocity and, hence, the delay of optical signals.

The effective variable time delay within this structure is associated with dispersion wavelength dependence of the dispersion-shifted(DS) and high-dispersion(HD) fiber. Figure 2.10 shows the relationship. The measured slopes indicated the relative time delay as a function of wavelength, with dispersion computed as the derivative of delay versus wavelength and normalized to the fiber length. Figure 2.10(squares) shows that there is some residual dispersion of the DS fiber that increased with wavelength. Similarly, Figure 2.10(crosses) shows the much higher dispersion of the HD fiber that also has some wavelength dependence. The wavelength dependence of the dispersion affects the relationship between the tuning wavelength and the time delay, which is no longer linear. The use of near-constant dispersion HD fiber that is becoming available with prelude potential detrimental effects.

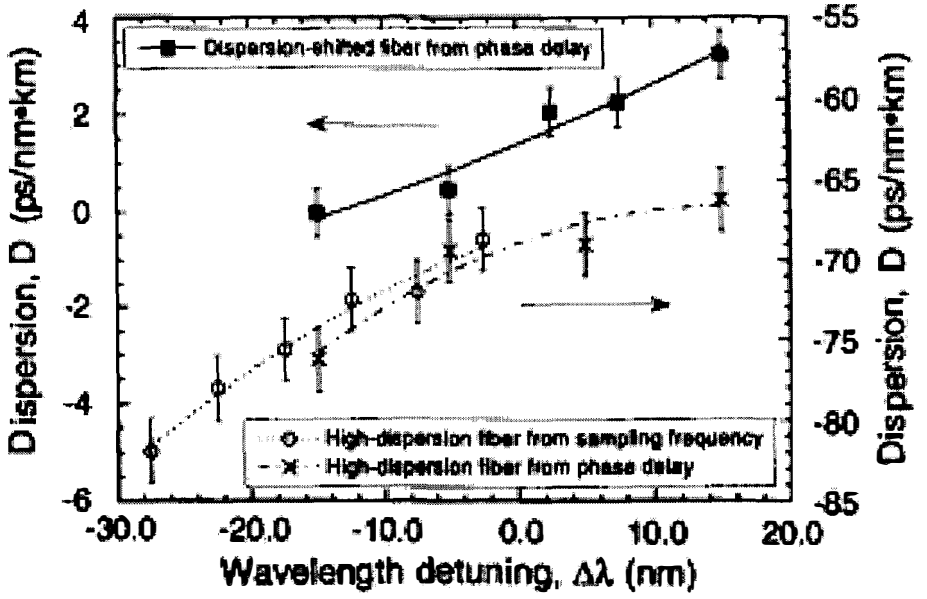

Figure 2.10: Measured dispersion coefficient of DS fiber and HD fiber [34]

The unit delay time within this architecture can be represented as:

$$\triangle\tau_s = l_{HD} \int \triangle\lambda(D_{DS}(\lambda) - D_{ds}(\lambda))d\lambda \tag{2.9}$$

where $\triangle\lambda = \lambda - \lambda_0$, $D_{HD}(\lambda)$ $D_{DS}(\lambda)$ are the HD and DS fiber's dispersion coefficients. Its sampling frequency can be: $f_s = 1/\triangle\tau_s$. Figure 2.11 shows a 8-tap filter characteristics. Since the laser applied in the system is a tunable laser, its wavelength can be tuned continuously, therefore, the sampling frequency can be varied continuously. The filter shows a Q of 30 and a pass band continuously tunable over 8.9 GHz to 18.2 GHz.

2.4.3 Fiber grating based tunable RF filter

Photonic RF signal processing based on fiber-Bragg gratings [23, 56, 57] in conjunction with wavelength-division multiple(WDM) technology provides a very powerful approach, enabling high capacity signal processors of high resolution, wide-band and adaptability.

The high sampling techniques using fiber grating components are demonstrated in Figure 2.12.

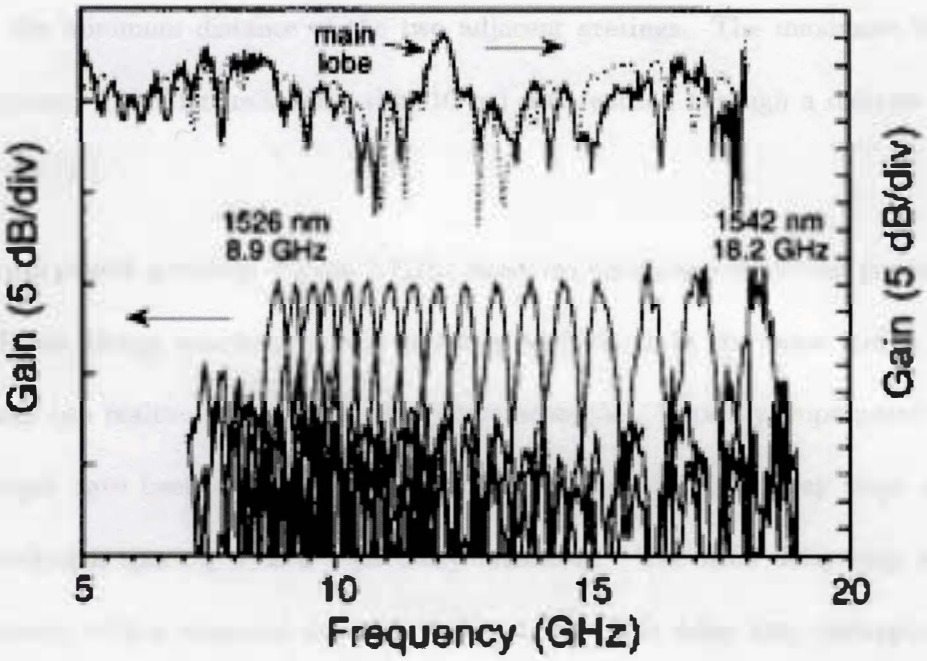

Figure 2.11: 8-tap filter characteristics. Top curves show that the comparison between measured (solid) and calculated (dashed) filter response at 1538nm. Bottom curves show the filter passband tuning as the wavelength varies by 1nm [34]

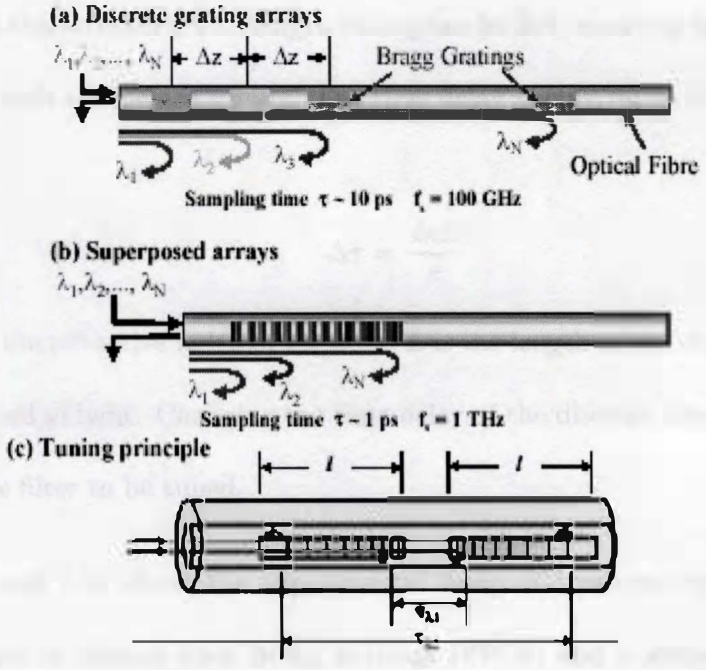

Figure 2.12: High speed sampling techniques using grating elements [49]

- **Discrete grating arrays**: In Figure 2.12(a), the minimum unit delay time is limited by the minimum distance of the two adjacent gratings. The maximum sampling frequency 100 GHz(unit delay time:10 ps) was realized through a discrete grating arrays [38].

- **Superposed grating**: Figure 2.12(b) based on multiple overwritten gratings with different Bragg wavelengths and coupling coefficients in the same length of fibre which can realize even smaller delay increments [58]. Recently, superposed grating designs have been shown to be capable of realizing 32 time delay steps at 1 nm wavelength spacing with a 1 ps delay increment. The time delay step has high linearity with a standard deviation below 1.7%. This delay step corresponds to a sampling frequency of 1 THz.

- **Chirped grating**: Figure 2.12(c) is based on controlling the basic unit time delay by changing the wavelength and shifting point of light reflection along a chirped fiber grating. In this structure, wavelength tuning can be fast, enabling agile programming capability with continuous tuning. The time delay tuning range is given by :

$$\Delta\tau = \frac{4nL}{c} \tag{2.10}$$

  where n is the refractive index of the fiber, L is the length of the chirped grating and c is the speed of light. Changing the time delay of the discrete time signal processor enables the filter to be tuned.

Figure 2.13 and 2.14 shows the experimental setup and results reported in [46]. It is based on a pair of chirped fiber Bragg gratings (FBGs) and a section of active fiber. The filter can have high-resolution bandpass RF response and it is tunable. Its tuning

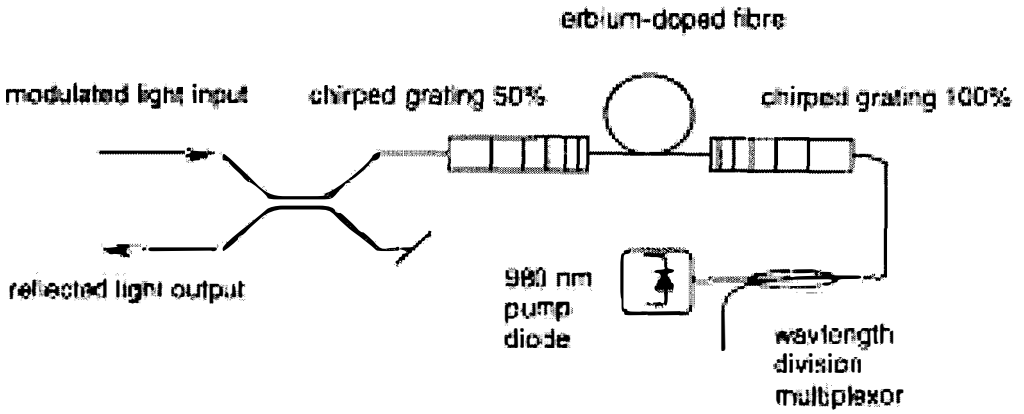

Figure 2.13: Configuration of tunable bandpass filter. [46]

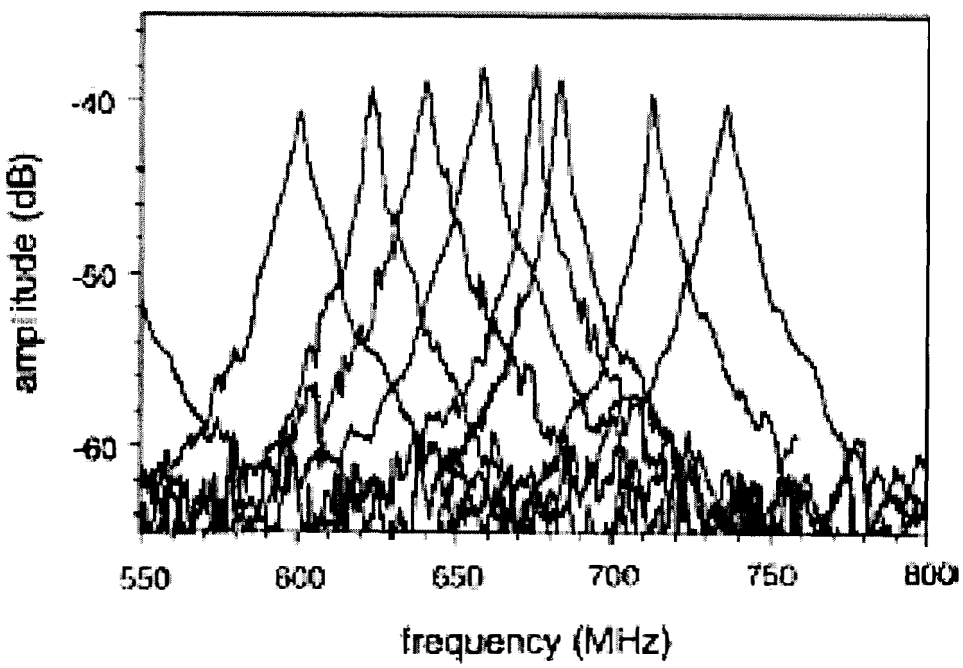

Figure 2.14: Tunable bandpass filter response [46]

is obtained via wavelength selectivity of the Bragg gratings. Wide, continuous tunability has been demonstrated, together with high performance characteristics. A 20% fractional tuning range has been achieved, and this can be readily extended using longer gratings or shorter cavity. The demonstrated technique is simple and compact, and enables wide-band continuously tunable filters with high Q factor and fast tuning speed.

2.4.4 AWG based tunable RF filter

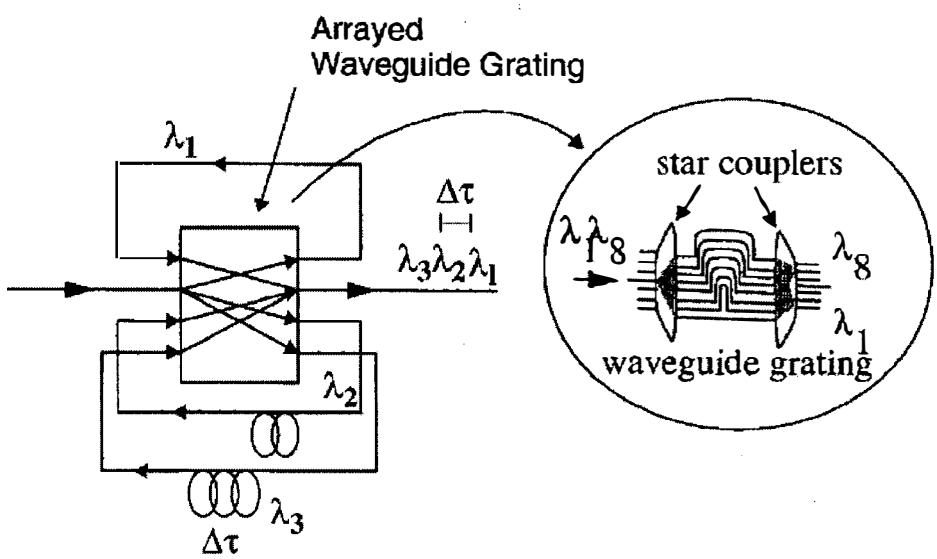

Figure 2.15: Schematic diagram of the wavelength - selective true time delay consisting of an arrayed-waveguide grating de-multiplexer in a symmetric feedback configuration [36]

Tunability can also be achieved using a novel wavelength-selective variable time delay [36]. Figure 2.15 shows the principle of AWG true time delay. A signal entering the center input will emerge from different outputs depending on its optical wavelength. Each output is then fed-back to its symmetric input with optic fiber of different length. The light will then be focused by the grating to the common output port. The time delay experienced by different optical beam is therefore a function of the optical wavelength. Figure 2.16 shows the frequency response of the filter at three different wavelengths. It is obvious that

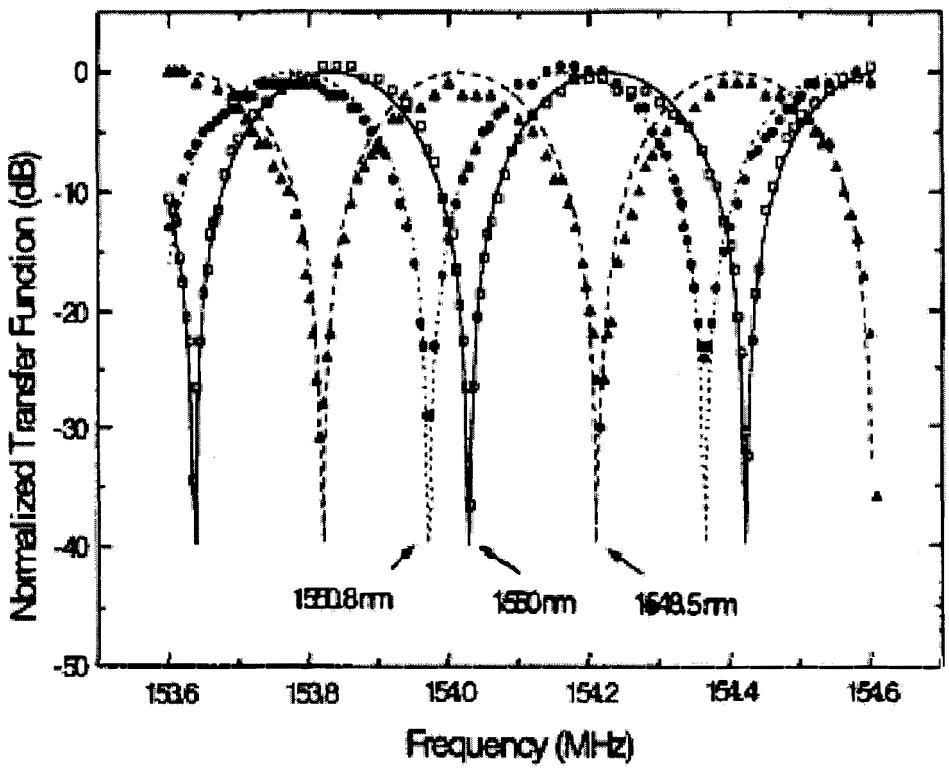

Figure 2.16: Frequency responses at three different wavelengths: 1548.5nm(open square), 1550nm(close triangle) and 1550.8nm (close triangle) [36]

the null of the filter can easily be tuned by changing the wavelength of optical carrier.

2.4.5 Reconfigurable and tunable RF filter

To realize fully reconfigurable and tunable photonic RF filter, it is important to be able to control tap weights and time delays within the photonic RF filter. Several reports [7, 24, 48, 50] demonstrate reconfigurability of RF filter.

Optical transversal RF filters using optical coherent interference can express arbitrary tap-weighting coefficients and therefore process signals without inherent combining power loss. RF Filters using optical fiber delay-line under coherent operation have been proposed [7,29,59], however the stability of the filter's response is not good since time delays within those architectures cannot be precisely determined.

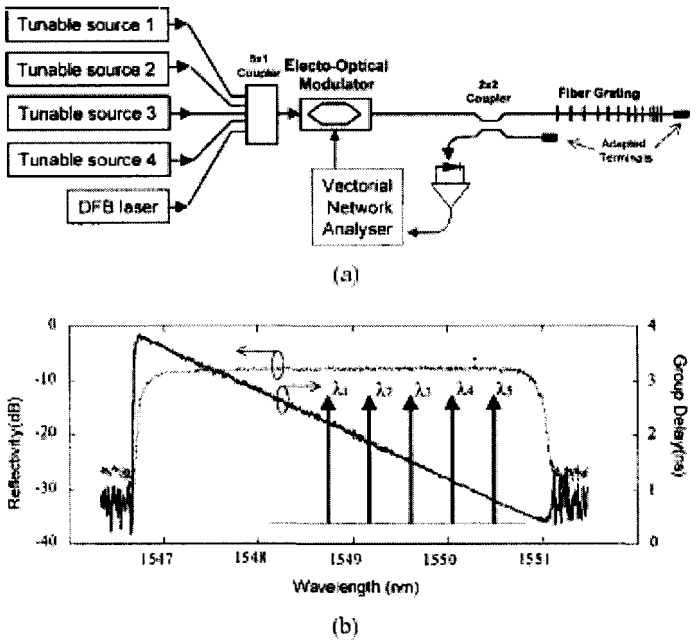

Figure 2.17: Layout of the filter with a laser array of five elements and a linearly chirped fiber grating [48]

Capmany and co-authours [48] proposed and experimentally demonstrated a novel class of compact, reconfigurable, tunable transversal RF filters based on combination of

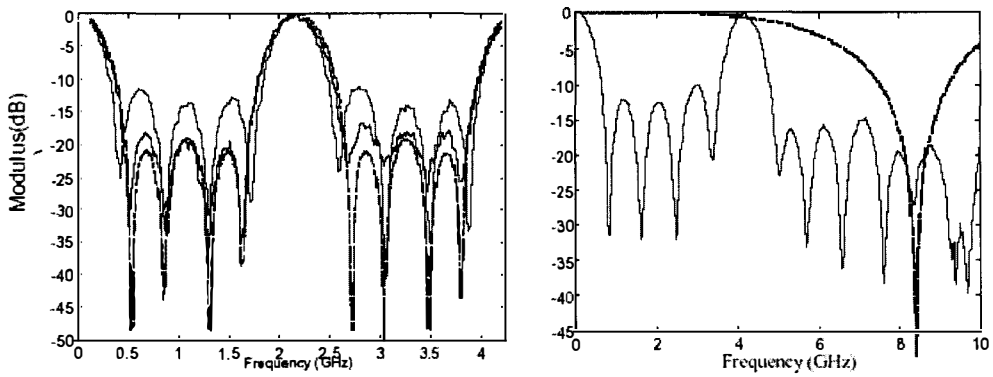

Figure 2.18: (a) Filter reconfigurability demonstration. (b) Filter tunability demonstration [48]

a linearly chirped fiber grating and tunable laser array. The layout of their experimental setup is shown in Figure 2.17. The filters are fully flexible, enabling fast and independent reconfiguration and RF tunability. Figure 2.18(a) and (b) show the results using a 5 stage uniform gratings where weights are given by a truncated Gaussian window function. Different colors in Figure 2.18(a) represents the filter's frequency responses by setting different weights from the laser sources. Figure 2.18(b) demonstrates results obtained for a uniform (solid trace) filter. The filter's free spectral range has been doubled to a value of 4.25 GHz, proving that filter tunability is possible. The carrier-suppression effect, shown as well in the figure, yields a spectral null around 8.5 GHz, and this is responsible for the suppression of the third spectral resonance in the filter. Nevertheless, this deleterious effect can be overcome by employing single-side band(SSB) RF modulation.

Instead of using a tunable laser array to tune the tap weights dynamically, another approach using an array of 8 gratings with a tunable laser source was reported by Yu [50].

The use of multiple wavelength sources of variable power levels and separations have been proposed [24] to generate reconfigurable bandpass characteristics. The system lay out is displayed in Figure 2.19.

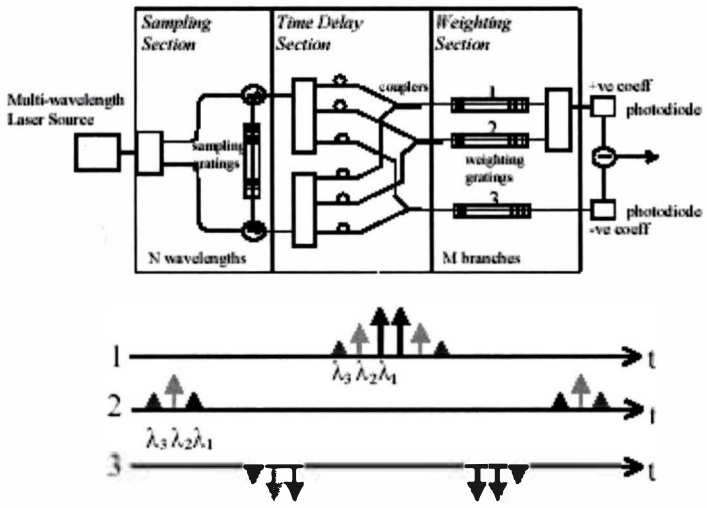

Figure 2.19: (a) WDM processor topology. (b) Symmetric taps generated in branches 1 to 3 [24]

2.5 Overview on incoherent in-fiber RF signal processing

The in-fiber RF signal processors we discussed so far are based on incoherent condition that the intensity of the modulated light outputs from all taps are summed linearly. It does not require any control of optical phase, therefore, it is not sensitive to external perturbations(e.g., temperature, vibration and stress). RF signal processor working in this condition is stable, repetitive, and more attractive for practical implementation. However, one important consequence of incoherent summation is that the negative weighting of taps cannot be accomplished optically, and the filter always has a maximum value at a DC point of its frequency transfer function, therefore, its transfer characteristics can not be arbitrarily reconfigured. The long optical delay line applied in the filter also limits the filter's free spectral range(FSR).

In principle, high coherence laser can be utilized in photonic RF signal processing where coherence time τ_c is longer than the unit time delay in the processor. However, under this working condition, the optical phase of each tap plays a predominant role in

the filter's frequency response, and each minor fluctuation in the propagation characteristics of any part of optical processor(length, refraction index, etc) can introduce serious phase-induced intensity noise to its response. Such coherent systems can be difficult to implement practically and are usually more complicated [7]. For this reason, coherent working condition which depends on the phase of optical carrier, is avoided for in-fiber RF signal processing.

2.5.1 Multimode laser source

To realize incoherent operation of in-fiber RF signal processing, and achieve an acceptable high signal-to-noise ratio, the optical source must have high power and its coherence length should be substantially less than the shortest unit delay in the processor, suppressing the undesirable coherent optical effects.

Multimode laser diodes(MMLDs), superluminescent diodes(SLDs) and superfluorecent fiber sources are commercially available [29, 40] and can be used as the incoherent laser sources for photonic RF signal processing. The linewidths of these sources are broad enough to produce the required short coherence length. However this solution is not practical in the modern telecommunication applications where a high coherence laser(such as DFB laser) is necessary to overcome systems's dispersion effects. The broad spectral width of such sources will severely degrade the performance of optical communication system.

2.5.2 Coherent-to-incoherent conversion

With more demanding from high speed optical network, all optical signal processing subsystem becomes more important and necessary. Parolari et al in their work [2] presented a

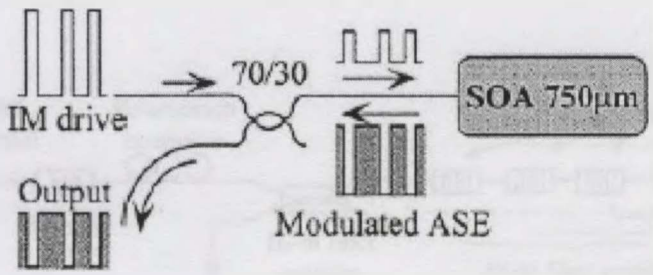

Figure 2.20: Schematic diagram of ASE converter device [2]

coherent-to-incoherent light conversion which is achieved by an all-optical amplified spontaneous emission (ASE) converter that can be locally employed before entering the fiber signal processing subsystem. The communication optical signal, whose carrier can have any spectral linewidth and most likely a narrow one, is thus locally converted into an optical signal having a low coherence time. The converter employs a semiconductor optical amplifier (SOA) and exploits the cross-gain modulation (XGM) phenomenon. The locally generated ASE is cross-modulated by the incoming optical signal, and the output light has the same coherence time of ASE, which can be estimated in hundreds of femtoseconds. Figure 2.20 shows their coherence-to-incoherence converter.

2.5.3 Hi-Bi fiber

Alternative schemes were demonstrated in [60, 61] where the coherence limitation of laser source was removed by making use of two orthogonal polarizations in hi-birefringence (Hi-Bi) fiber or Hi-Bi fiber grating. In their demonstrations, polarization syntheses has been introduced to realize incoherent operation, thus overcoming coherence limitation and increasing the free spectral range of an optical fiber delay line filter. By using a Hi-Bi fiber Bragg grating array, a large, tunable free spectral range has been obtained.

The experimental setup and results are shown in Figure 2.21. Since only two taps can

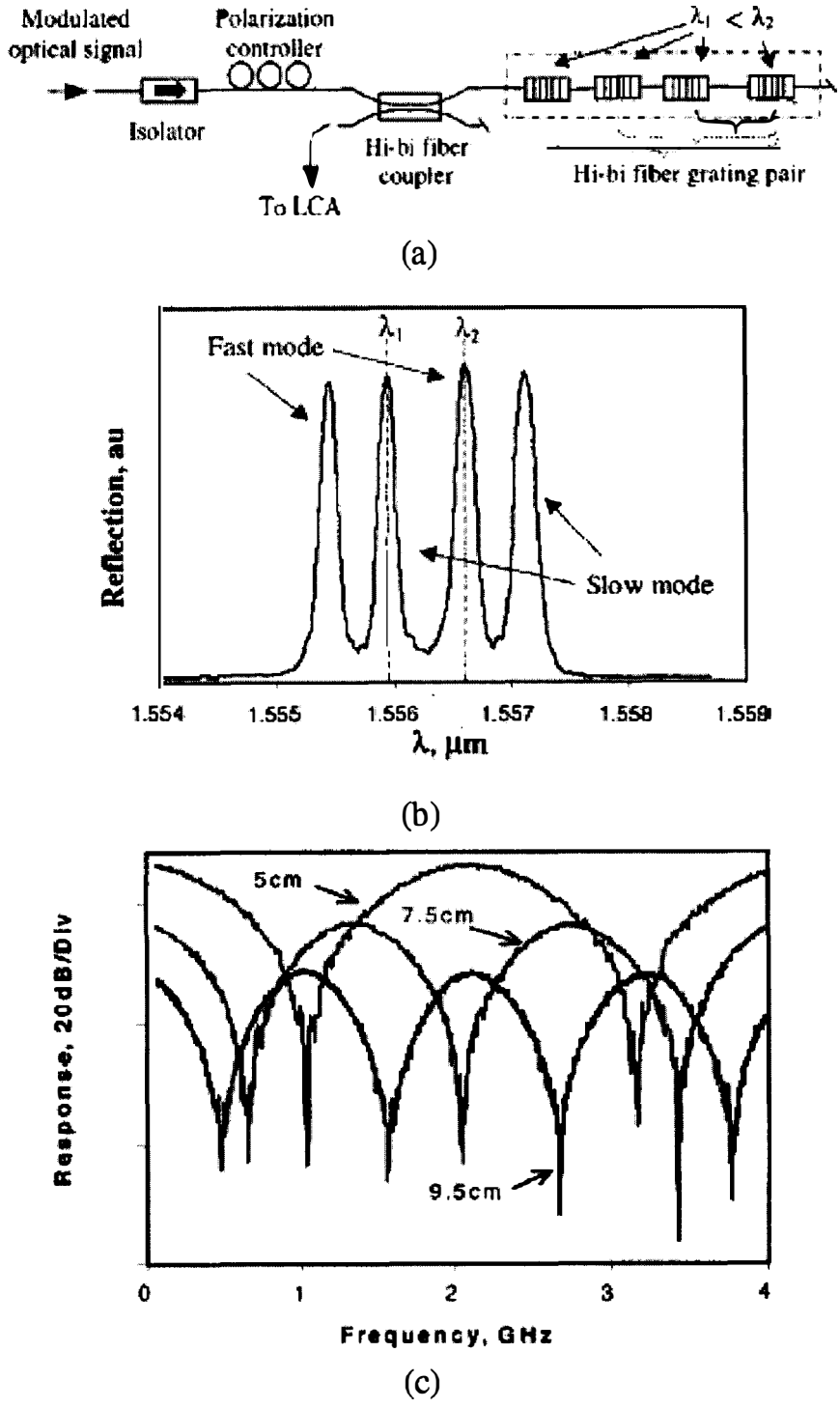

Figure 2.21: (a) Tunable configuration using Hi-Bi fiber coupler and grating array. (b) Reflections from a pair of Hi-Bi fiber gratings. (c) Frequency responses with tunable free spectral range [60]

be realized within this device, its tunability is very limited.

More works on this principle have been carried out by Yi [62] and Chen [63]. The filters they proposed can be continuously tuned and operate stable. Since more tunable laser sources and Hi-Bi fibers or fiber gratings are used within the filters, making them very complicated to manipulate. These filters are also bulky and expensive.

2.5.4 Negative tap weight generator

The optical transversal RF filters we discussed so far are working in incoherent regime. Within their architectures, only positive taps or positive weighting coefficients are possible. The filter's capacity is therefore limited. Without negative taps, it is difficult to manipulate the complex impulse responses to synthesize the required characteristics of filter, for example, high bandpass or flat top characteristic filter is hard to realize.

The technique [64] shown in Figure 2.22 uses the gain saturation in a semiconductor optical amplifier(SOA) to perform an inversion of analogue intensity modulation. Therefore, negative taps and and substraction of intensity modulated signals is made possible, regardless of the coherent length of optical source.

To realize negative taps in incoherent regime, an opto-electrical approach has been proposed, where the tap signals are detected by a pair of matched photodetectors and combined electrically [29, 64].

2.5.5 Multiple wavelength WDM signal processor

The application of multiple wavelength sources with wavelength-selective delays [65–67] is a powerful tool to afford the possibility of generating arbitrary transfer functions, since the tap weight can be implemented within the filter. Since the signals recombining at photodetector are at different wavelengths, the noises due to random phase noises of lasers

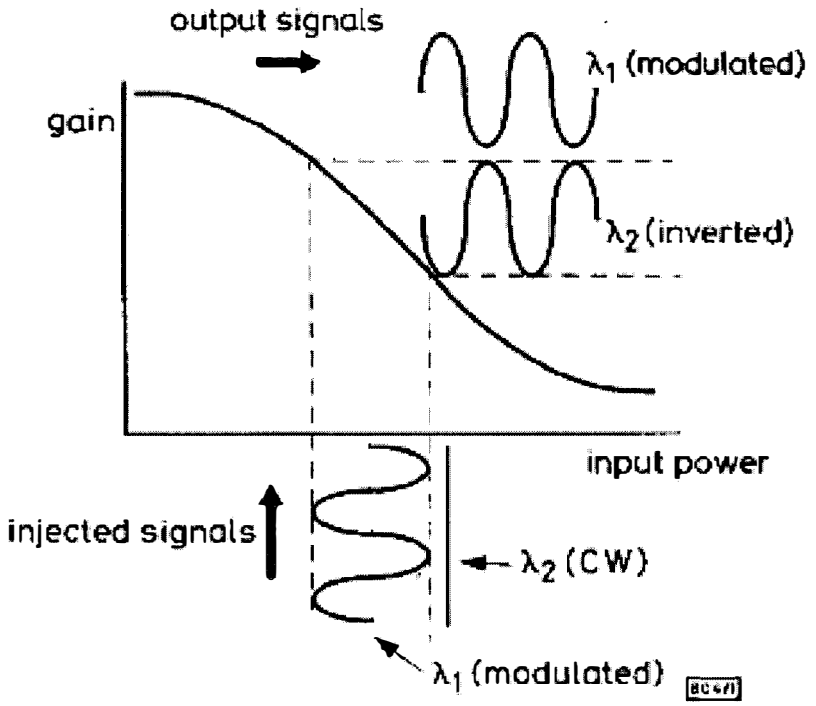

(a)

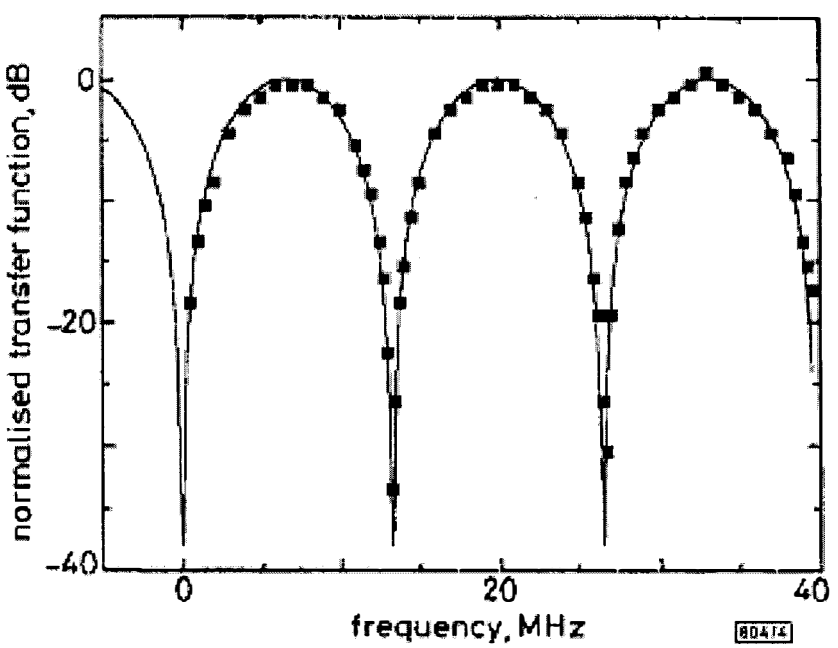

(b)

Figure 2.22: (a) Schematic diagram of inversion inside semiconductor optical amplifier. (b) Frequency response of two-tap optical transversal filter [64]

will appear at the beat frequency corresponding to the wavelength separation instead of appearing at the baseband. The beat frequency is very high and falls outside the bandwidth of photodetector, therefore these filters are free of laser coherence effects.

However, for high resolution filter characteristics, this technique is impractical because it requires either a large number of wavelengths in accurate separation or dynamically apodized fiber Bragg gratings for controlling the power levels of each wavelength source.

2.6 Related Optical Technologies

In this section, we discuss some key optical elements for photonic RF signal processing. With the rapid progress in optical technology, it will have a significant impact on photonic RF signal processing.

2.6.1 Laser source

The development of the first laser in 1960 [68, 69] marked a new era of optical communication. Continuously developments in semiconductor laser which can operate at room temperature made it a preferred source for optical communication [70]. Its capability of direct modulation via injected current was soon explored and has enabled the rapid developments of fiber optics applications in telecommunication and data communication with bit rates in multi-Gbit/s range. Laser diodes are also used to transmit analog signals over optical fibers with applications such as radar systems, cable television systems, and cellular systems for mobile communications.

Recently progresses in tunable lasers integrated with electro-absorbtion modulator(EAM) [71] and Vertical Cavity Surface Emitting Laser(VCSEL) diode array make reconfigurable and parallel RF signal processing more economic and practicable.

2.6.2 External Modulator

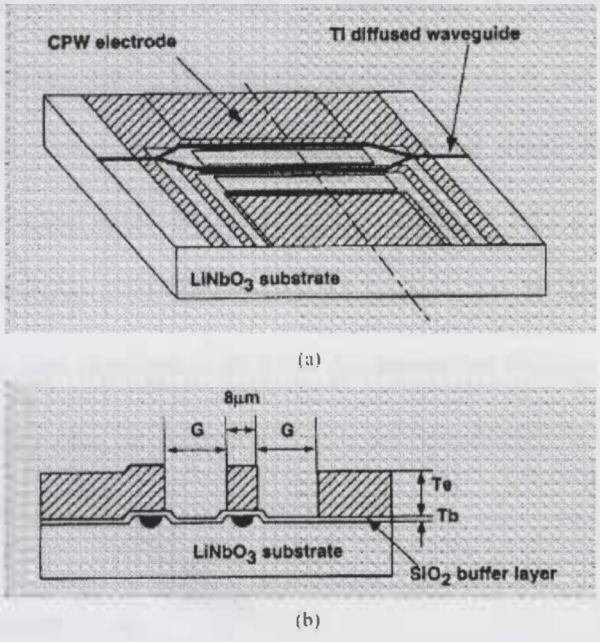

Figure 2.23: (a) Top view of an integrated electro-optical modulator. (b) Cross section of millimeter-wave $Ti : LiNbO_3$ Mach–Zehnder modulator [14]

To realize high speed and wide band RF signal processing, it is necessary to be able to modulate the optical source at high RF frequency with high bandwidth. External modulators are attractive because of their high performance characteristics, including broad modulation bandwidth, large extinction ratio, excellent spectral purity of the transmitted signal, high optical power handling capability and low modulation distortion.

Interferometric modulators using lithium-niobate and GaAs technologies have been realized with 3 dB electrical bandwidths in excess of 40 GHz [72–75]. Figure 2.23 shows the configuration of a millimeter-wave bandwidth lithium-niobate modulator. Impressive results have also been shown for the GaAs system with 3 dB electrical bandwidths of over 50 GHz and V_π of 13 V for a 1 cm -long modulator [73].

Recently, there has been strong interest in electro-optic polymer modulators with 3 dB electrical bandwidths exceeding 40 GHz, values of 10 V and fiber-to-fiber insertion losses

of 10 dB being reported [76]. Operation at 110 GHz has also been demonstrated [77].

Electro-absorption modulators operate by converting the incident light into photocurrent in their absorbing state. Waveguide modulators using the Franz-Keldysh effect in bulk semiconductor materials or the quantum confined Stark effect in quantum-well materials have been studied extensively. Bulk modulators at 1.53 μ m have achieved with 3 dB electrical bandwidths of 50 GHz under 3.5 V drive for 20 dB extinction ratio and fiber-to-fiber insertion loss of about 8 dB [76]. An attractive feature of electro-absorption modulators is that they can be integrated with semiconductor lasers to form compact optical sources capable of ultrafast modulation [78].

2.6.3 Photodetector

The photodetector generates an electrical current proportional to the incident optical power. Among its various high performance requirements, high sensitivity in the wavelength range of interest, minimum addition of noise to the system and a fast response speed of sufficient bandwidth are most important. It should also be insensitive to temperature variation, be of compatible physical dimensions, reasonable cost and long operating life.

Metal-semiconductor-metal (MSM) photodetectors have been used in a number of photonic RF systems. The main attraction has been their compatibility for integration with field-effect-transistor devices in optically controlled monolithic microwave integrated circuits(MMICs). Bandwidth as high as 78 GHz has been reported [79] with an external quantum efficiency of 7.5 % due to electrode blockage effects. Avalanche photodiodes offer internal gain, at the expense of higher operating voltages and temperature sensitivity. Using superlattice technology, 72 % quantum efficiency and an avalanche gain 10 have been obtained at a modulation frequency of 13 GHz and wavelength 1.55 μ m [79]. For high-speed operation, waveguide photodiodes with light incident parallel to the junction plane

have been extensively studied [80], with multimode designs offering 110 GHz bandwidth with 50% quantum efficiency [81].

The difficulty of interfacing photodiodes with subsequent amplifiers can be eased by monolithic integration, and impressive demonstrations of this technology have already been reported [82].

Recent progresses on photodiode array and the related technology have been reported by Lin [83] where a 1×12 MSM photodetector array was fabricated on a semi-insulated GaAs wafer with the external quantum-efficiency and 3 dB bandwidth of 0.4 A/W and 2.648 GHz respectively.

2.6.4 Passive components

Passive components from which photonic circuits are built include waveguides, couplers, gratings, mirrors, circulators, multimode interference (MMI) devices and AWG devices. The developments on components based on electro-holography which uses a spatial light modulator(SLM) as the holographic medium technology and inventions on photonic crystals [84] will certainly have great impacts on future photonic RF signal processing systems.

2.7 Conclusions

In this chapter, we reviewed various architectures and technologies of in-fiber adaptive RF signal processing. A survey of the latest development in relevant optical technologies is also covered. In next Chapter, we will present the proposed MicroPhotonic reconfigurable RF signal processor.

Chapter 3

MicroPhotonic Reconfigurable RF Signal Processor

In this Chapter, we discuss the use of MicroPhotonic processors to control optical power distribution in photonic signal processing structures, achieving adaptive photonic RF filtering with arbitrary transfer functions. A new MicroPhotonics-based photonic signal processing architecture is presented, in which fibre collimator arrays, Opto-VLSI processors, and a WDM combiner are integrated within an optical substrate to control the gains and weights of numerous active fibre Bragg grating cavities of different lengths. MicroPhotonic technology provides a cost-efficient and reliable means for controlling the gains and the input power of the Bragg cavities. Simulation results show that a reconfigurable 64-cavity photonic filter structure can generate arbitrary transfer characteristics at RF frequencies. We also investigate the impact of EDFA gain fluctuations on the response stability of Opto-VLSI based photonic filters.

3.1 Introduction

In last Chapter, we reviewed various technologies to realize adaptive in-fiber RF signal processing. Existing technologies cannot meet the requirements of next-generation photonic RF signal processors, namely, fully reconfigurable, high-resolution and cost effective.

MicroPhotonic integrating photonics and microelectronics technologies offers many advantages for RF signal processing, including the high-bandwidth capability of photonics, low insertion loss of optical media, the immunity to electromagnetic interference (EMI), and the intelligence of microelectronics.

RF signal processing based on emerging MicroPhotonic technologies can efficiently achieve adaptability [85]. To generate arbitrary RF transfer characteristics, we propose a novel multi-cavity structure that features high frequency resolution, precise cavity input signal power control, and accurate EDFA gain control. The novel structure integrates Opto-VLSI processors that dynamically split the input signal and pump beam and accurately couple them into the various active Bragg grating-EDFA cavities, achieving a transversal photonic RF filter with arbitrary transfer characteristics. Results show that for 128-cavity MicroPhotonic filter structure, high-rejection, low-ripples tunable RF bandpass or bandstop(notch) characteristics can be realized.

We also investigate the impact of EDFA gain fluctuations on the response stability of Opto-VLSI based photonic filters, and evaluate the passband ripple level for different skirt rejection characteristics. Simulation results show that for a gain fluctuation of 0.1 dB, and maximum allowed ripple level of 1 dB, the minimum attainable shape factor of a 128-cavity Opto-VLSI based photonic RF filter is 5.5, which is 1.5 times that attained by an EDFA-fluctuations-free photonic RF filter.

3.2 Architecture of Opto - VLSI processor

The architecture of Opto-VLSI processor consists of an array of liquid crystal (LC) cells, with a VLSI backplane [86,87]. Liquid crystals are generally birefringent, where the optical

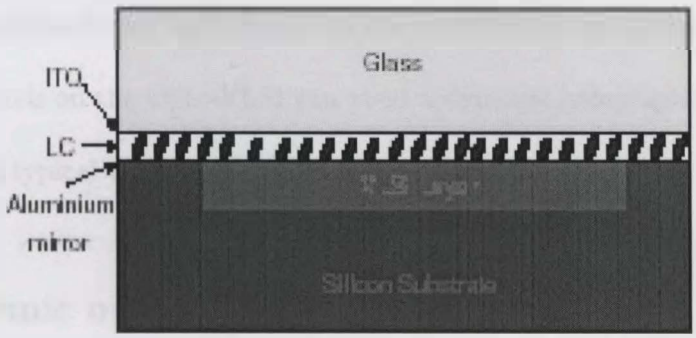

Figure 3.1: The layout of liquid crytal cell

axes of the two indices of refraction are controlled by the electric field across the LC cell. Therefore, by applying voltage across the LC cell, the index of refraction in the direction perpendicular to the plane of the cell can be altered. Figure 3.1 shows the layout of a typical LC cell.

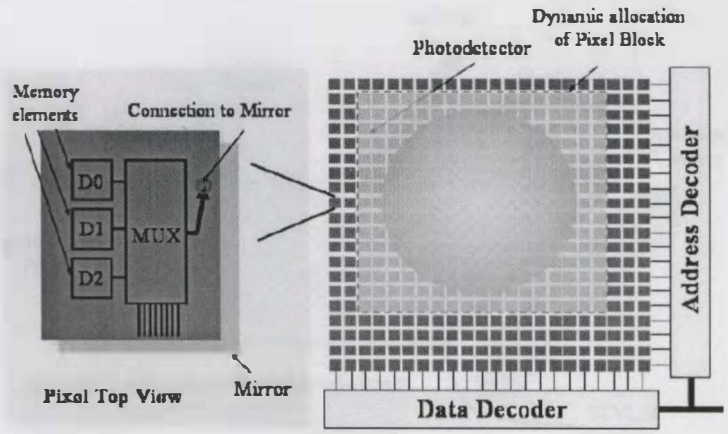

Figure 3.2: Schematic diagram of Opto-VLSI processor

The Opto-VLSI processor can be function as both transmissive and reflective spatial light modulator. We prefer to use reflective Opto-VLSI processor since it is easy to be integrated with its backplane VLSI circuit. A typical Opto-VLSI processor is a two-dimensional array of pixels made of electro-optic materials. Each pixels can be addressed electronically and be driven individually by the electric field on it, therefore the combination of these pixels on the Opto-VLSI can yield a dynamic holographic grating structure. The layout of a typical Opto-VLSI is shown in Figure 3.2.

3.3 Dynamic optical beam splitting approach

Free-space beam splitting can be accomplished by utilizing an Opto-VLSI processor, consisting of an array of Liquid Crystal(LC) pixels, independently addressed by a VLSI circuit to generate a reflective, multicasting phase-only holographic diffraction grating, in which the diffraction orders are deliberately enhanced to adaptively split the power of an incident optical beam along specific directions. This multicasting capability of Opto-VLSI processors provides efficient intelligence in photonic RF signal processing structures.

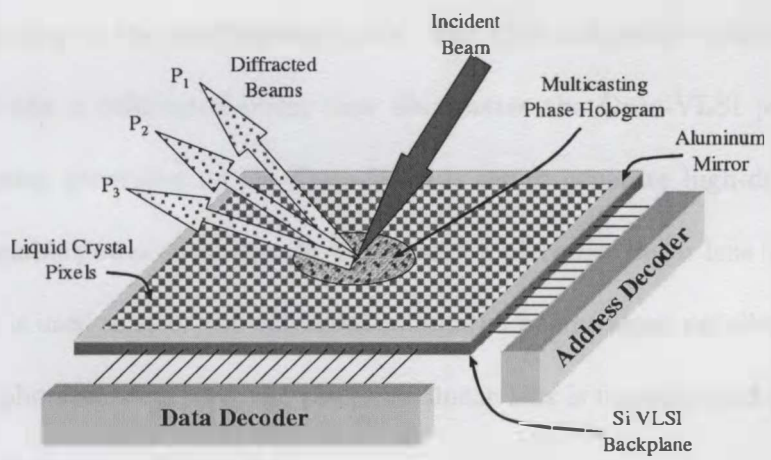

Figure 3.3: Multicasting capabilities of Opto-VLSI processors.

Figure 3.3 illustrates the multicasting potential of Opto-VLSI processors, which can

be fabricated by silicon processes to accommodate several hundred millions of transistors to drive few millions of LC pixels and process a very large number of optical beams at one time with high spatial resolution. Multi-phase Opto-VLSI processors can also be made polarization insensitive by incorporating a thin quarter-wave-plate (QWP) layer between the LC layer and the VLSI backplane. This latter feature makes the Opto-VLSI processor a competent platform for next-generation reconfigurable photonic systems.

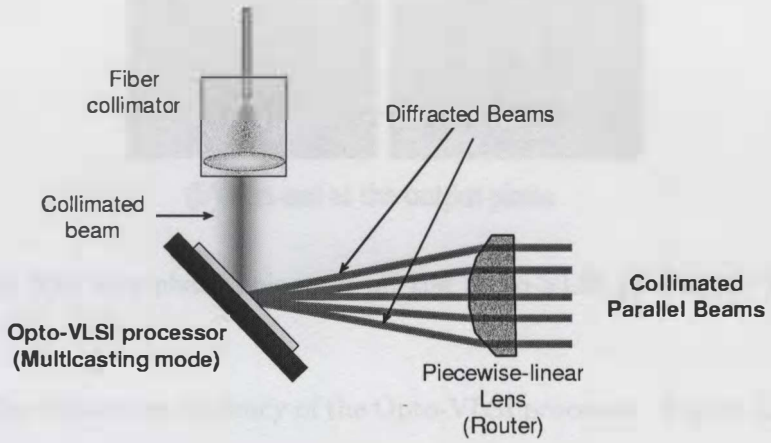

Figure 3.4: Routing of beams emerging from an Opto-VLSI processor operating in the multicasting.

Figure 3.4 shows the principle of routing the beams diffracted from an Opto-VLSI processor operating in the multicasting mode. The fibre collimator converts the in-fibre optical signal into a collimated beam that illuminates the Opto-VLSI processor. The diffraction grating generated by the Opto-VLSI is set to generate high-diffraction order beams with variable power along specific directions. A piecewise linear lens (or equivalently a prism array) is used to steer the diffracted collimated beams along parallel directions. In an integrated photonic structure, the piecewise linear lens is implemented as a diffractive optical plate, as shown in Figure 3.4.

Extensive researches [88, 89] have been carried out on the hologram algorithms which are used to generate the prescribed far-field fan-out subjecting to a phase-only constraint

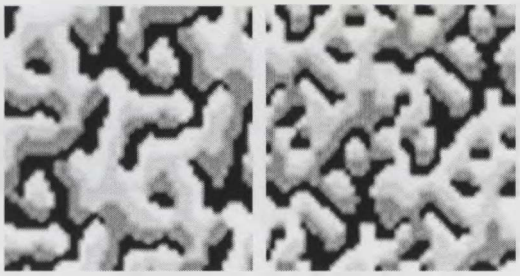

(a) Hologram on SLM

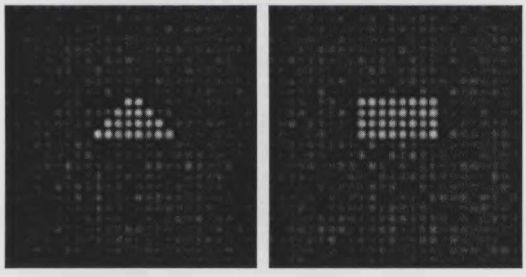

(b) Fan-out at the output plane

Figure 3.5: (a) The four-phase hologram on the Opto-VLSI processor. (b) Fan-out of hologram

and optimize the diffraction efficiency of the Opto-VLSI processor. Figure 3.5(b) shows the simulation results of the fan-out based on different holograms (shown in Figure 3.5(a)). The simulation is done by the free version of Holomaster 2.0 software, with four-phase hologram. From the figure, it is obvious that by changing the phase distribution on the Opto-VLSI, the number of fan-out and the intensity of each fan-out can be controlled. In section 3.6 we will show some experimental results.

3.4 Single- and Dual- Cavity photonic RF filter designs

A single-cavity photonic bandpass filter is shown in Figure 3.6(a). The transfer characteristic of that filter is also depicted in Figure 3.6(b). The shape factor S of the filter is defined as:

$$S = \frac{BW_{-30dB}}{BW_{-3dB}} \tag{3.1}$$

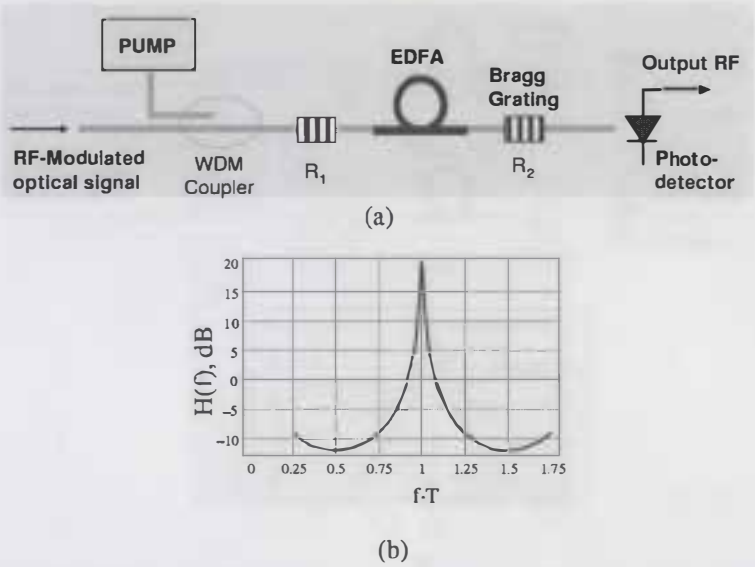

Figure 3.6: (a) Simple photonic bandpass filter structure. (b) Frequency response

where BW_{-3dB} is the $-3dB$ bandwidth and BW_{-30} is the $-30dB$ bandwidth. For an ideal filter, the value of the shape factor should be as low as possible, so that the filter passes a certain range of frequencies and strongly rejects all adjacent frequencies.

The transfer function of the simple bandpass filter shown in Figure 3.6 is given by

$$H(Z) = \frac{g\,(1 - R_1)\,(1 - R_2)}{1 - g^2 R_1 R_2 Z^{-1}} \tag{3.2}$$

where $Z = \exp(j2\pi T f)$, f is the RF frequency, g is the optical gain of active region, R_1 and R_2 is the first and second grating reflectivity, $T = (2n_0 L)/c$ is the round trip delay time corresponding to the cavity length L that is used to set the filter center frequency, n_0 is the fibre refractive index and c is the speed of light. Although the bandwidth of this structure can be controlled by the cavity closed loop gain $g^2 R_1 R_2$, its shape factor is independent of the loop gain, hence, it can not be customized.

Alameh et al. [23] have demonstrated the high-skirt selectivity of a photonic bandpass filter structure, consisting of a pair of active Bragg-grating cavities of equal lengths and different gains, as shown in Figure 3.7 (a). The optical gain offset Δg, which is controlled by the pump powers launched in the upper and lower cavities, generates a sharper bandpass

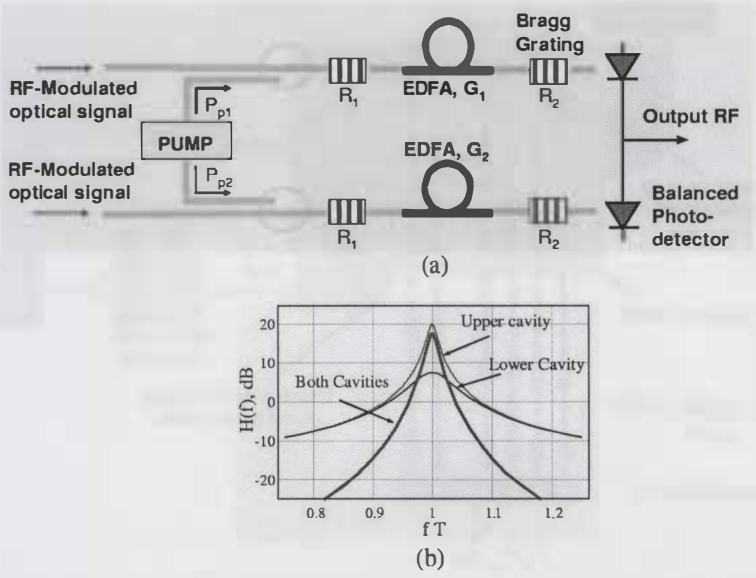

Figure 3.7: (a) Topology of the dual-cavity parallel fibre-based bandpass filter. (b) Frequency response

response around the center frequency in the lower arm than the response of the upper arm bandpass filter, whereas, far away from the center frequency the responses of both arms are nearly identical, see Figure 3.7 (b). By using a balanced photodetection process to subtract these two responses, the output response is slightly sharper around the center frequency than the single arm response, but most notably, response of the region far away from the center frequency is nearly significantly attenuated, leading to a large reduction in shape factor.

3.5 Novel, Multi-Cavity Microphotonic RF signal processor

Figure 3.8 shows the novel, reconfigurable MicroPhotonic RF signal processor, consisting of N gain-offset Bragg-grating cavity pairs and an optical substrate in which two Opto-VLSI processors, two microlens arrays, a WDM beam combiner and micro-optics are integrated. The cavity lengths are the same for each pair, while pairs are assigned different lengths. The output collimated beam of a high-power 980 nm pump source illuminates an

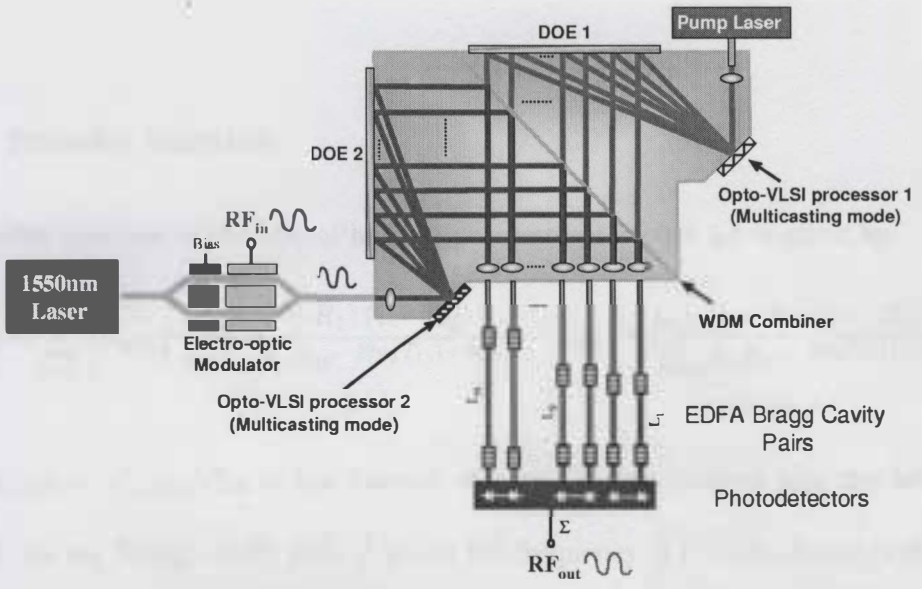

Figure 3.8: Topology of Multi-Cavity MicroPhotonic RF signal processor

Opto-VLSI processor, which generates a multicasting diffractive grating that diffracts the pump optical beam along various directions with arbitrary power distribution profile. The diffractive optical element (DOE1) is optimized to transform the diffracted pump beams into parallel collimated beams that can easily be coupled into the output Bragg cavities via a fibre collimator array. The capability of Opto-VLSI processor to dynamically couple arbitrary pump powers into the various Bragg cavities allows precisely control of the gains of the EDFAs, hence reconfiguring the quality factors (Qs) of the cavities. A 1550 nm optical carrier is modulated by the input RF signal via an electro-optic modulator. Using another Opto-VLSI processor with an optimized diffractive optical element (DOE2), the RF modulated optical signal is split into parallel collimated beams of arbitrary powers. The signal and pump collimated beams are combined with an integrated 980 - 1550 nm WDM combiner and coupled into the output EDFA Bragg cavity pairs via the output fibre collimator array. Each of the N EDFA Bragg cavity pairs consists of two cavities of equal lengths (but different gains) and whose output photocurrents are subtracted using a balanced photodetection process, making available positive and negative cavity processor

weights.

3.5.1 Transfer function

The transfer function of the MicroPhotonic processor of Figure 3.8 is given by:

$$H(f) = \sum_{n=1}^{N} \left[\alpha_{n,1} \frac{g_{n,1}\,(1-R_1)\,(1-R_2)}{1 - g_{n,1}^2 R_1 R_2 e^{-j2\pi f T_1 (1+n\beta_n)}} - \alpha_{n,2} \frac{g_{n,2}\,(1-R_1)\,(1-R_2)}{1 - g_{n,2}^2 R_1 R_2 e^{-j2\pi f T_1 (1+n\beta_n)}} \right] \tag{3.3}$$

where $\alpha_{n,1(2)} = P_{n,1(2)}/P_{tot}$ is the fraction of signal power coupled into the left (right) cavity of the n_{th} Bragg cavity pair, f is the RF frequency, $T1 = (2n_0 L_1)/c$ is the round trip delay of the first cavity, c is the speed of light, n_0 is the EDFA refractive index, L_n is the length assigned to the n_{th} cavity pair, and $\beta_n = (L_n - L_1)/L_1$. The cavity length increments are chosen to cover a desired RF band over which arbitrary transfer characteristics can be achieved. Practically, the parameters β_n can be measured once the Bragg cavities have been fabricated. The cavity weights α_n and gains g_n are the parameters that can be reconfigured to optimally fit $H(f)$ with an RF transfer characteristic target.

3.5.2 The impact of EDFA gain on the transfer function

To quantitatively evaluate the impact of EDFA gain fluctuations on the RF frequency response, the EDFA gains can be expressed as:

$$g_{n,i} = g_{n,i}^0\,(1 + k_{n,i}) \tag{3.4}$$

where $g_{n,i}^0$ is the average EDFA gain of the n_{th} cavity and $k_{n,i}$ is a random variable uniformly distributed in the range $-\frac{\delta g}{g_{n,i}^0}, \frac{\delta g}{g_{n,i}^0}$ with δg represents the maximum EDFA gain deviation. The EDFA gain fluctuations generate undesirable ripples in the RF response. The level of these ripples depends on the Q of the Bragg cavities used in the filter architecture.

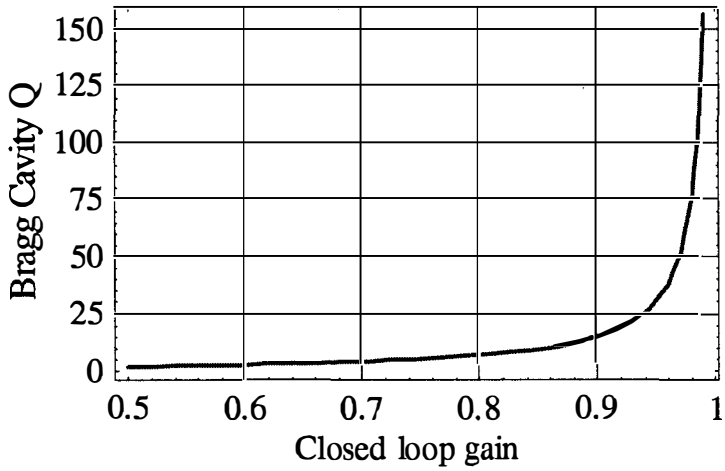

Figure 3.9: Bragg cavity Q versus closed loop gain.

Figure 3.9 shows the Q of a single Bragg cavity versus its closed loop gain. It is obvious that at low Q, the closed loop gain is small, and EDFA gain fluctuations cause insignificant change in the Q of the Bragg cavity, whereas at high Q, the closed loop gain is close to 1.0 and small EDFA gain fluctuations substantially change the Bragg cavity Q.

3.6 Results

In order to experimentally demonstrate the multicasting capability of the Opto-VLSI processor, we have set up a proof of concept experiment as shown in Figure 3.10 (a). A fibre collimator array was used to convert the input optical signal into a collimated beam. A diffraction grating plate was used to steer that beam onto the center of the Opto-VLSI processor, which was loaded by a multicasting hologram that diffracted the input collimated beam along two directions. The first direction was chosen to retrace the path of the input beam and hence it was coupled into the input fibre collimator port and routed through the circulator into the first output port. The second beam, which was diffracted along another direction, was coupled into the second collimator port via a second diffraction grating plate. A simulated annealing optimization algorithm was used

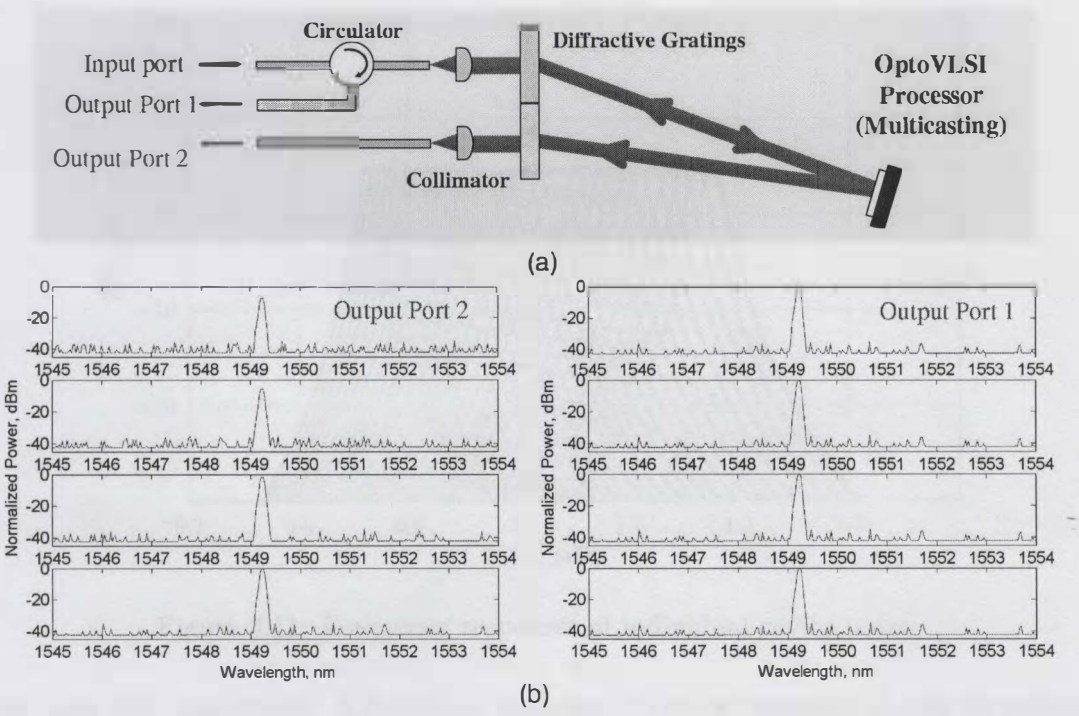

Figure 3.10: Experimental demonstration of multicasting capability of the Opto-VLSI processor.

to generate appropriate multicasting hologram which varied the power of the second beam while keeping the power of the first beam constant. Figure 3.10(b) shows the measured optical power at the two output ports. It is evident that adaptive optical power control (or equivalently filter coefficient adjustment) can be achieved through reconfiguration of the Opto-VLSI processor.

Computer simulations were carried out to tune the transfer characteristics by reconfiguring the weights and gains of the Bragg cavities of the photonic filter. Results were focused on reconfiguring the photonic structure to realize objectives of high-Q, low shape factor and multi-band bandpass RF filters. In the simulation, we assume $R_1 = R_2 = 0.5$. Figure 3.11 shows the responses of the individual cavity pairs for a cavity length offset of 1% and optical gain offset of 6.5%, together with the response of the simple bandpass filter discussed in Section 3.4. It is obvious that the proposed MicroPhotonic RF signal processor has the ability to generate narrow, low shape factor, bandpass responses over

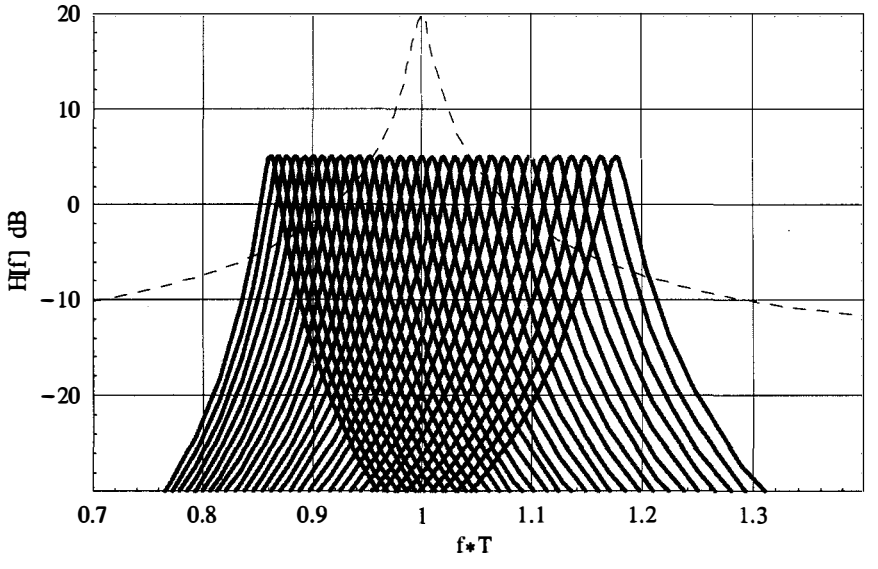

Figure 3.11: Frequency responses of individual cavity pairs

more than 30% bandwidth. A bandpass response of centre frequency f_i can be realized by:

- driving the second Opto-VLSI processor with an appropriate phase hologram that diffracts the optical signal beam falling on it only along the optical axes of i_{th} Bragg cavity pairs
- driving the first Opto-VLSI processor with an suitable phase hologram that couples the required pump powers into the i_{th} Bragg cavity pairs.

By using appropriate multicasting phase holograms are generated on both Opto-VLSI processors, the signal and pump powers coupled into the various Bragg cavities can arbitrarily be adjusted to generate multiple RF responses, whose sum results in an arbitrary RF response.

3.6.1 Bandpass filter

Computer simulations were carried out to realize bandpass characteristic by reconfiguring the weights and gains of the Bragg cavities of the photonic filter. Results were focused

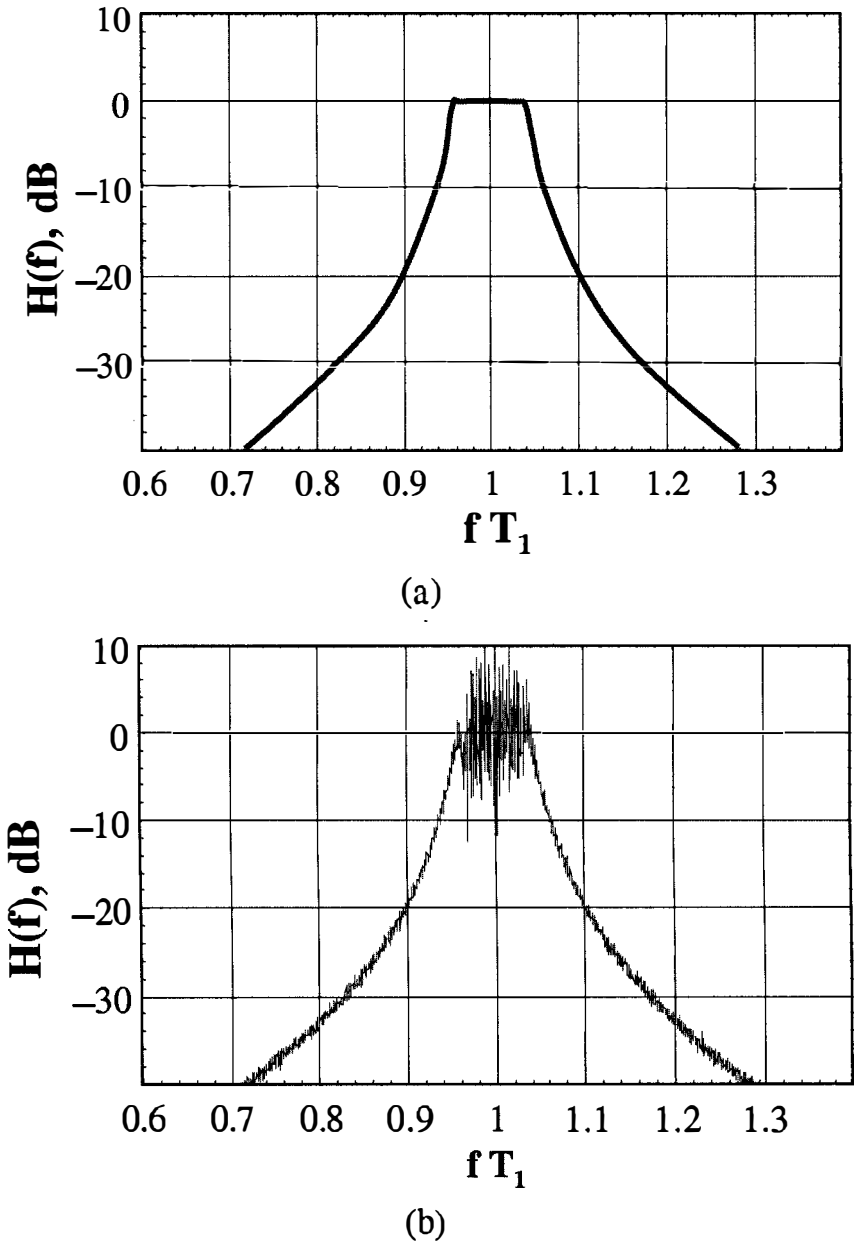

Figure 3.12: Frequency responses of the high gain 32-cavity filter. (a) No EDFA gain fluctuations. (b) 0.1 dB EDFA gain fluctuations

on reconfiguring the photonic structure to realize a low shape factor objective of 3.5. In the simulation, we assume R1= R2= 0.5, and all parameters $\beta_n = 0.005$. Figure 3.12 (a)shows the RF frequency response of the photonic filter, when the EDFA gains of each cavity pair are 1.97 and 1.875, respectively. The 3dB-to-30dB shape factor is 3.55. Figure 3.12(b) shows the RF frequency response when the EDFA gain fluctuations is 0.1 dB. In this case, substantial passband ripples are seen for small gain fluctuations. The calculated standard deviation of the ripples is around 5 dB.

Figure 3.13(a) shows the RF frequency response when the high and low EDFA gains are 1.875 and 1.65, respectively. In this case the -30 dB shape factor is 6. Figure 3.13(b) shows the RF response for 0.1 dB gain fluctuations. It is evident that the ripples are significantly lower than those of the high-gain photonic filter.

Figure 3.14 shows the standard deviation of the passband ripples versus the maximum attainable shape factor, for various EDFA gain fluctuations. It is noticeable that for a low shape factor objective, small EDFA gain fluctuations causes unacceptable passband ripples, whereas for a high shape factor target, the photonic filter is more tolerant to EDFA gain fluctuations. Finally, for 0.1 dB EDFA gain fluctuations and a passband ripples of less than 1 dB, the minimum attainable shape factor is 5.5. This is 1.5 times higher than the shape factor of a gain-fluctuation-free Opto-VLSI based photonic filter.

Figure 3.15(a) shows the frequency response of the 64-cavity filter for a signal power profile shown in Figure 3.15(b). Also shown in Figure 3.15(a) is the response of a single-cavity filter. All parameters β_n were assumed to be 0.01. For each cavity-pair, the EDFA gains are 1.9 and 1.3 for the high-gain cavity and low-gain cavity, respectively. The 3 dB - to - 30 dB shape factors of the 64-cavity and the single-cavity filters are 2.6 and 30, respectively. This shows that the multi-cavity filter results in more than 10-fold

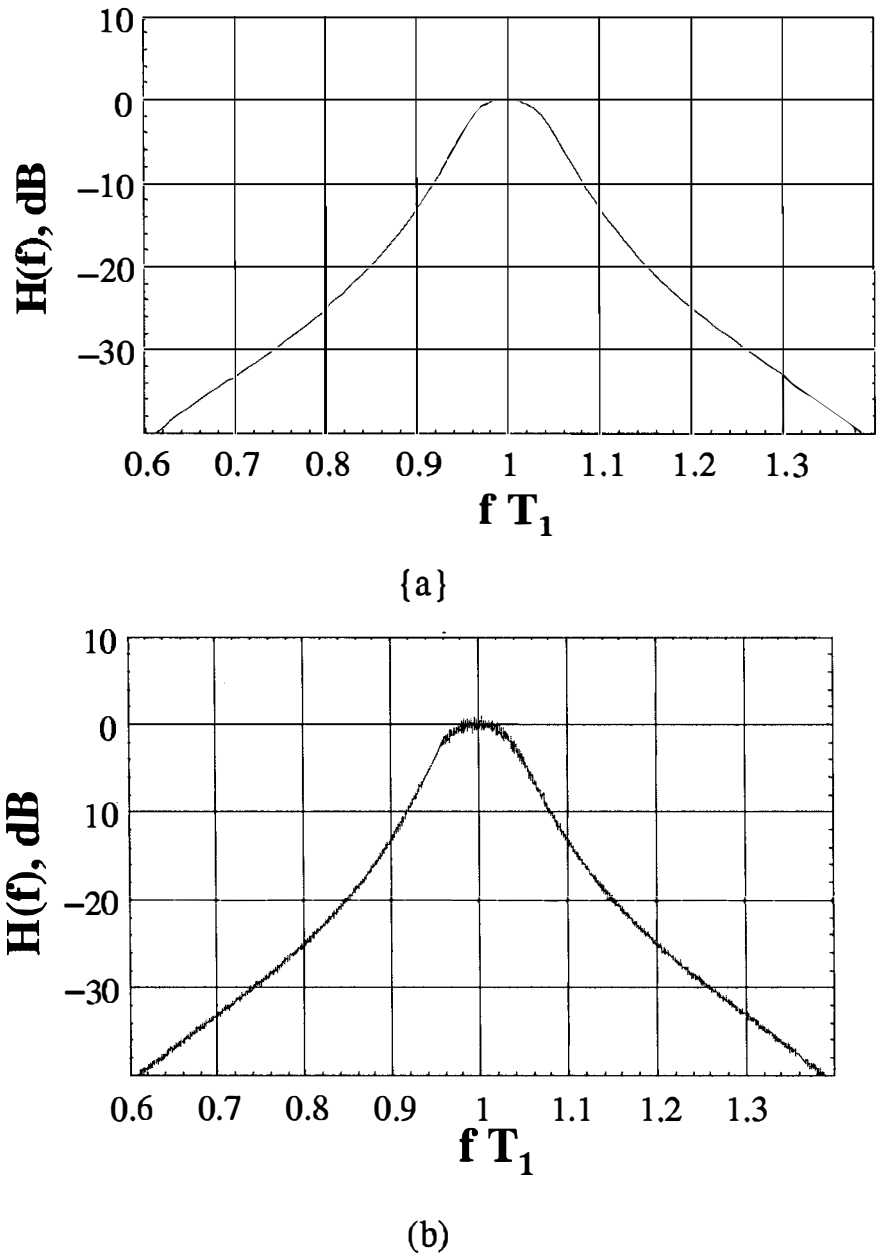

Figure 3.13: Frequency responses of the low gain 32-cavity filter. (a) No EDFA gain fluctuations, (b) 0.1 dB EDFA gain fluctuations.

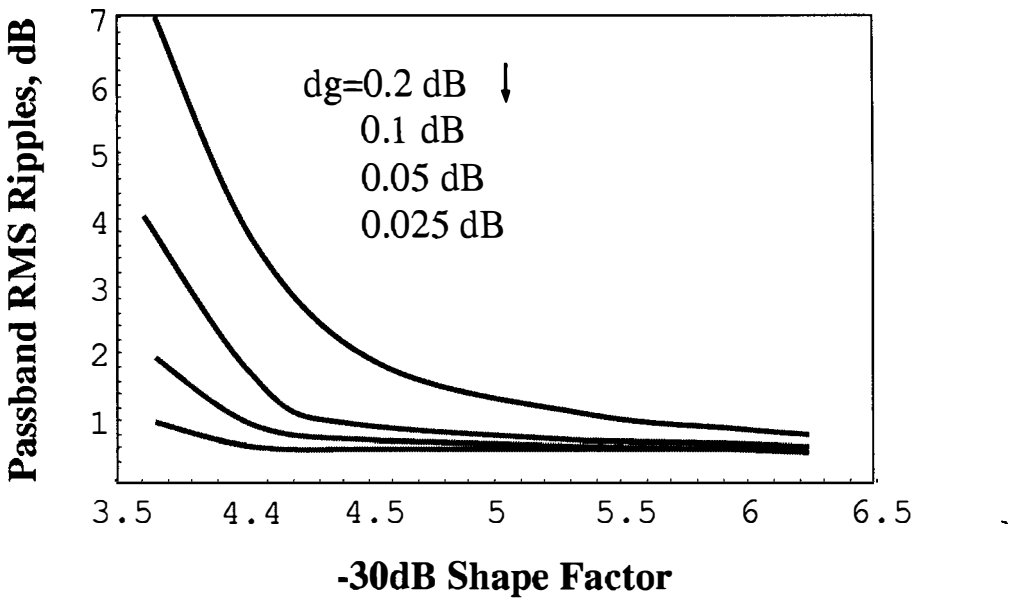

Figure 3.14: Passband ripples versus 3 dB - to -30 dB shape factor, for different EDFA gain fluctuations.

enhancement in shape factor, which is the highest, reported to date.

3.6.2 Notch filter

The MicroPhotonic RF signal processor is also capable of generating notch characteristics, which are crucial for mitigating RF interference. Figure 3.16(a) shows a notch filter response of unity normalized center frequency. The high and low gains of all Bragg cavity pairs were 1.85 and 1.45, respectively, and a cavity length offset of 2%. The optimum signal power profile, which is shown in Figure 3.16(b), results in more than 30 dB notch depth and less than 1 dB ripples over 65 % frequency band.

Figure 3.17(a) shows a notch filter response with the normalized centre frequency being tuned to 1.225. The high and low gains of the all cavity pairs were 1.85 and 1.45, respectively, and a cavity length offset of 2%. The optimum signal power profile, which is shown in Figure 3.17(b), results in more than 30 dB notch depth and less than 1 dB ripples over 65% frequency band.

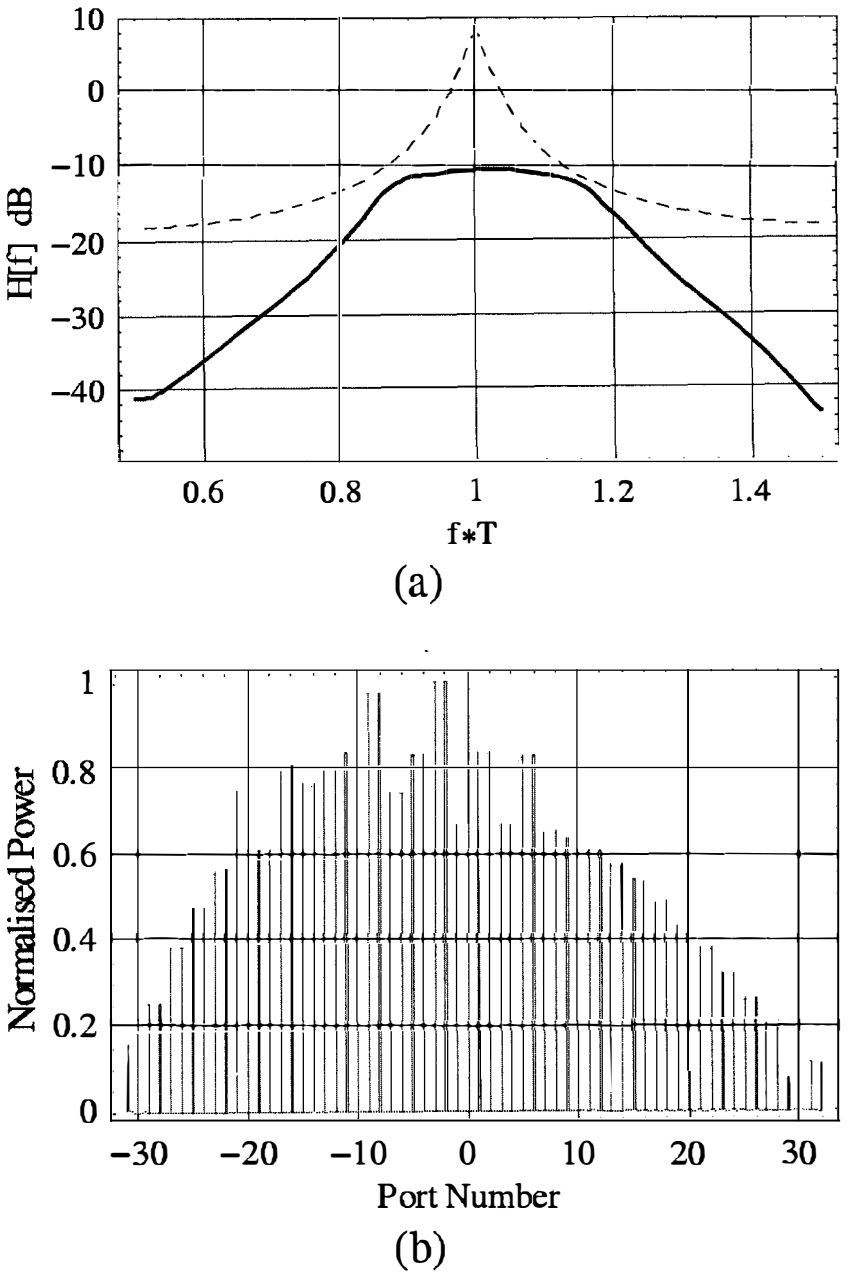

Figure 3.15: (a) Frequency responses of the 64-cavity filter (solid) and the single cavity filter(dashed). (b) Corresponding profile of signal power coupled into the cavity ports versus output port number. Upper and lower cavity gains = 1.9 and 1.3, respectively.

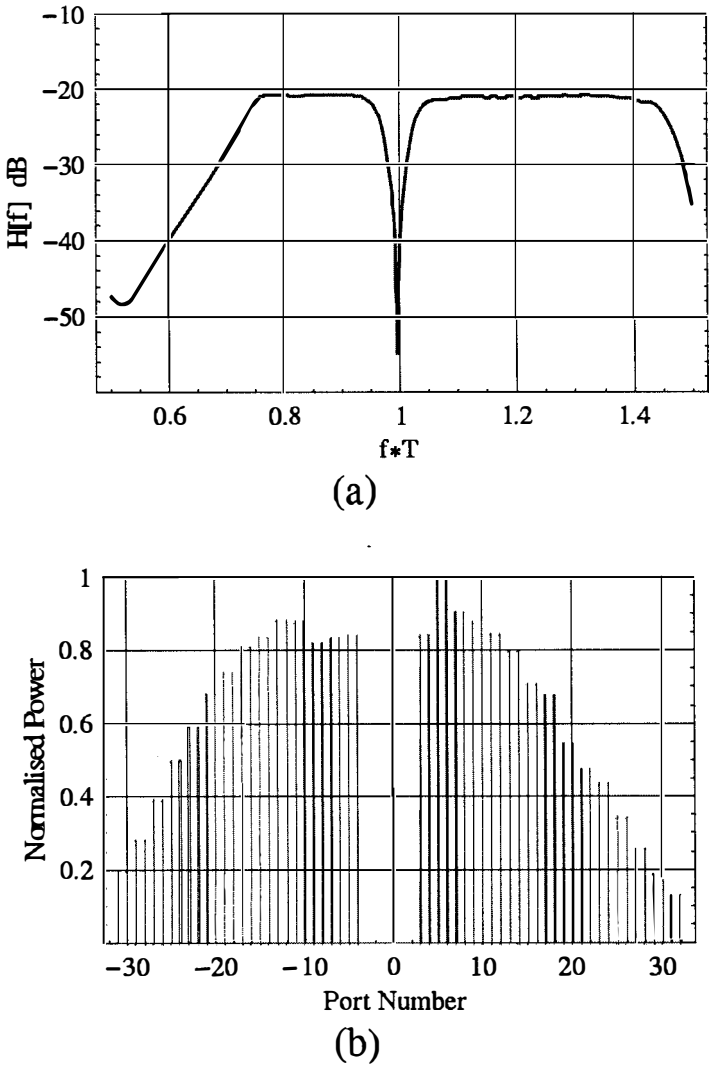

Figure 3.16: (a) Frequency responses of the 64-cavity filter. (b) Corresponding profile of signal power coupled into the cavity ports versus output port number. Upper and lower cavity gains = 1.85 and 1.45, respectively.

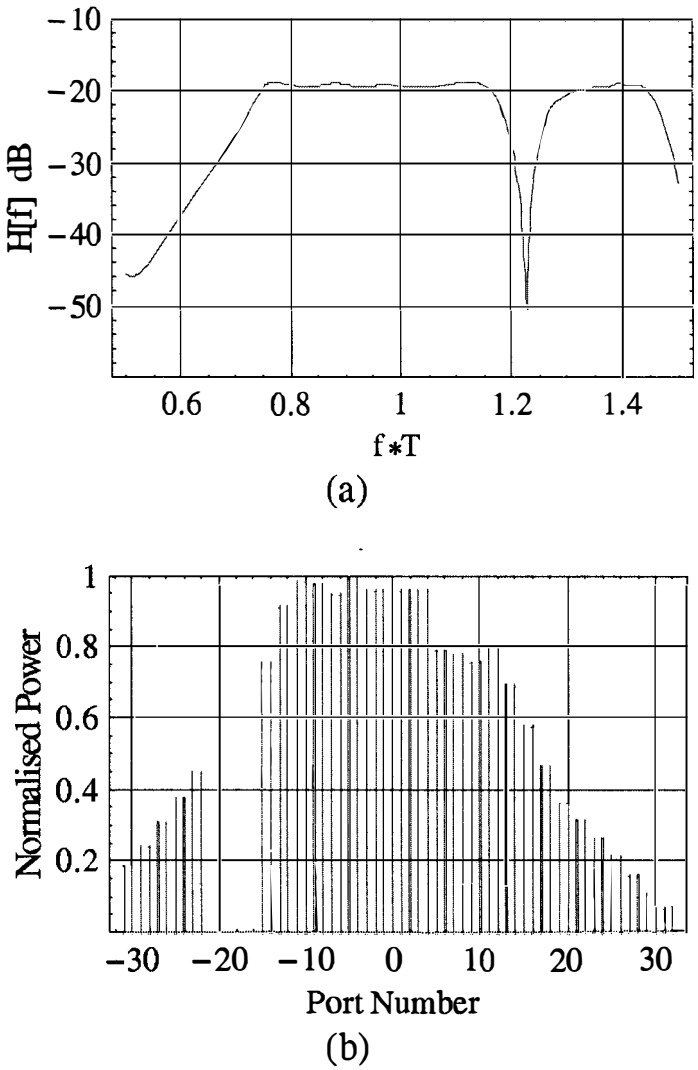

Figure 3.17: (a) Frequency responses of the 64-cavity filter. (b) Corresponding profile of signal power coupled into the cavity ports versus output port number. Upper and lower cavity gains = 1.85 and 1.45, respectively.

3.7 Conclusions

A novel MicroPhotonic reconfigurable photonic RF processor has been presented. The processor utilizes Opto-VLSI processors to generate reconfigurable diffraction gratings which in conjunction with optimized micro-optics, control the optical signal and pump power distributions in EDFA fibre Bragg grating cavities. The Opto-VLSI technology provides a cost-efficient and reliable means for implementing MicroPhotonic RF signal processor. Results have shown that for a 64-cavity structure a wide passband filter response with a shape factor as low as 2.6 is feasible, which is the highest reported to date. The impact of EDFA gain fluctuations in Opto-VLSI-based reconfigurable photonic signal processors was also discussed. The use of several high-Q Bragg cavities can achieve a bandpass response with low shape factor. However, in high-Q Bragg cavities, small fluctuations in EDFA gains can cause substantial passband ripples that degrade the performance of the photonic signal processor. We have quantitatively evaluated the passband ripples of Opto-VLSI based photonic filters for different EDFA gain fluctuations. We found that low-Q Bragg cavities are more tolerant to the EDFA gain fluctuations than high-Q cavities. Simulation results showed that for gain fluctuations of 0.1 dB, and maximum allowed passband ripple level of 1 dB, the minimum attainable shape factor of a 32-cavity Opto-VLSI based photonic RF filter is 5.5, which is 1.5 times that attained by a gain-fluctuations-free photonic RF filter.

Tunable notch characteristics have also been obtained with less than 1 dB passband ripples over more than 65% operating frequency band. The results have shown that the new MicroPhotonic processor can be reconfigured to tune the center frequency while maintaining a low shape factor. The processor can also be reconfigured to generate arbitrary characteristics.

The MicroPhotonic reconfigurable RF signal processor we proposed can realize the fully reconfigurable transfer function by controlling the intensity in each cavity of the filter. The tuning of the weight is limited by the length of EDFA in the cavity and it is sensitive to the laser coherency. In next Chapter, we analyze how the laser coherency affects the performance of the photonic RF filter.

Chapter 4

Coherence Effects on Photonic Signal Processor

Laser coherence effects on photonic signal processor are investigated in this Chapter. When optical interference is generated due to reflections in fiber delay line or any imperfect connections, the interference of optical carrier and that of the modulation RF signals generate beat noise that falls within the RF band. These two interference effects introduce the phase-to-intensity noise(PIIN), causing unstable operation.

In this Chapter, we investigate the RF frequency responses of two typical photonic RF filters, namely, transversal RF filter(FIR), fiber Febry-Parot cavity RF filter(IIR), and single-mode fiber recirculating delay line(RDL) notch filter under coherent light illumination. Results show that the coherence length of laser has a substantial impact on the performance of all types of photonic RF signal processors.

4.1 Introduction

Fibers have been used to transmit radio frequency(RF) or microwave signals as delay lines and other signal processing elements at megahertz or gigahertz frequencies [29, 51, 90]. Among the various applications of photonic RF signal processors [14], one particular interesting area is the radio-frequency (RF) notch or bandpass filters which are based on the use of true-time delay lines [48, 55, 65].

Optical interference occurs in systems under long coherence length laser illumination, where the delayed RF-modulated optical signals, which may be originated by multiple reflections, connectors, or splices in the optical systems, can be converted to intensity noises that fall within the RF band and cannot be filtered out.

The analysis of phase-induced intensity noise(PIIN) has been extensively studied [91–94]. Tur and co-authors have theoretically and experimentally investigated the phased-induced intensity noise power spectrum of a fiber recirculating loop [91]. They showed that this noise significantly degrades the performance of a photonic signal processor and limits its high-frequency operation range. Moslehi has obtained a universal expression for the phase-induced intensity noise of a general optical RF signal processor [94, 95]. Although both have accurately evaluated the optical interference, both have ignored the interaction between the interference caused by the optical carrier and the modulating RF signal.

In this Chapter, the RF frequency responses of photonic signal processors are analyzed under coherent operation. Firstly, in Section 4.2, the concept of laser coherence is introduced. In Section 4.3, the RF frequency response of a photonic RF signal processor is analyzed, including the interference introduced by optical carrier and the RF modulation signal. General expression for the RF frequency response is obtained for a laser source of Lorentzian spectral line shape. Section 4.4 investigates the RF frequency response of a

4-tap photonic RF filter under coherent illumination and the PIIN is analyzed. In Section 4.5, we analyze a fiber Fabry-Perot cavity notch filter's response under coherent operation. Section 4.6 discusses the frequency response of a fiber RDL RF notch filter, the real time RF frequency responses are simulated by disturbing time delay of the fixed loop in the range of one optical cycle time. The results show that the photonic RF filter is unstable under coherence operation and sensitive to the minor environmental disturbances.

4.2 Laser coherence time

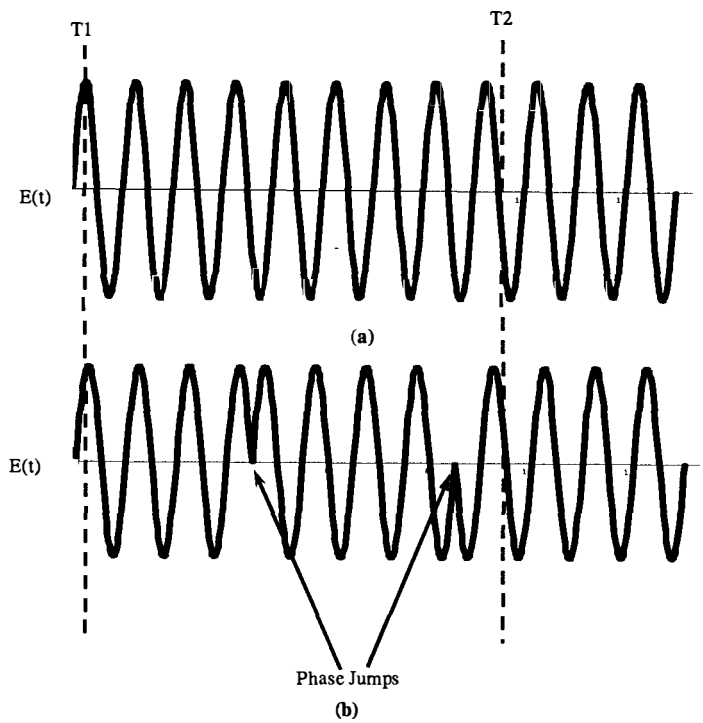

Figure 4.1: Concept of laser coherence. (a) Coherent light: The phase of the optical field is predictable across time interval(T2-T1). (b) Low coherence light: The phase of the optical field is uncertain across the time interval(T2-T1) because of random phase jumping

The laser coherence time τ_c is a measure of the spectral purity of laser frequency over time. In two-path interferometers, the degree to which an optical wave interferes with a time-delayed portion of itself depends on the coherence time of the wave with respect to

the optical delay. The coherence time is reduced by random events, such as spontaneous emission in the laser cavity, which alters the phase or frequency of the laser-output field. This is illustrated in Figure 4.1.

In Figure 4.1(a), since the phase is predictable during the interval of time $T_1 - T_2$, the coherence time is longer than that of Figure 4.1(b). In Figure 4.1(b) random phase changes cause uncertainty in the phase relation between time T_1 and T_2. The coherence time, τ_c, varies inversely with the laser linewidth, $\triangle\upsilon$. For a Lorentzian lineshape spectrum, the laser coherence time is defined as

$$\tau_c = \frac{1}{\pi\triangle\upsilon} \tag{4.1}$$

As laser linewidth increases, its coherence time decreases. Another parameter related to the laser coherence is laser coherence length L_c. The coherence length of a laser is related to its coherence time by:

$$L_c = \upsilon_g \tau_c \tag{4.2}$$

where, υ_g is the velocity of the light within the propagation medium, $\upsilon_g = \frac{c}{n_g}$, n_g is the group velocity index, which is approximately 1.47 in optical fibers.

As an example, consider a laser with a linewidth of 10 MHz, its coherence time and coherence length are about 32 ns and 6.5 m respectively.

4.3 RF response of photonic RF signal processor

The general architecture of a photonic RF signal processor is shown in Figure 4.3 where a laser source, an electro-optic modulator, an optical signal processing unit and a photodetector are used.

To investigate the impact of laser coherence on RF frequency response of a photonic RF filter, we assume that the laser source is a DFB laser of typical Lorentzian-shape spectrum

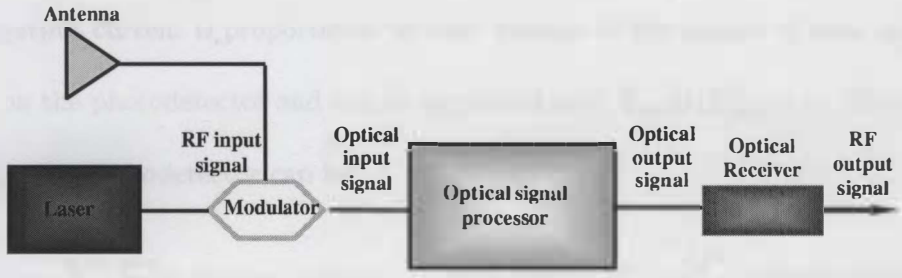

Figure 4.2: General architecture of photonic RF signal processor

modulated by an RF sinusoid signal. The electric field of the input RF-modulated optical signal is given by:

$$E_{in}(t) = [1 + M\cos\omega_{RF}t]e^{j\omega_0 t}\varepsilon(t) \tag{4.3}$$

where M is the modulation index, ω_0 is the radian frequency of the optical source. ω_{RF} is the RF signal frequency and $\varepsilon(t)$ is the slowly-varying envelop of the RF-modulated optical field [96], which is given by:

$$\varepsilon(t) = \int_{-\infty}^{\infty} \tilde{\varepsilon}(\omega)e^{j\omega t}d\omega \tag{4.4}$$

Using Wiener-Khintchine theorem, the autocorrelation function of optical field can be defined as:

$$\Gamma(\tau) = \Gamma^*(-\tau) = \langle\varepsilon(t)\varepsilon^*(t-\tau)\rangle \tag{4.5}$$

where $\langle\rangle$ represents an ensemble, or time-averaging process. Without loss of generality, we assume that $\varepsilon(t)$ is normalized such that $\Gamma(0) = 1$.

The output field $E_{out}(t)$ transmitted through the photonic delay line processor can be expressed as:

$$E_{out}(t) = \sum_{n=0}^{N} k_n\varepsilon(t_n^{'}) \cdot [e^{j\omega_0 t_n^{'}} + \frac{M}{2}e^{j(\omega_0+\omega_{RF})t_n^{'}} + \frac{M}{2}e^{j(\omega_0-\omega_{RF})t_n^{'}}] \tag{4.6}$$

where $t_n^{'}$ is the delay time of the processor for each optical path. Equation 4.6 shows that the output field $E_{out}(t)$ impinging on the photodetector has three spectral components which are at ω_0 and $\omega_0 \pm \omega_{RF}$.

The output current is proportional to time average of the square of total optical field incident on the photodetector and can be expressed as $< E_{out}(t)E^*_{out}(t) >$. Therefore, the current on the photodetector can be:

$$I_{RF}(t) =< \sum_{m=0}^{N}\sum_{n=0}^{N} k_n k_m \varepsilon(t-nT)\varepsilon(t-mT)[(e^{j(\omega_0(m-n)T} + \frac{M^2}{4}(e^{j(\omega_0\pm\omega_{RF})(m-n)T}) + \frac{M}{2}(e^{j(\omega_0(m-n)T\pm\omega_{RF}(t-mT))} + e^{j(\omega_0(n-m)T\pm\omega_{RF}(t-nT))}) + \frac{M^2}{4}(e^{j(\omega_0(m-n)T\pm\omega_{RF}[2t-(m-n)^{1/2}>T])}) > \quad (4.7)$$

When the photodetector's response time τ_d is sufficiently short, that is: $\omega_{RF} \ll 1/\tau_d \ll \omega_0$, three frequency components are dominant in the response, namely: dc, ω_{RF} and $2\omega_{RF}$, which are referred to as the dc, RF and second-harmonic currents, respectively. By proper RF filtering, the dc and second-harmonic currents are usually filtered out, and will not be discussed here. Therefore, the RF response of the filter can be expressed in terms of its amplitude A_{RF} and phase ϕ_{RF} functions.

$$I_{RF}(t) = A_{RF} * e^{j(\omega_{RF}t+\phi_{RF})} \quad (4.8)$$

4.4 Transversal photonic RF filter

4.4.1 Analysis

The architecture of a conventional transversal photonic RF filter is shown in Figure 4.3. The laser output is modulated by an electro-optic amplitude modulator, amplified by a following Erbium-Doped Fiber amplifier (EDFA) and fed into a $1 \times N$ optical power splitter. The split signals are delayed and then recombined with a $N \times 1$ optical combiner and then detected by a photodetector.

For laser with a Lorentzian spectral shape, the autocorrelation function of optical field

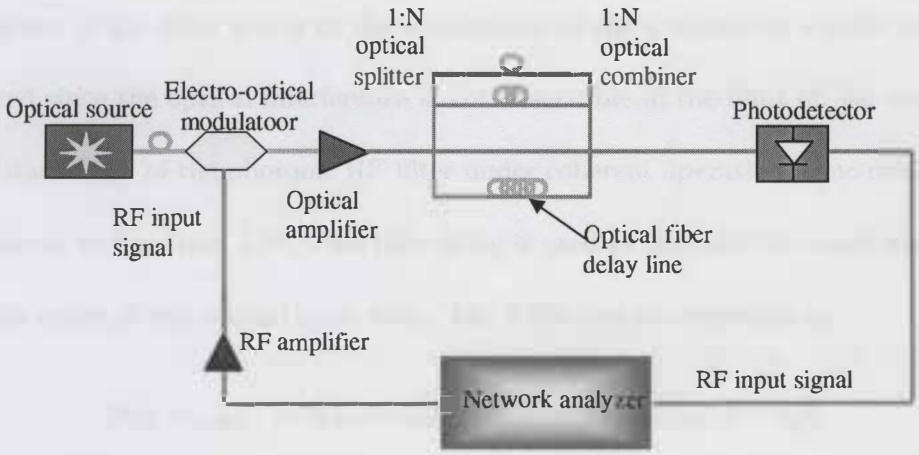

Figure 4.3: Configuration of the transversal RF optical filter

is given by:

$$\Gamma(\tau) = e^{-|\delta\omega\tau|} \tag{4.9}$$

Substituting Equation 4.9 into Equation 4.7 yields,

$$A_{RF} = (\sum_{n=1}^{N}(\sum_{m=1}^{N} k_n k_m e^{-|\delta\omega(m-n)T|}\cos((m-n)\omega_0 T)(\cos(m\omega_{RF}T) + \cos(n\omega_{RF}T)))^2$$
$$+ (\sum_{n=0}^{N}(\sum_{m=0}^{N} k_n k_m e^{-|\delta\omega(m-n)T|}\cos((m-n)\omega_0 T)(\sin(m\omega_{RF}T) + \sin(n\omega_{RF}T)))^2 \tag{4.10}$$

where N is the number of optical splitter's ports. T is the unit delay time for each optical path. k_i is the coupling ratio for each branch of optical splitter and $\sum_{i=1}^{N} {k_i}^2 = 1$ if the splitter is lossless.

Physically, the $(m-n)^{th}$ term in the series is due to the interference of optical carrier having completed $(m-n)$ times travel with those of frequency of $\omega_0 \pm \omega_{RF}$ having journeyed the optical path m times.

For light with a very broad bandwidth, $\Gamma(\tau) = 0$ for $\tau \neq 0$. The amplitude of RF component can be deduced immediately from Equation 4.10 and 4.11 as:

$$A(\omega_{RF}, T) = (\sum_{m=n=1}^{N} 2k_m k_n \cos(m\omega_{RF}T))^2 + (\sum_{m=n=1}^{N} 2k_m k_n(\sin(m\omega_{RF}T)))^2 \tag{4.11}$$

The response of the filter is due to the interference of the modulation signals only. This is expected since the optical interference is not observable in the limit of: $\delta\omega \dashrightarrow \infty$.

To obtain PIIN of the photonic RF filter under coherent operation, time delay τ_d of T is introduced, in Equation 4.10. This time delay is used to simulate the small disturbance and in the range of one optical cycle time. The PIIN can be expressed as:

$$PIIN(\omega_{RF}) = Maximum[A(\omega_{RF}, T) - A(\omega_{RF}, T - \tau_d)] \tag{4.12}$$

4.4.2 Simulation results

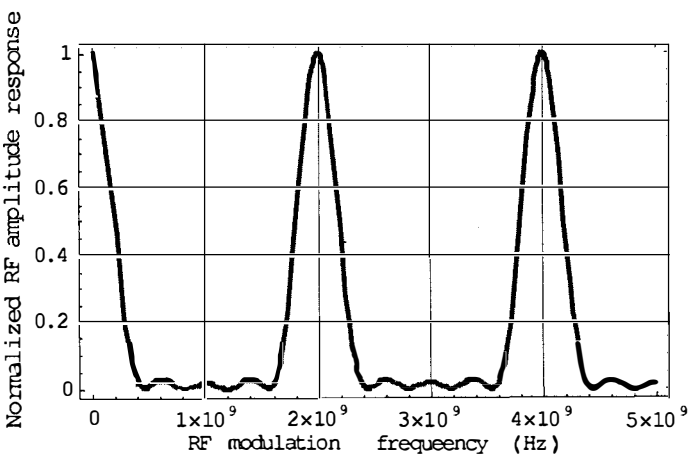

Figure 4.4: Normalized RF frequency response of a 4-tap RF filter.

Based on above discussions, Mathematica Software Package is used to simulate the PIIN of the conventional 4-tap RF filter. Assuming that the optical delay line in each of the optical path is 100 mm,200 mm.300 mm and 400 mm, the optical splitter splits the incoming signals evenly among its output ports therefore, $k_{1,2,3,4} = 0.5$, and wavelength of the laser is 1.5μm. Figure 4.4 shows the normalized frequency response of the 4-tap RF filter, which can be used as a band pass filter.

Figure 4.5 shows PIIN spectra of a 4-tap conventional photonic RF bandpass filter, under laser illuminations with various coherence lengths. The simulation is done under

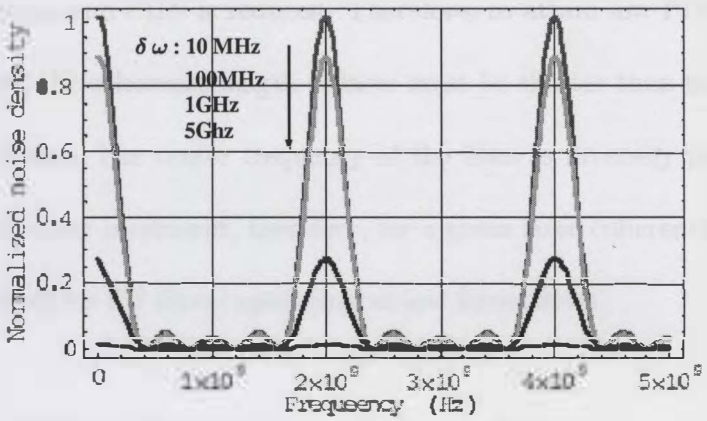

Figure 4.5: Normalized phase-induced intensity noise versus the laser coherence length.

conditions that the length of fiber delay line increases in 100mm step. The coherence length of laser is varied from 10m to 40mm. It is shown that at the peaks of RF response, the PIIN is quite significant. This degrades the performance of the bandpass filters seriously. It is also shown that when the coherence length varies from 10m to 40mm, the noise is reduced significantly over the whole RF band.

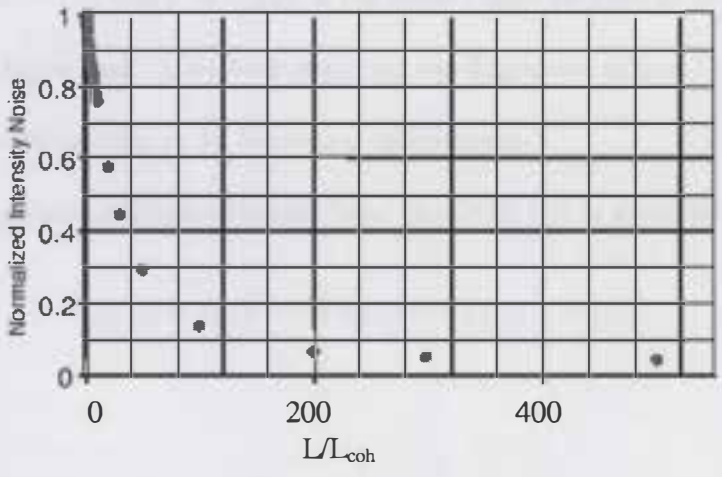

Figure 4.6: Normalized maximum phase-induced intensity noise versus different coherence length for a 4-tap transversal filter.

Figure 4.6 shows the normalized maximum PIIN versus the length of the fiber unit delay line under laser illumination with $l_{coh} = 10m$. Increasing the length of the fiber

unit delay, the maximum PIIN is reduced. Therefore, to attain low PIIN , hence a stable RF filter response, the coherence length of laser must be shorter than the delay increment in the filter structure. The center frequency of the filter is inversely proportional to the length of the unit delay increment, therefore, for a given laser coherence length, the PIIN can only be reduced for RF filters operating at low frequencies.

4.5 Fiber Fabry-Perot cavity notch filter

4.5.1 Analysis

For a fiber Fabry-Perot(FP) cavity of length L and reflectivity r, the output electric field that results from the input field expressed by Equation 4.3, is given by:

$$E_{tr}(t) = (1-r^2)\sum_{i=1}^{\infty} r^{2n}\varepsilon(t_n)\left[e^{j\omega_0 t_n} + \frac{M}{2}e^{j(\omega_0+\omega_{RF})t_n} + \frac{M}{2}e^{j(\omega_0-\omega_{RF})t_n}\right] \tag{4.13}$$

where $t_n = t-(2n-1)T$ and $T = n_g L/c$ is the transit time for light to traverse the cavity.

Note that in Equation4.13, we have neglected the dispersion caused by the FP medium and assumed the reflectivity to be frequency independent.

The RF component which is obtained from $\langle E_{tr}(t)E_{tr}^{\star}(t)\rangle$ is given by:

$$I_{RF}(t) = M(1-r^2)^2 Re\left[e^{j\omega_1 t}(T_1(t)+T_2(t))\right] \tag{4.14}$$

where

$$T_{1,2} = \frac{e^{-j\omega_{RF}T}}{1-r^4 e^{-j2\omega_{RF}T}}\left\{\Gamma(0) + \sum_{l=1}^{\infty} r^{2l}\left[\Gamma(\pm 2lT)e^{\pm j2l\omega_0 T} + \Gamma(\mp 2lT)e^{\mp jl(\omega_0\pm\omega_1)T}\right]\right\} \tag{4.15}$$

Physically, l_{th} term in the series is due to the interference of waves of frequency ω_0 having completed a round trip travel n times in the cavity with those of frequency $\omega_0 \pm \omega_{RF}$ having journeyed the cavity $n \pm l$ times.

For a low coherence length laser, $\Gamma(\tau) = 0$ for $\tau \neq 0$. The RF frequency response can be deduced directly from Equation 4.14 and 4.15:

$$A_{RF} = 2M(1-r^2)^2[1+r^8-2r^4\cos 2\omega_1 T]^{-1/2} \tag{4.16}$$

This response is due to the interference of RF modulation signals only. This is obvious because the optical interference is not observable in the time of $\delta\omega \to \infty$. The peaks of A_{RF} occur at $f_p = mc/(2n_gL)$, where m is an integer. For $r > 3^{-1/4}$, the full width between points of half maximum is:

$$\delta f_p = \frac{c}{\pi n_g L}\sin^{-1}\frac{\sqrt{3}(1-r^4)}{2r^2} \tag{4.17}$$

and it is independent of optical frequency ω_0.

For a laser source with the Lorentzian spectral shape, after some algebra, the filter's frequency response can be obtained from Equation 4.15 and is given by:

$$A(\omega_{RF}) = \frac{M(1-r^2)^2}{(1+r^8-2r^4\cos 2\omega_{RF}T)^{1/2}}\left|2+\frac{r^2e^{-2(\Delta\omega-j\omega_0)T}}{1-r^2e^{-2(\Delta\omega-j\omega_0)T}}+\frac{r^2e^{-2(\Delta\omega+j\omega_0)T}}{1-r^2e^{-2(\Delta\omega+j\omega_0)T}}\right.$$
$$\left.\frac{r^2e^{-2(\Delta\omega+j(\omega_0+\omega_{RF}))T}}{1-r^2e^{-2(\Delta\omega+j(\omega_0+\omega_{RF}))T}}+\frac{r^2e^{-2(\Delta\omega-j(\omega_0-\omega_{RF}))T}}{1-r^2e^{-2(\Delta\omega-j(\omega_0-\omega_{RF}))T}}\right| \tag{4.18}$$

4.5.2 Simulation results

Figure 4.7 shows the relationship of $A(\omega_{RF})$ with the parameters: r, $\omega_0 T$ and $\Delta\omega T$. The simulations were carried out under the conditions that the wavelength of the laser is 1.5 μm and the reflectivity of the mirrors is 0.8. To illustrate the coherence effects, all curves are normalized with respect to the peak response of the filter. Generally, when the coherence length is comparable to or shorter than the length of cavity, the filter's response is determined mainly by the interference of RF modulation signals (as shown in Figure 4.7

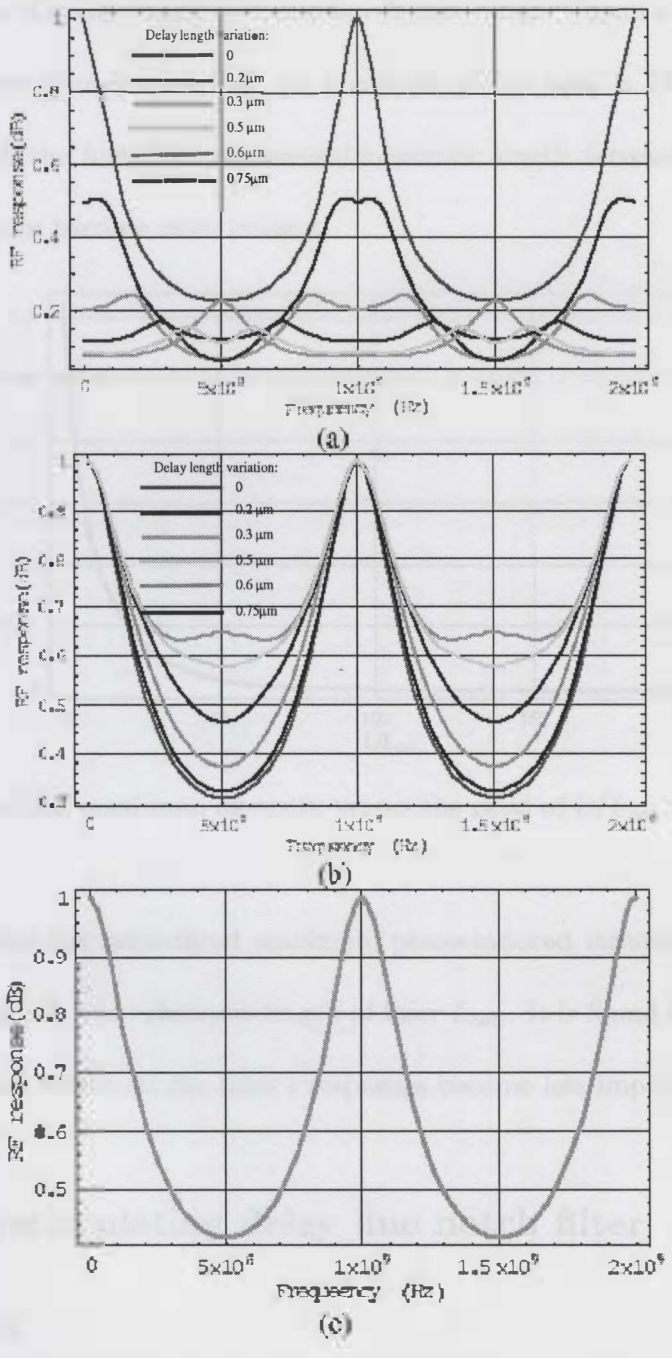

Figure 4.7: The effects of laser linewidth on RF response with the 100 mm cavity length. (a) 20 MHz.(b) 200 MHz.(c) 2 GHz

(c)) and they are insensitive to environment disturbances. If the coherence length increases to nearly 20 times of the cavity length, the noises in the response become apparent even when the variation of cavity length is in one wavelength range. Figure 4.7(a) and (b) shows the responses under illumination that the linewidth of the laser is 20MHz and 200MHz respectively. With the linewidth decreasing(coherence length increasing), the effects of the optical coherence become more evident.

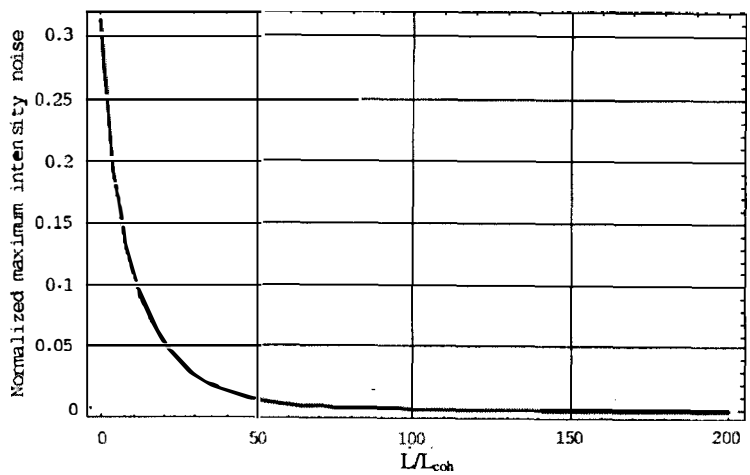

Figure 4.8: Normalized maximum intensity versus the ratio of L/L_{coh} for fiber F-P notch filter

Figure 4.8 shows the normalized maximum phase-induced intensity noise versus the rati0 of cavity length L and coherence length of laser L_{coh}. It is found that when $L_{coh} << 100L$, the coherence effects on the filter's responses become less important.

4.6 Fiber recirculating delay line notch filter

4.6.1 Analysis

The configuration of a fiber RDL processor is shown in Figure 4.9. Its core component is a 2×2 fiber directional coupler and the relevant parameters of the coupler are shown in Figure 4.10.

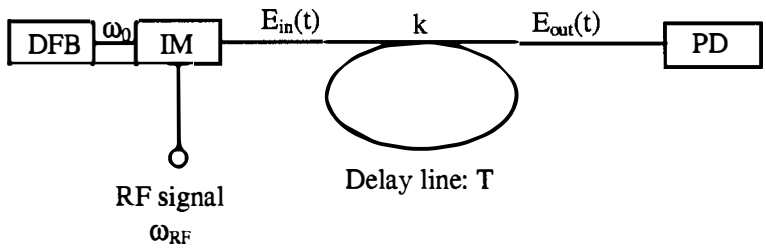

IM: Intensity modulator
PD: Photodetector
k: Coupling ratio

Figure 4.9: Fiber recirculating delay line notch filter

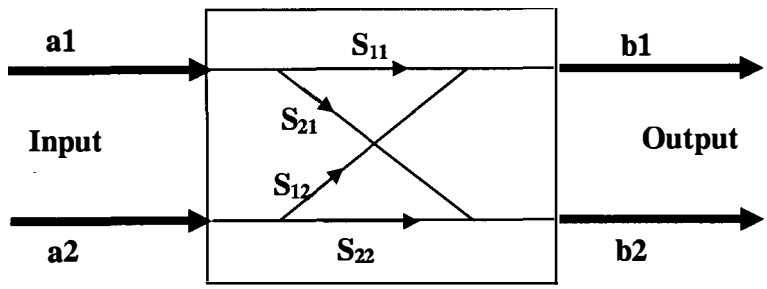

Figure 4.10: 2×2 coupler with relevant parameters of the Jones matrix

The input and output fields meet the following 2×2 unitary matrix which is known as Jones matrix.

$$\begin{bmatrix} b_1 \\ b_2 \end{bmatrix} = \begin{bmatrix} S_{11} & S_{12} \\ -S_{12}^{\star} & S_{11}^{\star} \end{bmatrix} \begin{bmatrix} a_1 \\ a_2 \end{bmatrix} \tag{4.19}$$

where S_{11}, S_{12} are complex variables and $S_{11}^2 + S_{12}^2 = 1$. To count excess loss from the coupler, the above equation can be rewritten as $S_{11}^2 + S_{12}^2 = 1 - \gamma$, where γ represents the excess power loss of the coupler. Therefore, S_{11} and S_{12} are:

$$S_{11} = \sqrt{(1-\gamma)(1-k^2)} \tag{4.20}$$

$$S_{12} = jk\sqrt{1-\gamma} \tag{4.21}$$

Let L be the length of the fiber delay line, with the input field given by 4.3, the output field at the photodetector is:

$$E_{out}(t) = \frac{|S_{11}|^2}{|S_{12}|} \sum_{n=0}^{\infty} C_n \varepsilon(t_n') \cdot [e^{j\omega_0 t_n'} + \frac{M}{2} e^{j(\omega_0+\omega_{RF})t_n'} + \frac{M}{2} e^{j(\omega_0-\omega_{RF})t_n'}] \tag{4.22}$$

where the length of the coupler is ignored since it is relatively short comparing to L. In Equation 4.22, $C_0 = -|S_{12}/S_{11}|^2$, $C_n = {S_{12}}^n$ for $n \geq 1$, ${t_n}' = t - nT$, and $T = n_g L/c$ is the transmission time for the light in delay line. n_g is the refractive index of the fiber. c is light speed in vacuum.

By calculating the autocorrelation of optical field, the RF component of the output will be:

$$I_{RF}(t) = M\frac{|S_{11}|^4}{|S_{12}|^2} Re[e^{-j\omega_{RF}t}(R_1 + R_2)] \tag{4.23}$$

where

$$\begin{aligned} R_1 = \Gamma(0) &\left[\left|\frac{S_{12}}{S_{11}}\right|^4 + \frac{|S_{12}|^2 e^{-j\omega_{RF}T}}{1-|S_{12}|^2 e^{-j\omega_{RF}T}}\right] + \left[-\left|\frac{S_{12}}{S_{11}}\right|^4 + \frac{|S_{12}|^2 e^{-j\omega_{RF}T}}{1-|S_{12}|^2 e^{-j\omega_{RF}T}}\right] \\ &\cdot \sum_{l=1}^{\infty}\left[(S_{12}^*)\Gamma(lT)e^{-jl\omega_0 T} + (S_{12}^l)\Gamma(-lT)e^{-jl(\omega_0+\omega_{RF})T}\right] \end{aligned} \tag{4.24}$$

$$\begin{aligned} R_2 = \Gamma(0) &\left[\left|\frac{S_{12}}{S_{11}}\right|^4 + \frac{|S_{12}|^2 e^{-j\omega_{RF}T}}{1-|S_{12}|^2 e^{-j\omega_{RF}T}}\right] + \left[-\left|\frac{S_{12}}{S_{11}}\right|^4 + \frac{|S_{12}|^2 e^{-j\omega_{RF}T}}{1-|S_{12}|^2 e^{-j\omega_{RF}T}}\right] \\ &\cdot \sum_{l=1}^{\infty}\left[(S_{12}^*)\Gamma(lT)e^{-jl(\omega_0-\omega_{RF})T} + (S_{12}^l)\Gamma(-lT)e^{-jl\omega_0 T}\right] \end{aligned} \tag{4.25}$$

For the laser with Lorentzian spectral shape, the filter's frequency response can be expressed as:

$$\begin{aligned} A(\omega_{RF}) = M(1-\gamma)^2(1-k^2)^2 \Bigg| & 2\left(\frac{k^2}{1-k^2} + \frac{e^{-j\omega_{RF}T}}{1-(1-\gamma)k^2 e^{-j\omega_{RF}T}}\right) \\ & + \sqrt{(1-\gamma)}\left(-\frac{1}{(1-\gamma)(1-k^2)} + \frac{e^{-j\omega_{RF}T}}{1-(1-\gamma)k^2 e^{-j\omega_{RF}T}}\right) \\ & \Bigg[\frac{-jke^{-(\Delta\omega-j\omega_0)T}}{1+j\sqrt{(1-\gamma)}ke^{-(\Delta\omega-j\omega_0)T}} + \frac{jke^{-(\Delta\omega+j\omega_0)T}}{1-j\sqrt{(1-\gamma)}ke^{-(\Delta\omega+j\omega_0)T}} \\ & + \frac{jke^{-(\Delta\omega+j(\omega_0+\omega_{RF}))T}}{1-j\sqrt{(1-\gamma)}ke^{-(\Delta\omega+j(\omega_0+\omega_{RF}))T}} + \frac{-jke^{-(\Delta\omega+j(\omega_0-\omega_{RF}))T}}{1+j\sqrt{(1-\gamma)}ke^{-(\Delta\omega+j(\omega_0-\omega_{RF}))T}}\Bigg]\Bigg| \end{aligned} \tag{4.26}$$

The first term in Equation 4.26 is due to the interference of modulation signals alone. The effects of the optical interference are represented by the second term of $\omega_0 T$ and $\Delta\omega T$.

4.6.2 Simulation results

When the coherence length of optical carrier is short, the filter's frequency response can be simplified as:

$$A(\omega_{RF}) = 2M[(1-\gamma)^2((1-\gamma+k^2(-1+2\gamma))^2 - \frac{4k^2(2k^2-1)(\gamma-1)\sin^2(\omega_{RF}T/2)}{1+k^4(-1+\gamma)^2\cos(\omega_{RF}T)}] \tag{4.27}$$

The fact that $A(\omega_RF)$ is independent of $\omega_0 T$ is a clear indication that it is the result of interference of RF modulation signals only. $A(\omega_RF)$ has notches at $N \cdot L = (m+\frac{1}{2})\lambda_1$ with a minimum value of:

$$A(\omega_{RF})_{min} = 2M|\frac{|S_{11}|^4 - |S_{12}|^4 - |S_{12}|^2}{1+|S_{12}|^2}| \tag{4.28}$$

If $|S_{11}|^4 = |S_{12}|^4 + |S_{12}|^2$, $A(\omega_{RF})_{min}$ vanishes; for example, the notches become nulls. By choosing proper S_{11} and S_{12} given in Equation 4.21, the condition of generating the maximum notch is: $k^2 = \frac{1-\gamma}{3-2\gamma}$. In other words, sharp notches occur if the loss in the recirculating delay line is small and $k^2 = \frac{1}{3}$.

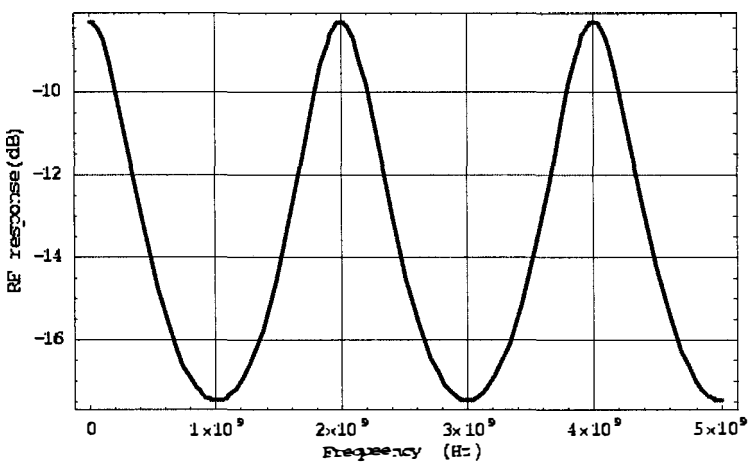

Figure 4.11: The RF response of fiber RDL notch filter under incoherent illumination

Figure 4.11 depicts the RF frequency response under incoherent operation. The filter can work robustly and it is insensitive to the frequency or phase of optical carrier.

For an optical source with small linewidth, the optical interference effects represented in the terms of $\omega_0 T$ and $\Delta\omega_0 T$ can not be omitted from Equation 4.26. This causes the RF response sensitive to the environmental disturbances.

Figure 4.12 shows the RF response of the fiber RDL notch filter under conditions: $L = 100mm$, $k = 0.5732$, and $\gamma = 0.05$ with different laser linewidth that corresponds 20 MHz, 200 MHz and 2 GHz respectively. In each figure, random loop length disturbances are introduced to simulate the environmental disturbance which can always be translated to the loop length variation. The disturbance is not longer than one wavelength. It is shown that the optical coherence effect is not noticeable when $l_{coh} \sim NL$. As l_{coh} increases, the effect of optical interference becomes increasingly apparent. The amplitudes of filter's response at the notches are very sensitive to the changes in L when $l_{coh} < 100L$ while the peaks don't change very much.

Figure 4.13 presents the results under the conditions that $\Delta\omega_0 = 20MHz$, $k = 0.5732$, and $\gamma = 0.05$ with different delay L. Figure 4.13(a),(b) and (c) shows the RF responses of delay line with 10 m, 1 m and 100 mm respectively. The stable RF frequency response can only be obtained when the delay line is 100 times shorter than the laser coherence length. This also limits the fiber RDL notch filter's working frequency to very low value.

Figure 4.14 shows normalized maximum phase-induced intensity noise versus the ratio of cavity length L and the laser coherence length L_{coh}. It is found that when $L_{coh} << 100L$, the coherence effects becomes less important.

4.7 Conclusions

Optical coherence effects on photonic RF signal processor have been studied. The common expression of RF response of photonic RF filter under coherent operation is obtained. The

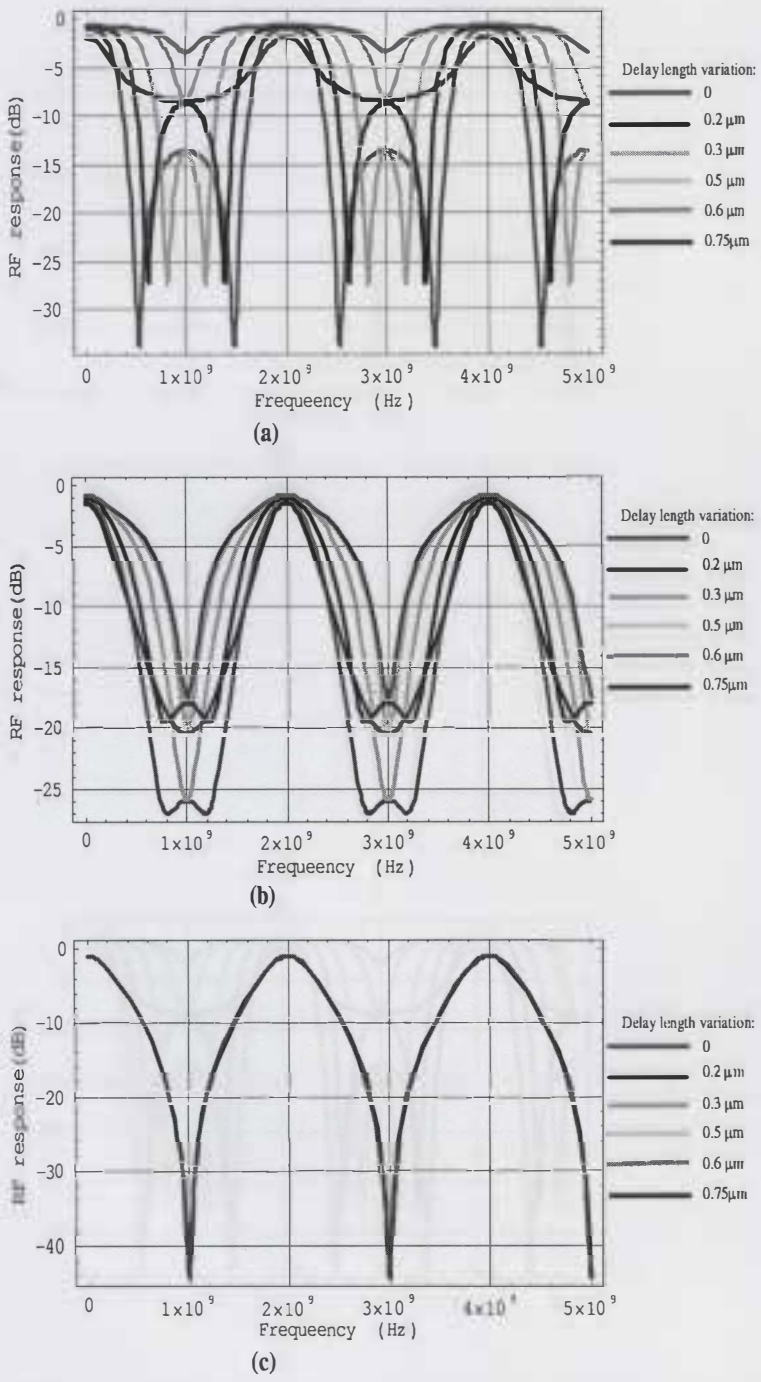

Figure 4.12: The effects of coherence length on RF response with the 0.1 m delay length.(a) 20 MHz. (b) 200 MHz. (c) 2 GHz

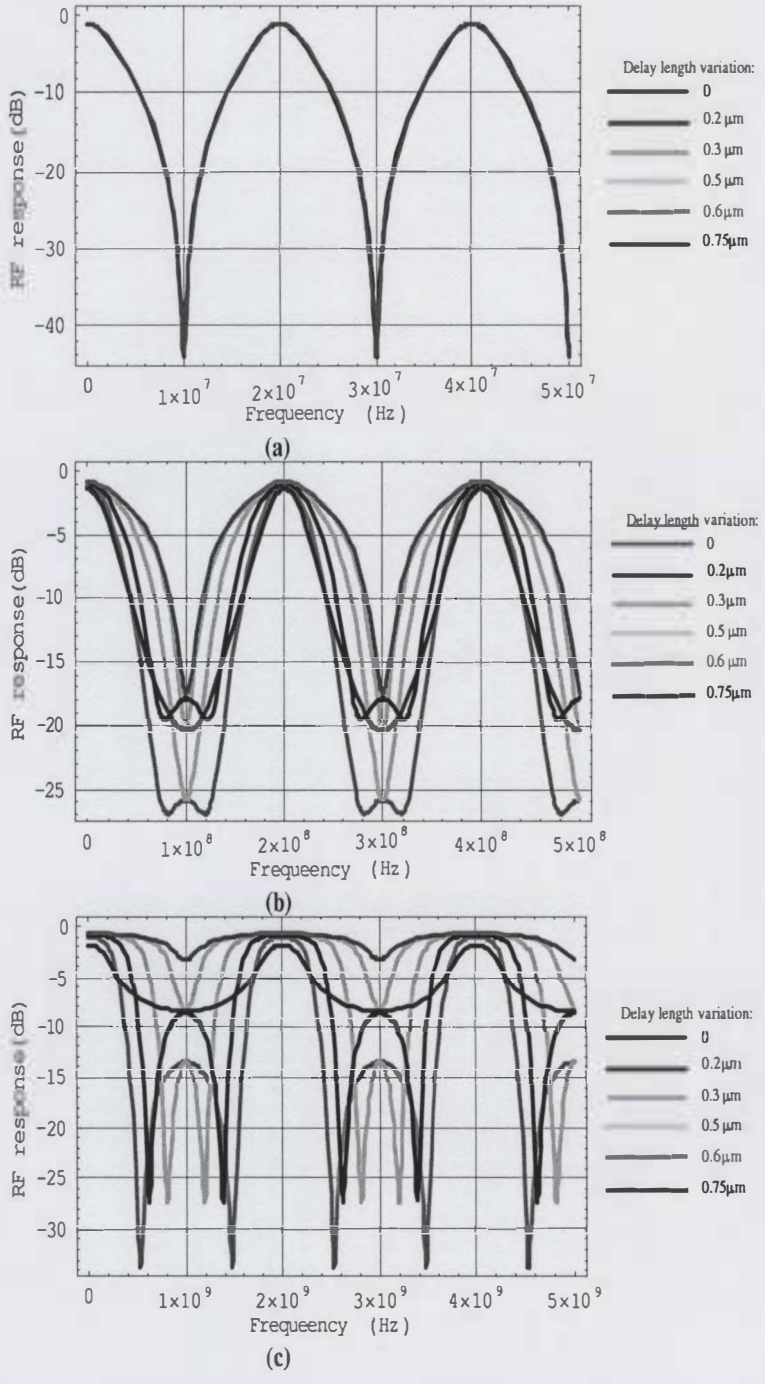

Figure 4.13: The effects of coherence length to RF response. The linewidth of the laser is 20 MHz. (a) 10 m. (b) 1 m. (c) 0.1 m

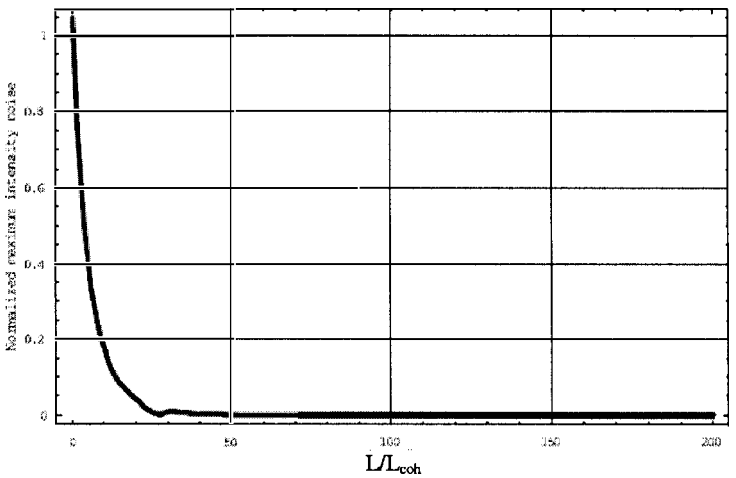

Figure 4.14: Normalized maximum intensity versus the ratio of L/L_{coh} for RDL notch filter

combination effects of optical interference and the interference of RF signals are examined for three types of photonic RF filter namely, optical fiber FIR filter(4-tap transversal RF filter) and two types of fiber IIR filters, fiber Fabry-Perot cavity RF filter and fiber RDL RF notch filter.

Laser coherence can significantly affect the performance of photonic RF signal processors. The frequency responses of all in-fiber RF processors examined are sensitive to laser coherency. To attain a stable RF response, it is necessary that the coherence length of laser source be at least 100 times shorter than the minimum unit delay line of the processor. This limits the operation of photonic RF filters employing high coherent laser source to low RF frequency.

In the following Chapter, we propose an new approach based on phase modulating laser source to suppress the PIIN in photonic RF signal processors.

Chapter 5

Optical coherence control for noise suppression in photonic signal processors

In Chapter 4, we analyzed laser coherence effects on the performance of photonic RF signal processor. The phase-induced intensity noise can be ignored when the coherence length of laser source is 100 times shorter than the unit delay line of the system. However, this condition limits the maximum sampling frequency of in-fiber RF filters.

In this Chapter, we present a novel noise suppression method based on controlling the laser coherence property by an external phase modulator. By imposing pseudo-random binary sequence(PRBS) to the optical modulator, the laser linewidth can be broadened, leading to a shorter coherence length. Experimental results are also demonstrated, which verify the proposed approach.

This Chapter is organized as following: Section 5.1 is an overview on coherence control of laser. In Section 5.2, we describe measurement method for laser coherency. Section 5.3

proposes the new technique to tune the laser coherence property. Section 5.4 introduces the RF frequency response measurement followed by Section 5.5 reports the experimental results in terms of laser linewidth and PIIN suppression in the fiber RDL notch filter.

5.1 Laser coherence control technology

To suppress the phase-induced intensity noise in fiber link systems, several methods have been proposed [97–99]. In the early work reported in Blauvelt [100] where the laser is directly modulated by a high frequency signal, therefore its coherency can be reduced, leading to the reduction of phase-induced intensity noise in the optical fiber link. However, the laser can only become totally incoherent by directly modulation under a very deep modulation(where the laser output is pulse-like and each pulse is incoherent with the previous).

Another method was proposed by Pepeljugoski [97] and its setup is shown in Figure 5.1 where an external modulator was driven by a single RF tone at a frequency which is higher than the data bandwidth. The results showed that the noises in the fiber link at data frequencies were reduced.

All previous proposals were based on suppression the PIIN in fiber-link systems instead of photonic RF signal processing system.

For coherence control in photonic RF signal processing system, one on-site coherence-to-incoherence [2] control method has been proposed as discussed in Chapter 2.

In this Chapter, we propose a new method by applying an external phase modulator to the DFB laser source. The phase modulator is driven by PRBS sequence and therefore, the laser linewidth is broadened, hence the PIIN in photonic RF processor is suppressed. The advantage of our method is that we can tailor laser source coherency to the requirements

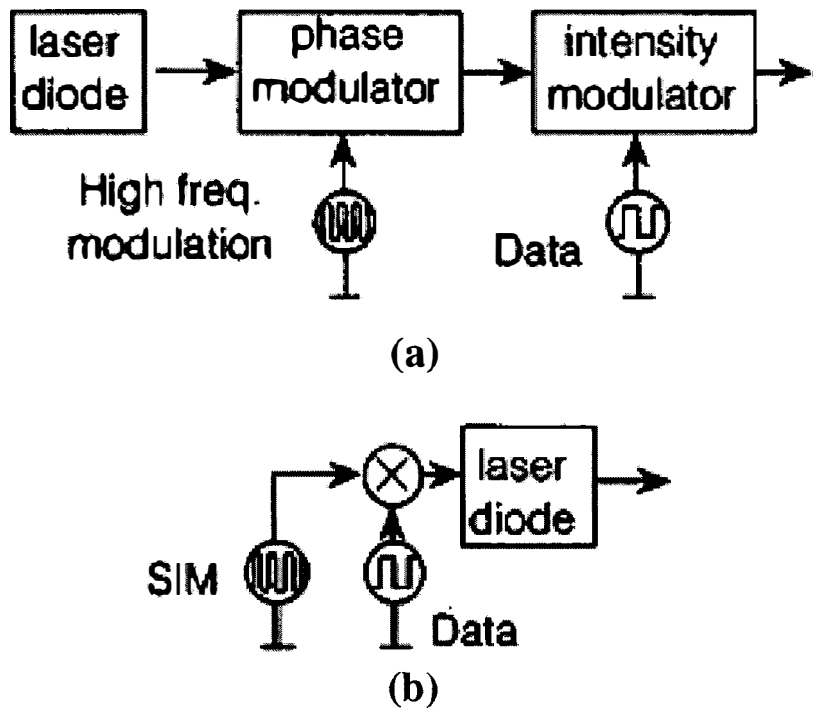

Figure 5.1: (a)External modulation. (b) Direct modulation

of photonic RF processor.

5.2 Laser linewidth measurement

To study laser coherence effects on photonic RF signal processors precisely, it is necessary to measure the linewidth of laser.

For high coherence laser, its finite spectral width is predominantly defined by the phase of optical field instead of its amplitude fluctuation. The typical linewidth of a DFB laser is 10 MHz. To measure this linewidth, a typical grating-based optical spectrum analyzer(OSA) would not meet the resolution requirement. Other scanning filter methods like scanning F-P filters and interference filters are not able to achieve the high resolution either.

To solve the issue of measuring laser linewidth, delayed self-heterodyning fiber interferometer technique shown in Figure 5.2, was previously proposed [101, 102], based on mixing (heterodyning) the laser field with a delayed version.

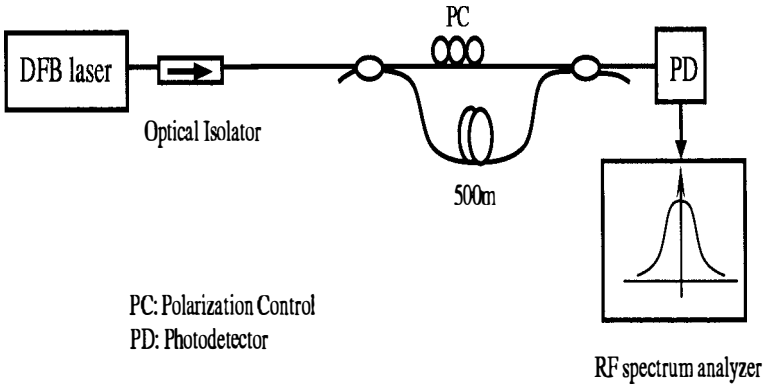

Figure 5.2: Configuration of delayed self-heterodyning technology

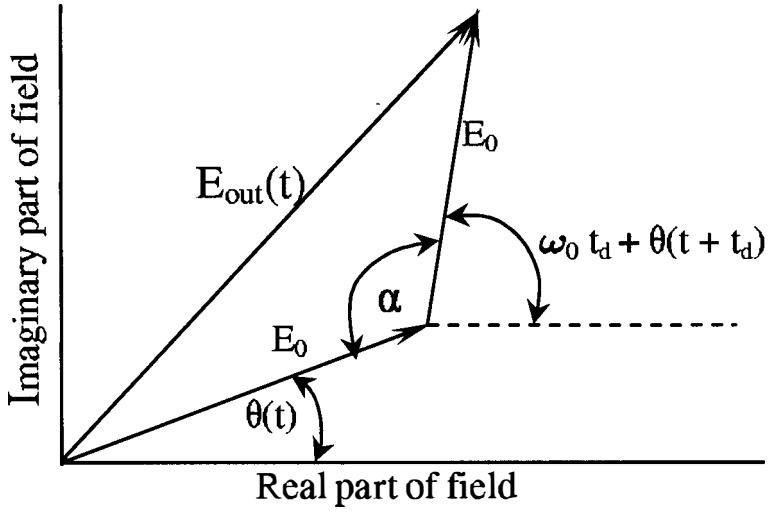

Figure 5.3: Construction showing that the total optical field at the detector.

Since the main fluctuation of a laser field is that of its phase rather than amplitude, we can approximate the laser field at the photodetector by the phasor(complex) representation, as illustrated in Figure 5.3, where,

$$E_{total} = \frac{1}{4}E_0 e^{j\theta(t)} + \frac{1}{4}E_0 e^{j[\omega_0 t_d + \theta(t+t_d)]} \tag{5.1}$$

For delays t_d that are considerably shorter than the coherence time τ_c of laser field,

the magnitude of the total field phasor is a constant as shown in Figure 5.3. Although the phase $\theta(t)$ varies randomly, the angle α that determines the magnitude of optical field E_{total} depends only on the phasor difference. At the limit of $t_d \ll \tau_c$, it does not change with time. The output current from the detector is constant, and nothing can be learned from it about the laser field spectrum. It is clear that in order to measure the laser spectrum, time delay t_d should meet the requirement: $t_d \gg \tau_c$.

The field spectrum measured can be generally given by:

$$S_d(f) = \frac{\Delta f}{\pi(f^2 + (\Delta f)^2)} \times [1 - e^{-2\pi\Delta f\tau_d}\cos(2\pi f\tau_d) - \frac{f}{2\Delta f}\sin(2\pi f\tau_d) - \frac{1}{2\pi^2 f}e^{-2\pi\Delta f\tau_d}\sin(2\pi f\tau_d) + 2\pi e^{-2\pi\Delta f\tau_d}\Delta f] \quad (5.2)$$

where Δf is $3dB$ linewidth and τ_d is the delay time. Assuming that the laser phase noise is only white noise and the propagation time of the light along the delay fiber is much longer than the coherent time, the measured field spectrum becomes Lorentzian function and can be expressed as:

$$S_d(f) = \frac{\Delta f}{\pi(f^2 + \Delta f^2)} \quad (5.3)$$

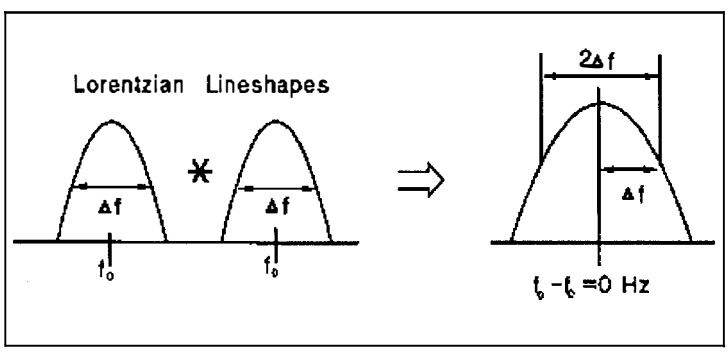

Figure 5.4: Autocorrelation process of measurement.

The autocorrelation process can be illustrated in Figure 5.4. It is shown that the 3 dB linewidth of optical spectrum is twice that of the laser linewidth Δf.

5.3 Laser coherence control

To provide a robust photonic RF filter, a new technique for optical source coherence control for noise suppression in photonic signal processors is designed and tested. The new coherence control method for RF signal processing is based on an external phase modulator which is driven by a PRBS signal. The drive signals can be modified to tailor the linewidth of laser source to the optimum value according to the requirements of photonic RF signal processor.

Phase Modulator The phase modulator shown in Figure 5.5 has a single optical

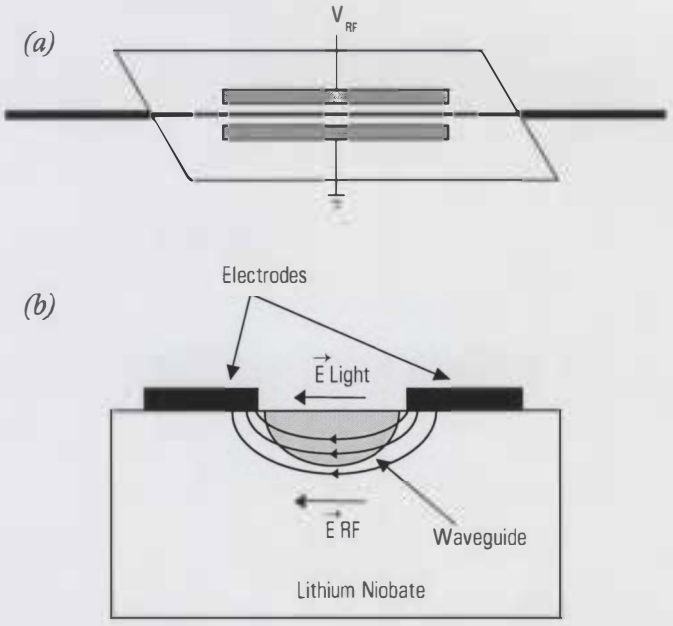

Figure 5.5: Electro-optic phase modulator. (a) Top view, (b) Side view

input of polarization maintaining (PM) fiber and a single optical output of PM or single-mode (SM) fiber. In a simple phase modulator, two electrodes surround the waveguide. The bottom electrode is grounded while the top electrode is driven by an outside voltage signal. As the voltage on the top electrode changes, the refractive index of the waveguide changes accordingly, alternating the light as the refractive index rises and falls. While this

modulates the phase of the light, the output intensity remains unchanged.

In the presence of an electric field, light traveling through the device experiences a change in propagation delay, $\Delta t = (\Delta nL)/c$, which is equivalent to a change in the phase of the light at the output and it is given by $\Delta\phi = \omega\Delta t = (\Delta n\omega L)/c$ where Δn is the absolute change in the refractive index due to the applied electric field, ω is the optical frequency, L is the interaction length, and c is the speed of light in the vacuum.

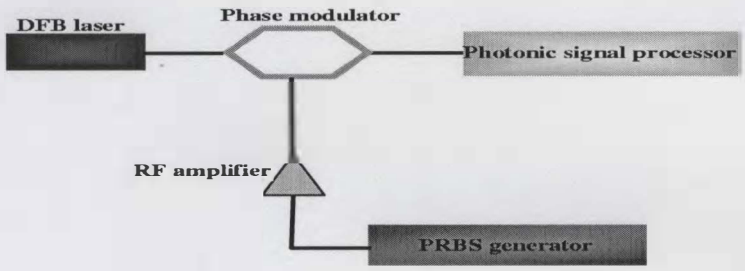

Figure 5.6: Coherence Controller

To control the laser coherency, the configuration of Figure 5.6 is applied, where an external phase modulator is used after the laser. By driving the phase modulator with pseudo-random binary sequence(PRBS) signal, the phase distribution of laser source can be modulated. Since PRBS signals include a series signals at different frequencies, therefore, the phase modulator imparts a controlled sinusoidal optical path length change (or retardation) within the modulator, thus varying the phase of output wave. This reduces the laser coherence length .

By reducing the coherence length of laser source in a controlled manner, a significant broadening of laser spectrum is obtained. Therefore, those interference effects which are introduced by the laser coherence in the photonic RF signal processor can essentially be canceled out.

Assuming that the laser linewidth shape is Lorentzian and the photon density doesn't fluctuate much in short time. Therefore the optical field on the photodetector can be approximated as:

$$E(t) = E_0 \cos(\omega_0 t + m\Psi(t))e^{|t|/\tau_c} \tag{5.4}$$

Where m is the modulation depth of PRBS signal. $\Psi(t)$ can be a single frequency signal ω_m, or complex frequency signals.

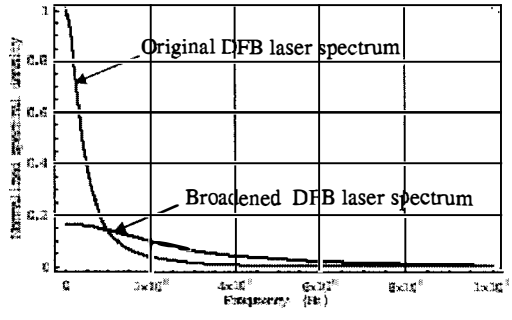

Figure 5.7: The linewidth of a DFB laser with Lorentzian spectral shape

Figure 5.7 shows the spectrum of a DFB laser with a Lorentzian spectral shape.

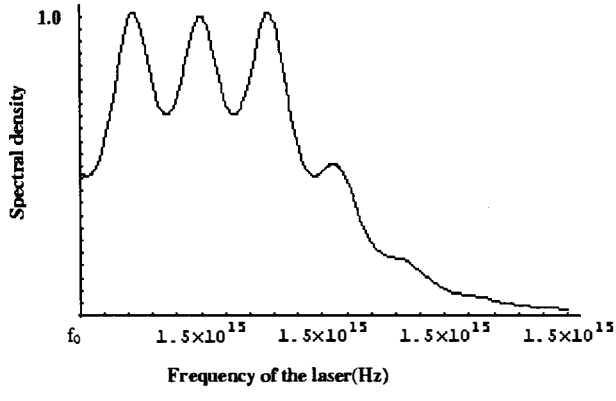

Figure 5.8: The spectral density of DFB laser with two modulation signals.

Figure 5.8 shows the linewidth of a modulated laser where two modulation signals $50MHz$ and $556MHz$ are used with modulation depth of 1 and 1.5 respectively. It can be seen that the laser linewidth is enhanced. However, chirps in the laser spectrum can mix with the RF signals, causing distortion in the information band. In order to suppress

these peak frequencies, wide band RF modulation signals can be more effective.

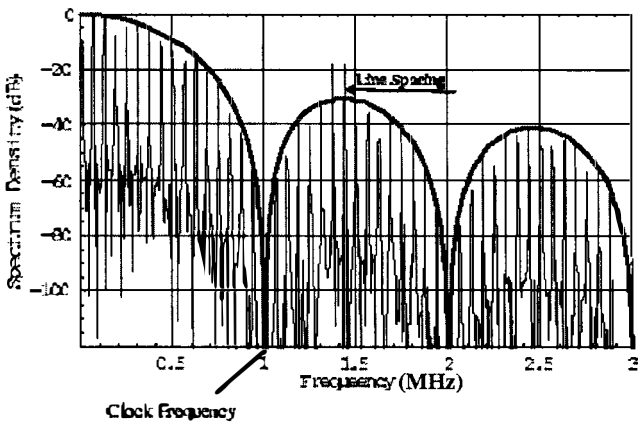

Figure 5.9: The spectrum density of the PRBS sequence

To generate wide band signals, a randomly generated bit sequence at high frequency can be used. A truly random signal generator might be inefficient since the bandwidth of signal cannot be controlled in a straightforward manner. The best solution is to use pseudo random bit sequence (PRBS) generator which has a very long periodicity (very dense discrete spectral components). In addition, the use of PRBS signals has the advantage that they can be reproduced in the experiments. Figure 5.9 shows spectrum of the PRBS. The signals in the frequency domain have $\frac{\sin x}{x}$ envelope. The first zero occurs at the clock frequency. The spacing of the individual spectral lines is the inverse of the period of the PRBS sequence. Figure 5.9 shows the spectrum of a $2^7 - 1$ length of the PRBS signal with a clock frequency at 100 MHz.

By applying the PRBS signal to the phase modulator, the laser linewidth is broadened as shown in Figure 5.7. Theoretical analysis about PRBS generator can be tracked in reference [103].

5.4 RF frequency response measurement

In order to measure the coherence effects on the RF frequency response of photonic RF signal processor, a microwave network analyzer is used, which, displays the transfer characteristics of the photonic RF filter in both frequency and time domains.

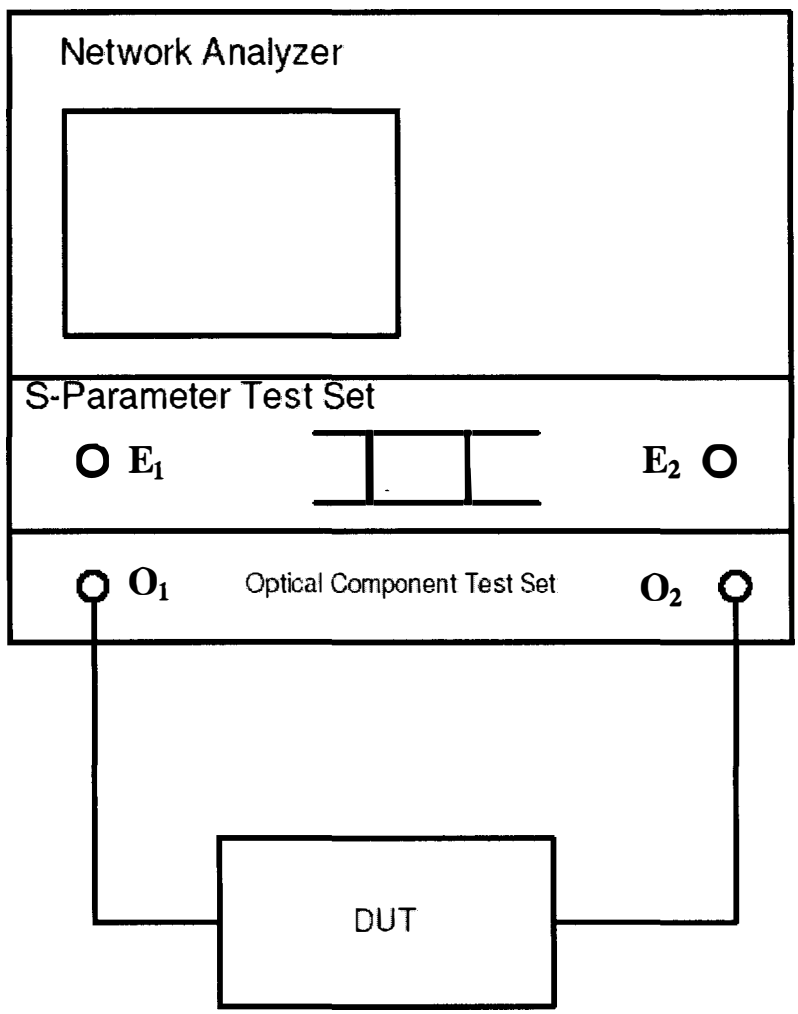

Figure 5.10: Transmission measurement configuration

A microwave(MW) vector network analyzer(VNA) was used, in conjunction with a high speed optical test set, including an electro-optic(E/O) and opto-electric(O/E) converters as shown in Figure 5.10, where different optical devices can be inserted between the optical ports of O_1 and O_2 and then tested. The optical devices can be delay line

structures, waveguides, fibers, interferometers, couplers, Y-junctions,filters, attenuators, optical amplifiers and mirrors.

The transfer function measured between the electrical ports E_1 and E_2 of VNA is the product of three parts, and given by:

$$H_{total}(\omega_{RF}) = H_{E/O}(\omega_{RF})H_{ODUT}(\omega_{RF})H_{O/E}(\omega_{RF}) \tag{5.5}$$

where $H_{total}(\omega_{RF})$ is the transfer function of the total system, $H_{E/O}(\omega_{RF})$ is the transfer function of E/O components, $H_{ODUT}(\omega_{RF})$ is the transfer function of optical device under detection and $H_{O/E}(\omega_{RF})$ is the transfer function of O/E components respectively. Since we are only interested in the RF frequency response of photonic device inserted between the optical ports O_1 and O_2, the effects of $H_{E/O}(\omega_{RF})$ and $H_{O/E}(\omega_{RF})$ can be removed through the following network analyzer's calibration :

$$H_{ODUT}(\omega_{RF}) = \frac{H_{total}(\omega_{RF})}{H_{E/O}(\omega_{RF})H_{O/E}(\omega_{RF})} \tag{5.6}$$

Similar to the definition of electrical scattering parameters, the optoelectronic S-parameters can be defined as:

$$S^0_{m,n} = \frac{b^0_m}{a^0_n} e^{j(\phi_{tm}-\phi_{in})} \tag{5.7}$$

Where:

$$a^0_i = I_{in} M cos(\omega_{RF} t + \phi_{in}) \tag{5.8}$$

$$b^0_t = I_{tm} M cos(\omega_{RF} t + \phi_{tn}) \tag{5.9}$$

where I_{in} and I_{tm} means the incident and transmitted average optical intensities respectively. ω_{RF} is the angular frequency of RF modulation while phase angles of incident and transmitted waves are distinguished by ϕ_{in} and ϕ_{tm}. Finally a very important fact must be recognized, since microwave VNAs display measured results in electrical S-parameter.

Due to electrical current-to-optical power and optical power-electrical current transformations in measurement system, the relation between investigated optoelectronic and the measured electrical S-parameters written as :

$$|S^{e}_{m,n}|e^{j(\phi^{e}_{im}-\phi^{e}_{in})} = |S^{0}_{m,n}|^{2}e^{j(\phi^{o}_{im}-\phi^{o}_{in})} \tag{5.10}$$

In our experiment, HP 83420A Lightwave Test Set, HP8515A S-parameter Test Set, HP 8340A Synthesised Sweeper, HP 8510B Network Analyzer were used and connected as shown in Figure 5.10.

5.5 Experiments and results

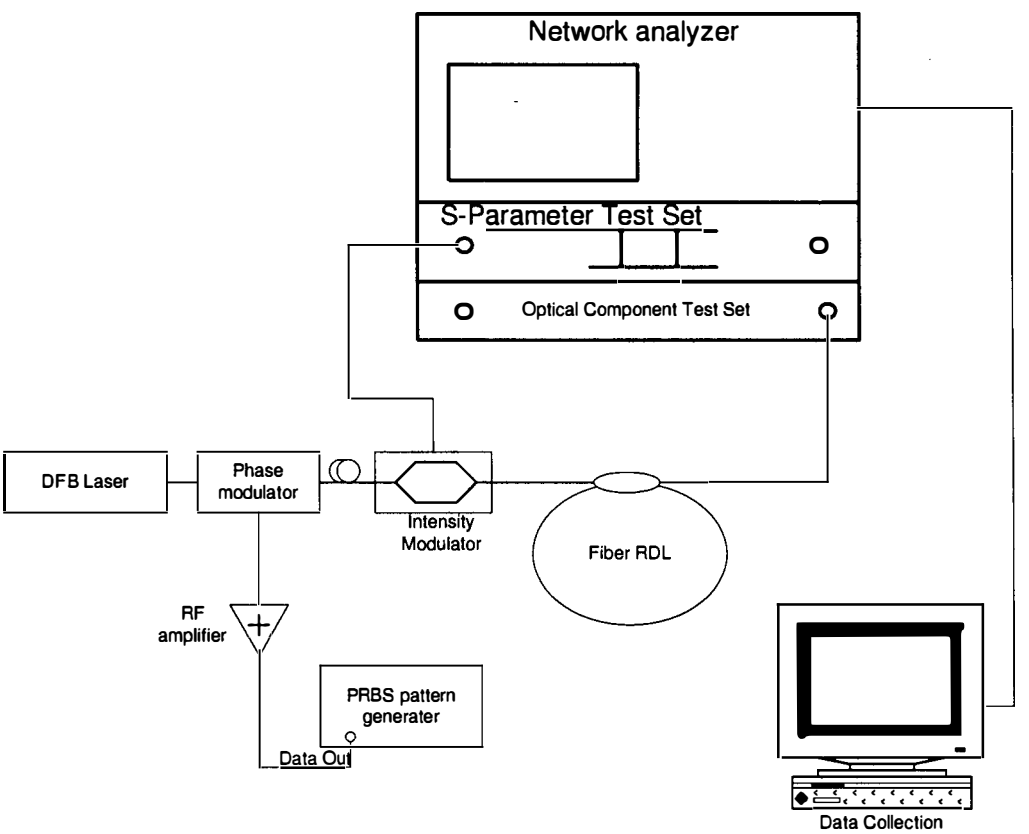

Figure 5.11: Experimental setup of coherence control for photonic RF filter

Figure 5.11 depicts the experimental setup for controlling the coherence length of the

laser source. In our experiment, we use a polarization controller in one path of the delay line to maximize the detected signals on the RF spectrum analyzer. In order to obtain high measurement resolution, a delay line difference of 200 m is necessary.

The laser source was a single-mode Fujisitsu FLD 150F1BJ distributed feedback laser with a linewidth of 10 MHz. It had a relatively long coherence length. The laser was firstly modulated by a $LiNbO_3$ phase modulator with the 3 dB bandwidth of 10 GHz. Then it transmitted through the polarization controller. After that the laser passed through an intensity modulator which was located inside of the HP 83420A Lightwave test set, then it was transmitted over the fiber recirculating delay line, and was measured by an optical receiver in the lightwave test set, the electrical signal was finally collected by network analyzer. The HP 8510 network analyzer provides swept frequency modulation electrical signals through its port1 to the intensity modulator. By measuring the transmit scattering parameter S_{21}, RF transfer function of the fiber RDL filter can be obtained. The RF frequency response can be collected by the computer through GPIB card and using Labview Software Package to process all the collecting data.

We first applied two sine signals to the phase modulator. The two signal frequency are 80 MHZ and 165 MHz respectively. Figure 5.12 shows the modulated laser spectrum under two tone modulation. It is obvious that the laser spectrum was slightly broadened.

Figure 5.13 shows the photonic RF filter response under the illumination with two control signals. It is shown that stability of the RF response is slightly improved however a fluctuating response was still observed.

To verify the principle of the new PRBS phase modulation technique of laser coherence control in relation to the requirements of the photonic signal processor, experimental setup of Figure 5.10 was applied. The fiber RDL notch filter employed a coupler of ratio 33:67,

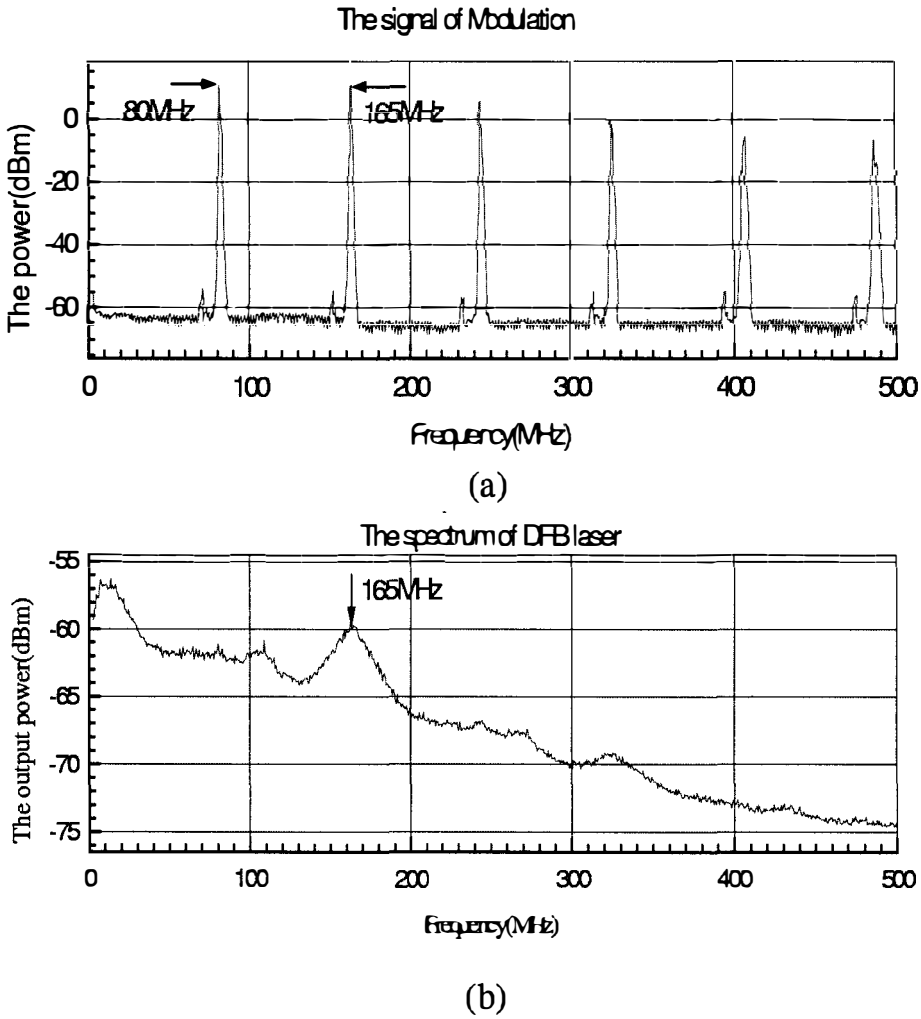

Figure 5.12: Measured spectrum. (a) The spectrum of the two tone signals (b)The spectrum of the modulated DFB laser

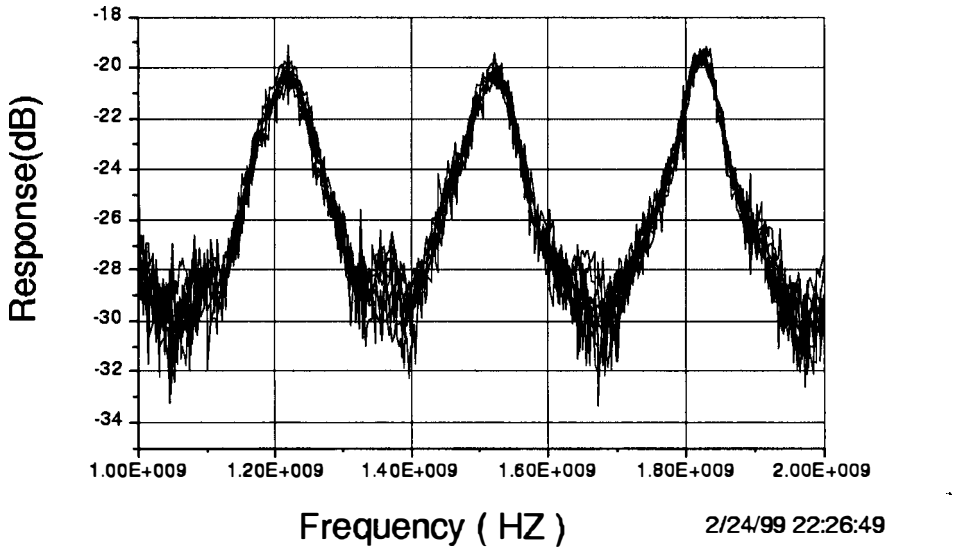

Figure 5.13: Measured RF filter response.

excess loss of 5 % and a 1.05 m recirculating fiber, corresponding to the FSR of 189.5 MHz. The optical phase modulator was driven by a PRBS sequence signal generated by an HP70841B Pattern Generator 0.1-3 Gb/s. To obtain enough modulation depth for the PRBS control signal, the PRBS was boosted by SHF-84B broadband amplifier of bandwidth 10 GHz, and its maximum gain is 40 dB.

The spectrum of the DFB laser, measured by self-heterodyne technique, is shown in Figure 5.14. Curve (i) in Figure 5.14 shows the spectrum of the DFB laser output, which exhibits a linewidth of 15 MHz. Curve (ii) in Figure 5.14 shows the spectrum of the laser after the PRBS phase modulation coherence control is applied. It is obvious that the spectrum of the laser has been transformed, and that it has been modified to around 160 MHz. The PRBS sequence used to drive the phase modulator had a pattern word length of $2^7 - 1$, a frequency of 200 MHz, and the phase modulation index of 1.1π.

The frequency responses of the photonic RF notch filter under the two illumination conditions are shown in Figure 5.15. Figure 5.15(a) shows a superposition of several

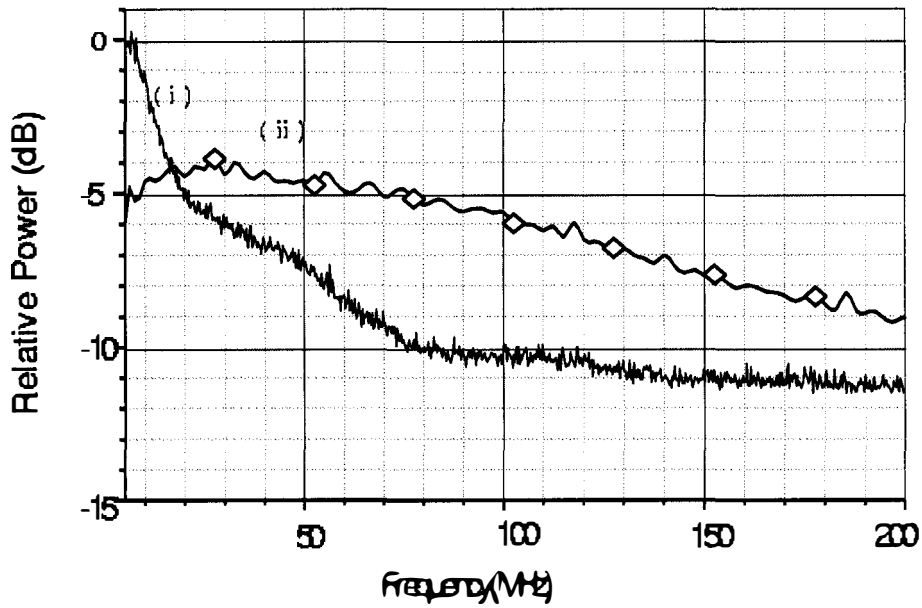

Figure 5.14: Measured spectrum of the optical source: (i) DFB laser spectrum, (ii) Spectrum after the PRBS phase modulation coherence control is applied

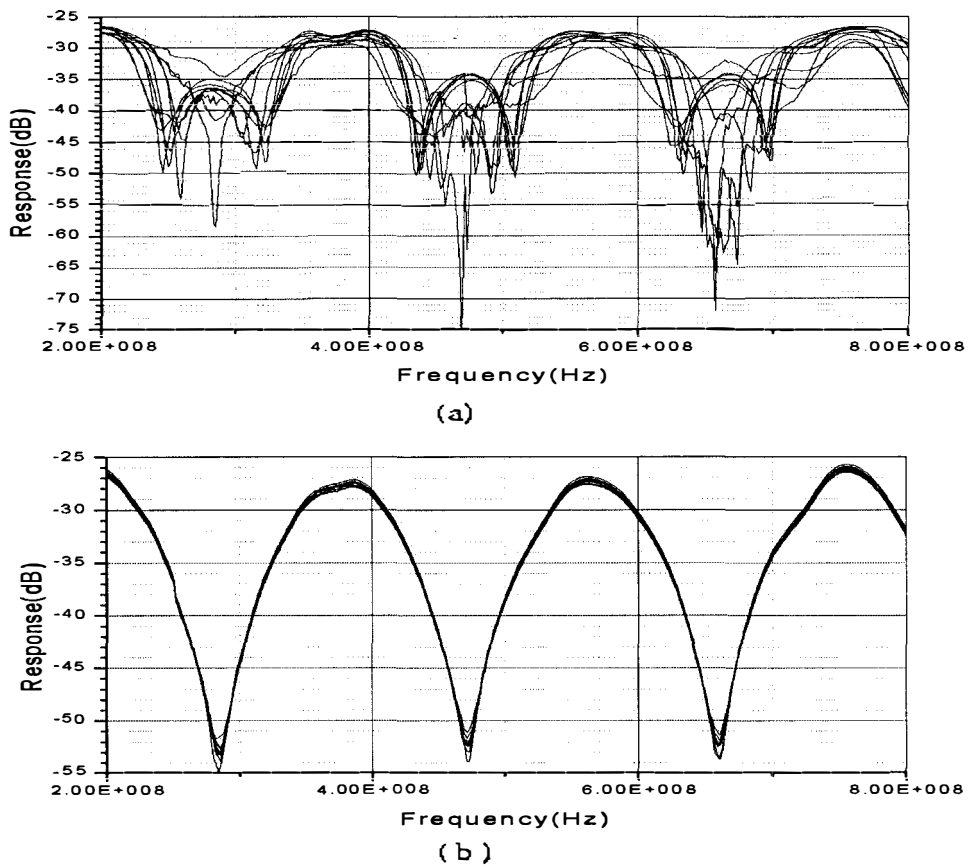

Figure 5.15: Measured RF frequency responses: (a) With DFB laser, (b) With PRBS modulated DFB laser

responses taken at sequential time intervals, when the DFB laser on its own is used as the optical source. The linewidth of DFB laser is comparatively small to the photonic filter's FSR frequency, and as expected, the resulting operation is in the coherent regime. Under this operation, the optical interference effects take place, it is very difficult to determine the exact RF response of the filter. In this case, the measured RF frequency response is strongly influenced by the optical source parameters and environmental conditions such as temperature or mechanical stress and it is extremely unstable and not suitable for practical applications. Figure 5.15(b) shows a superposition of responses at sequential time intervals when the PRBS phase modulation coherence control is applied. In this case, the source coherence has been transformed to the optimum value corresponding to the delay time of fiber RDL RF filter. The highly stable response can be observed, which is insensitive to small environmental disturbances, and it also exhibits the expected filtering behavior.

The phase modulator controlling by the PRBS signal provides a controlled way to reduce the unwanted phase induced intensity noise in photonic RF signal processing system, therefore, significantly improving the stability of photonic RF signal processing and makes the processor free of laser coherency limitation, hence it improves the performance of photonic RF signal processor.

5.6 Conclusions

In this Chapter, we demonstrated a new technique of laser coherence control for noise suppression in photonic RF signal processors. It is based on a PRBS phase modulation technique that transforms the laser coherency to the requirements of the photonic RF signal processor. The advantage of this technique is that it enables high quality laser sources such as DFB lasers and solid state lasers, which have high signal to noise ratio(SNR)

and dynamic range link capabilities to be used as optical sources in photonic RF signal processors.

The technique described is quite general which can tailor the laser linewidth to meet the requirements of photonic RF signal processors with arbitrary operating frequency. Experimental verification of this technique has been presented. Results have demonstrated that the PRBS phase modulation technique enables DFB laser to be used as an optical source for photonic RF signal processing, and its frequency response is highly stable. The new coherence control technique offers potential capability for the photonic based filters that they can be integrated into optical fibre microwave transmission systems.

In the next Chapter, we will discuss an integrated Microphotonic wideband RF interference mitigation filter which simultaneously meets the two requirements of adaptive RF filtering, namely, coherence insensitivity and reconfigurability.

Chapter 6

Integrated MicroPhotonic wideband adaptive RF filter

In previous chapters, we discussed the optical coherence effects on photonic RF signal processors, and proposed a new coherence control method to suppress the PIIN in photonic RF signal processing adaptively. In this Chapter a novel integrated MicroPhotonic architecture that integrates a photo-receiver array, a Vertical Cavity Surface Emitting Laser (VCSEL) array, and a multi-cavity optical substrate to realize a low-cost adaptive wideband RF filter is proposed. The new structure can be designed as multi-band adaptive RF notch filter or bandpass filter. Interference mitigation and high-Q can also be synthesized within the new architecture. This approach is initiated by integration of photonics and microelectronics technologies which offers many advantages for photonic RF signal processing.

6.1 Overview

The growing demand for wireless communication services has resulted in enormous radio-frequency interference all over the globe. For many RF applications such as square kilometre array (SKA) telescope and broadband radar systems, where the level of received RF signal is low, RF interferences can appear within one or several information bands, thereby limiting the system sensitivity. Dynamic RF interference mitigation devices are crucial for these applications. Consider for example, the SKA telescope receives, in addition to the RF information signals, unwanted RF interference noises resulting from a broad portion of the spectrum used for commercial and military purposes. This RF interference power often exceeds the power of the wanted RF signal, thereby limiting the sensitivity of the telescope.

A number of studies have been demonstrated in developing the photonic RF interference mitigation filters including fibre-Bragg grating based optical delay lines for the generation of transversal RF filters [23, 37]. The use of multiple wavelength sources of variable power levels and separations has also been proposed [24]. There are some limitations of those structures either they can not suppress the phased-induced intensity noise or are impracticable for application. Recently, an 8×8 true-time delay module that integrates holographic-grating couplers and graded index (GRIN) lenses on top of optical substrates, has been proposed for a K-band phased array antenna beamforming [104]. In their module, a portion of the substrate guided wave is extracted out each time the wave encounters the output holographic-grating coupler and focused back into optical fibres. However, coupling the optically delayed signals into optical fibres limits the maximum number of delays that can be synthesized.

In this Chapter, an integrated MicroPhotonic architecture that integrates a Vertical

Cavity Surface Emitting Laser (VCSEL) array, a 2D ultra-wideband photo-receiver array and a multi-cavity optical substrate is presented. The structure can generate a large number of optical true-time delays to achieve arbitrary, high-resolution RF filter transfer characteristics with no phase-induced intensity noise. Each optical cavity can realize an adaptive finite impulse response (FIR) filter of specific center frequency. By tuning the responses of the different optical cavities, a broadband adaptive FIR filter characteristic can be realized.

The unique feature of this proposed approach is that all the true-time-delay optical substrate, optical source and receiver will be integrated into one single substrate. A diffractive optical element(DOE) array will be made directly into the substrate. As a result, it significantly reduces the device size while eliminating the most difficult packaging problem associated with the delicate interfaces between optical fibers and optical substrate. Such a monolithic approach offers great precision for the RF phase control than the fiber-delay-lines due to the sub-micrometer accuracy of optical substrate. Also, the gain for each photodetector array can be individually set, making this structure more agile and robust.

6.2 Architecture of interference mitigation RF filter

Figure 6.1 illustrates the principle of the new architecture. The input RF signal is converted, via electrical-to-optical converters, to many RF-modulated collimated optical beams. The RF-modulated beams are then delayed directly in optical domain via the optical delay generator, which generates a large number of delayed optical beams. Each delayed optical beam is photo-detected by an element of a photo-receiver array and appropriately amplified by a post electrical- amplifier to produce a delayed RF signal with

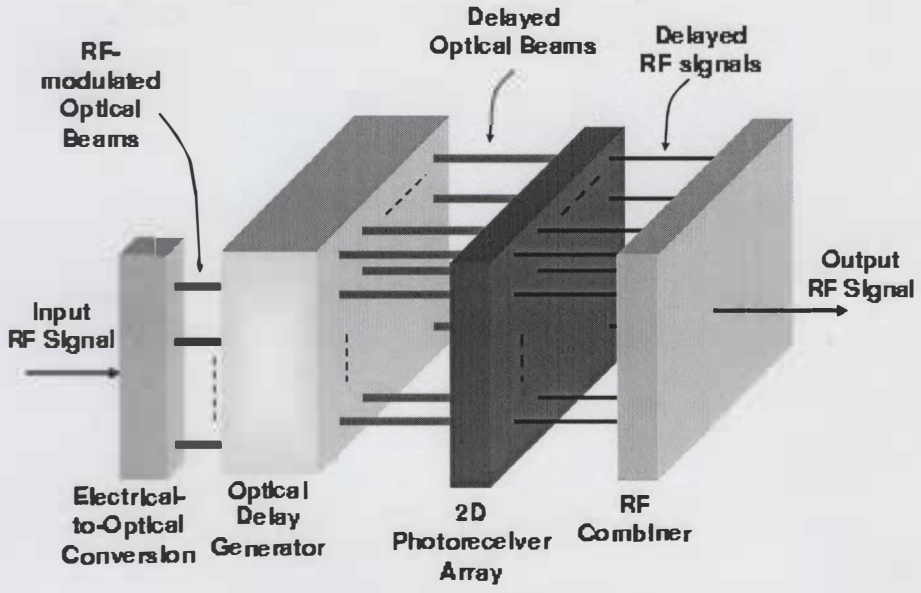

Figure 6.1: Principle of MicroPhotonic RF signal processing

appropriate amplitude. By combining the entire delayed RF signals, a FIR transversal RF filter characteristic is synthesized, which depends on the amplitudes and delay times of the combined RF signals.

Figure 6.2 shows the architecture of the MicroPhotonic RF filter. The low-noise amplifier (LNA) pre-amplifies the input RF signal to compensate for subsequent splitting loss and also to boost the modulation efficiency of the VECSEL array (where the first E stands for "external"). The RF splitter equally splits the input RF signal into N RF signals, which modulate the N elements of the $1 \times N$ 850 nm VECSEL array integrated on the VECSEL/photoreceiver chip. A VECSEL array can generate high optical power per element while maintaining fundamental mode oscillation. The diffractive optical element(DOE) collimates and routes the Gaussian beams generated by the VECSEL array. Each RF-modulated collimated optical beam generated by a VECSEL element propagates within the optical substrate and undergoes several reflections in a cavity whose width defined by one of the mirrors assigned to that VECSEL element and the DOE. Every time a beam bounces on the DOE, a small fraction of the power of that beam is transmitted

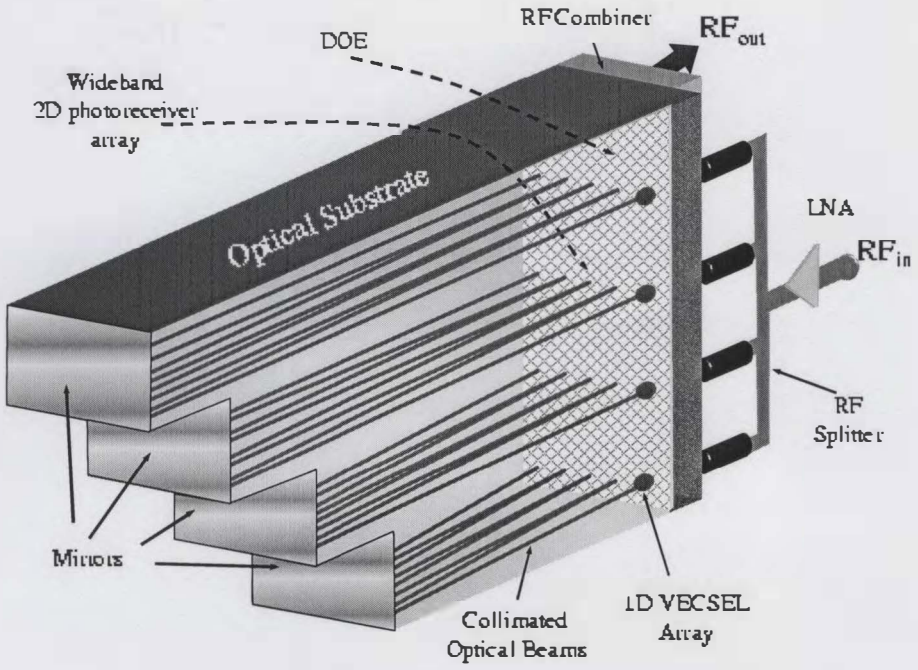

Figure 6.2: Architecture of MicroPhotonic RF filter

through the DOE for detection and amplification by an element of the wideband photoreceiver array that is integrated on the VECSEL/photoreceiver chip, while the remaining large fraction is reflected and routed to for subsequent delayed photodetection. An RF combiner adds (or subtracts) the amplified RF photocurrents to generate the output RF signal.

6.3 Transfer function

To easily comprehend the ability of the integrated MicroPhotonic RF filter to reconfigure its transfer characteristic, we examine the impulse response of the filter by driving the input with an RF impulse. In this case, each VECSEL element of the VECSEL array generates an optical impulse of power P_0. The optical impulse propagating inside an optical cavity of length L_m is sampled at a frequency:

$$\sqrt{4L_m^2 + d^2}\Big/_v \tag{6.1}$$

where d is the spacing between the photo-receiver elements, and ν is the speed of light inside the cavity. The power of the reflected impulse after n photo-detections is P_0R^n and that of the transmitted impulse is: $P_0(1-R)R^n$, where R is the reflectivity of the DOE. For example, if a 64×64 photo-receiver array is used with $R = 97\%$ and $P_0 = 10mw$, then the power of the optical impulse detected by the first photo-receiver element is 0.5 mw, while the power of optical impulse detected by the 64th photo-receiver element is 0.044 mw. By combining the arbitrarily-weighted current impulses, an adaptive Finite Impulse Response (FIR) transversal RF filter is realized. The frequency response of the filter is given by:

$$H(\omega) = \sum_{m=0}^{N-1} \sum_{n=0}^{N-1} \Re K_{VCSEL} P_0 (1-R) R^n G_{m,n} \exp\left[-jn\omega \frac{\sqrt{4L_m^2 + d^2}}{v}\right] \qquad (6.2)$$

where $\Re$ is the photo-receiver responsivity, $G_{m,n}$ is the current gain of the photo-receiver element (m,n), and $k_{VCSEL} = OMD/I_{RF}$ is the modulation response of the VCSEL elements, with OMD is the optical modulation depth and I_{RF} is the input RF current modulating the VCSEL element. The weights of the current impulses generated by the photo-receiver elements associated with an optical cavity can be changed by adjusting the gains of those photo-receiver elements.

Figure 6.3 schematically illustrates the interface between the VECSEL/photoreceiver chip and the optical substrate and also illustrates the propagation of the optical beams inside the optical substrate. The VECSEL element generates the high-power VECSEL beam using an external reflector. The glass layer is used over the VECSEL/photoreceiver chip for protection. The DOE is a thin holographic film inserted between the VECSEL/photoreceiver chip and the optical substrate. It comprises two sections. The first section is the VECSEL collimator, which is a hologram capable of collimating and steering VECSEL beam, while the second section (dashed) acts as a lens relay that prevents

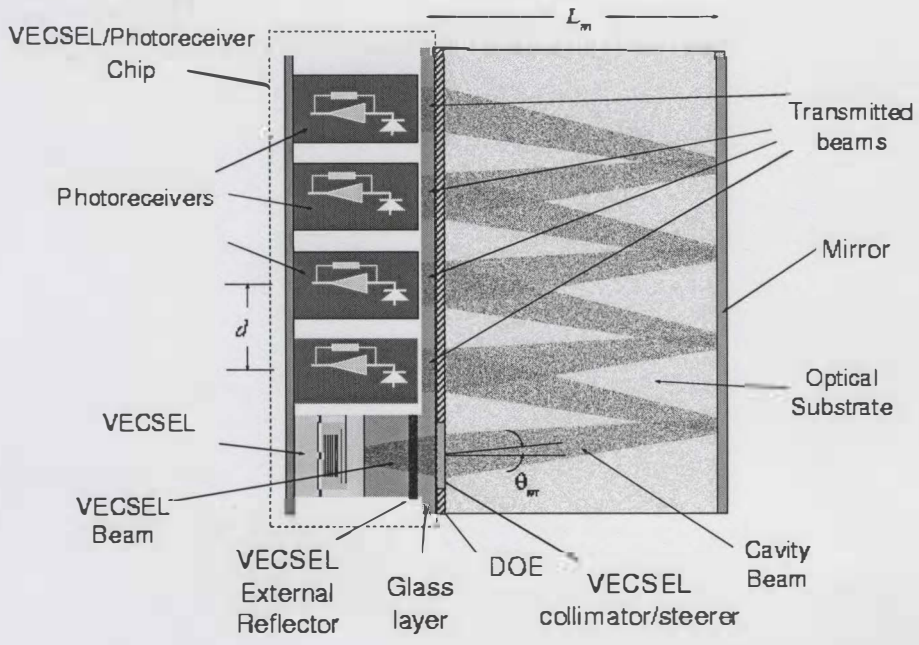

Figure 6.3: Interface between VECSEL/photoreceiver chip and optical substrate

the optical beam from diverging as it propagates within the cavity, and also maintains the beam diameter within an adequate range. The DOE can be appropriately coated to provide any desired reflectivity. As the cavity beam hits the DOE, a large portion of its power is reflected inside the optical cavity while a small fraction of its power is transmitted through the DOE and the glass layer and then detected by one of the photo-receivers.

6.4 Gaussian beam correction within the cavity

In order to design a reconfigurable RF filter with more flexibility, it is necessary to generate more taps within the cavity. Since the laser beam is a Gaussian beam, it will expand after it is transmitted in the cavity several times. The expanding beam will overlap each other on the photodetector arrays limiting the maximum number of taps.

Figure 6.4 shows the evolution of a gaussian beam as it propagates along the x-axis. When the Gaussian beam propagates in free space, its size and wavefront curvature vary

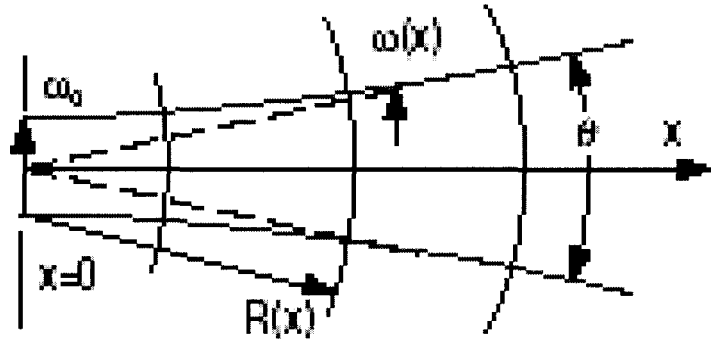

Figure 6.4: Gaussian beam propagation

with x. The following equations describe the Gaussian beam radius $\omega(x)$ and the wavefront radius of curvature R(x):

$$\omega^2(x) = \omega_0^2(1 + (\frac{\lambda x}{\pi\omega_0^2})^2) \tag{6.3}$$

$$R(x) = x(1 + (\frac{\lambda x}{\pi\omega_0^2})^2) \tag{6.4}$$

where ω_0 is the beam radius at $x = 0$ and λ is the wavelength. In our design, it is assumed to be $0.85\mu m$.

To correct the wavefront of propagating beam, a DOE is used, which appropriately focuses the diverging beam and maintain its diameter within an acceptable range. Figure 6.5 shows the cavity structure and the optical path of a typical optical beam propagating within the cavity.

For an input collimated Gaussian beam whose waist at the first photodetector is ω_0, the cavity length is L_m, the relationship between the input beam waist size and the distance of the beam transmitted in the cavity without any corrections is shown in Figure 6.6. It is obvious that if the input beam waist is small, its maximum working distance is short. For example, for $w0 = 0.05mm$, the maximum working distance before which the beam waist increases by 10% is only 4.3 mm, whereas, for $w0 = 0.5mm$, the maximum distance

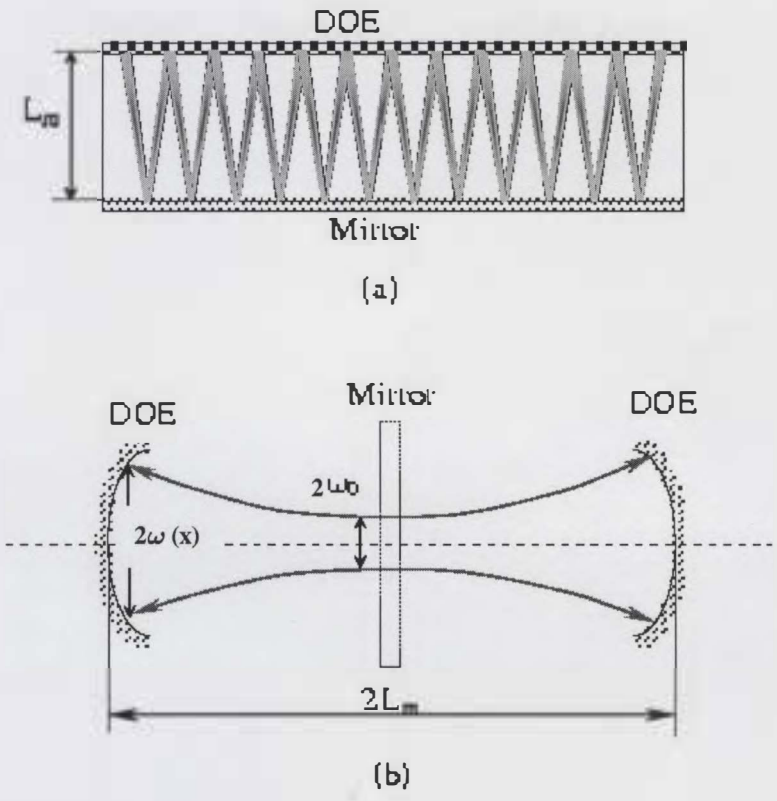

Figure 6.5: (a)Beam propagation in the cavity. (b)The optical path of a typical optical beam propagating within the cavity.

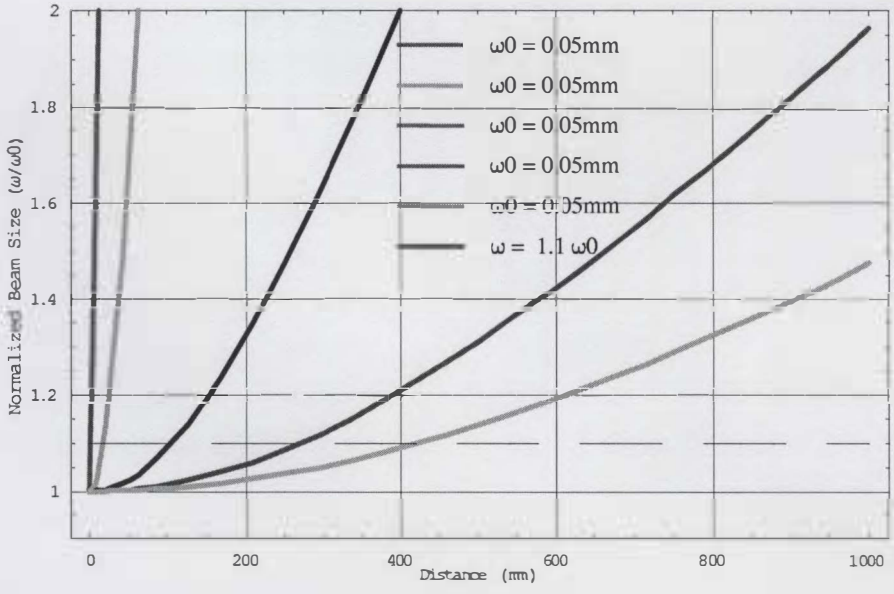

Figure 6.6: Normalized beam size on the DOE versus distance the beam transmitted in the cavity without correction, Cavity length = $20mm$

increases to 450 mm.

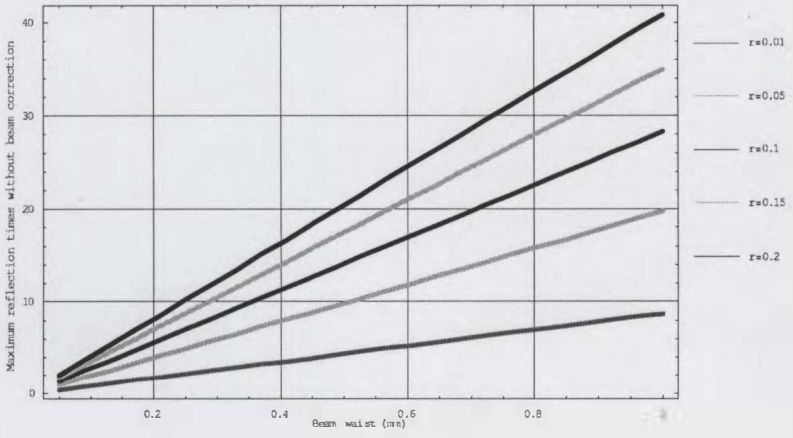

Figure 6.7: Maximum number of taps without beam equalization.

Figure 6.7 shows the maximum number of taps without beam equalization versus the input beam waist. For different relative beam size tolerance, which is defined by: $r = \frac{\omega_x}{\omega_0} - 1$. It is shown that increasing the beam waist increases the maximum number of allowed taps. When the tolerance reduced, the maximum number of taps is significantly decreased, causing more DOE to be implemented. The correction DOE can be practically implemented using the curvature defined by Equation 6.4.

For a cavity length of L_m and a photoreceiver array of spacing d, the maximum steering angle θ_m, of the DOE for the processor is:

$$\theta_m = \sin^{-1} \frac{2\omega_0(1+r)}{2L_m} \tag{6.5}$$

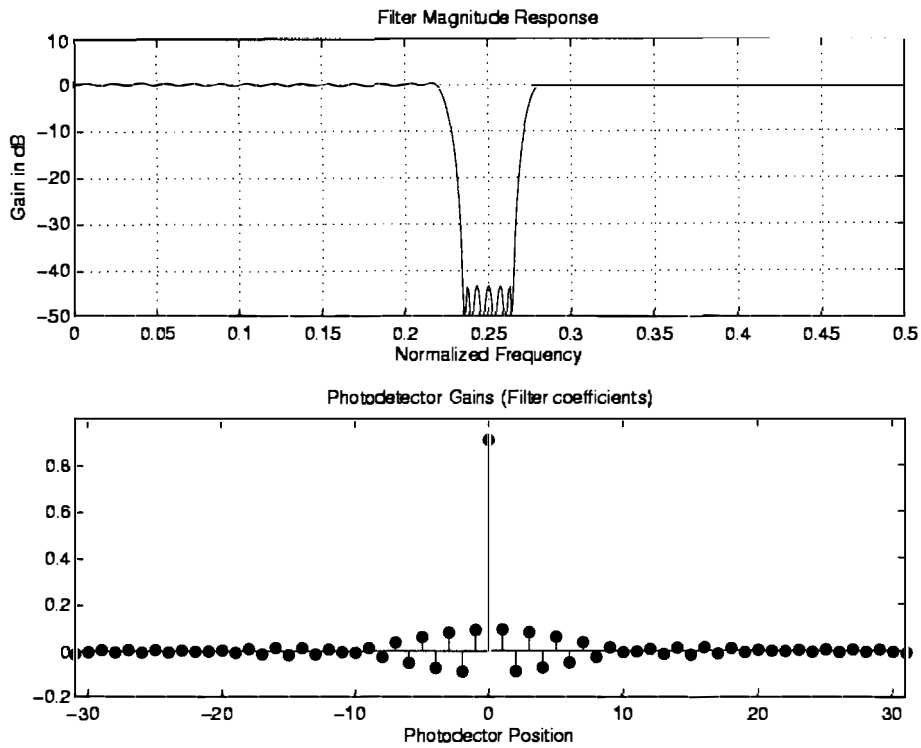

Figure 6.8: Microphotonic filter: (a) Magnitude response. (b) Filter coefficients.

6.5 Results

6.5.1 Computer simulation

Notch filter

Computer simulation were carried out to generate low shape factor tunable notch filter with minimum passband ripples by reconfiguring the gains of photoreceiver amplifiers of the MicroPhotonic filter. Results were focused on reconfiguring the photonic structure to realize a shape factor of less than 2, and multi-band notch RF filters objectives. Figure 6.8(a) and (b) show the frequency response and the corresponding photodetector gain profile for a 64-cavity MicroPhotonic RF filter, respectively. The gain profile was optimized to generate a response of relative center frequency of 0.5 using Remez exchange algorithm. This results in maximum passband ripple of 0.24 dB and a shape factor as low as 2 at -40 dB. For a cavity length of 10 mm, the notch frequency is 5 GHz.

By designing filter structure with more taps, MicroPhotonic RF interference mitigation filter can be synthesized adaptively and the notch responses can cover a wide frequency band.

Multi-band RF notch filter

Generally, with the availability of several cavities of different lengths, one can synthesize a large number of taps with reconfigurable weights, allowing adaptive RF interference mitigation over a wide frequency band.

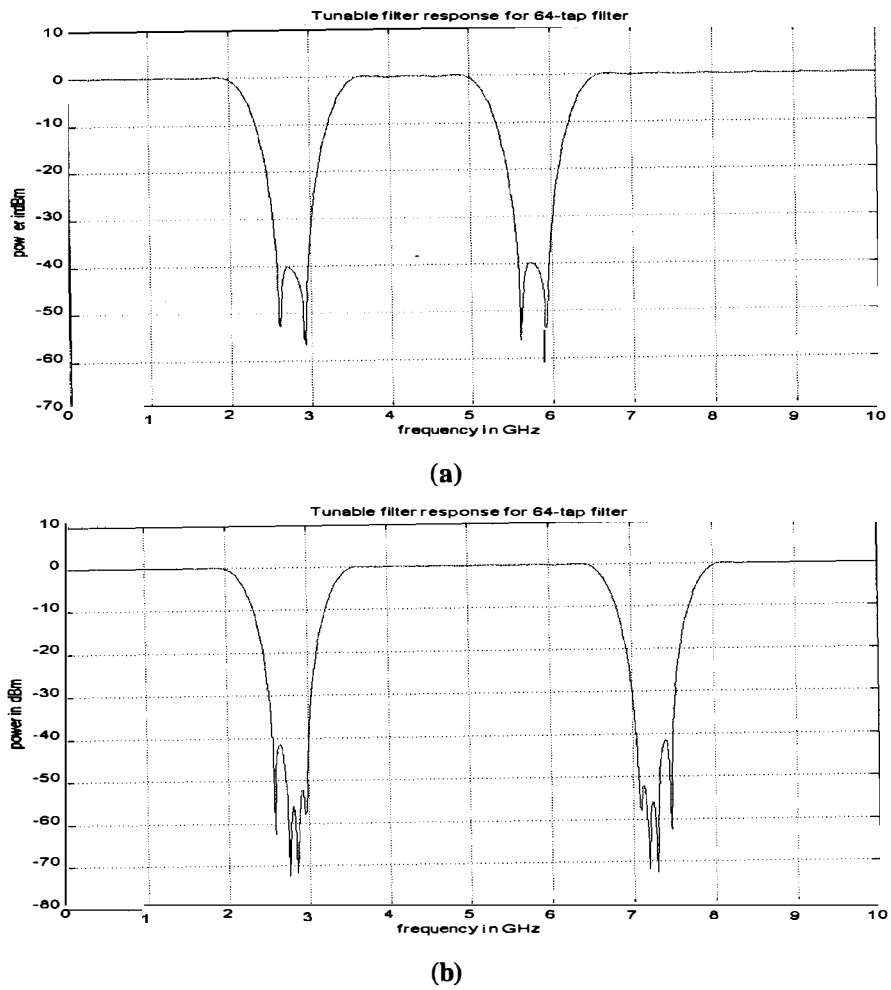

Figure 6.9: Tunable Dual-band MicroPhotonic RF interference mitigation filter response.

For a cavity length of 10 mm, the notch frequency is 5 GHz. Figure 6.9(a) shows a

dual notch response synthesized with 64-tap 10 mm cavity, with the weights optimized to generate notches at 2.5 GHz and 5.75 GHz, whereas in Figure 6.9(b) the weights were optimized to generate notches at 2.5 GHz and 7.25 GHz.

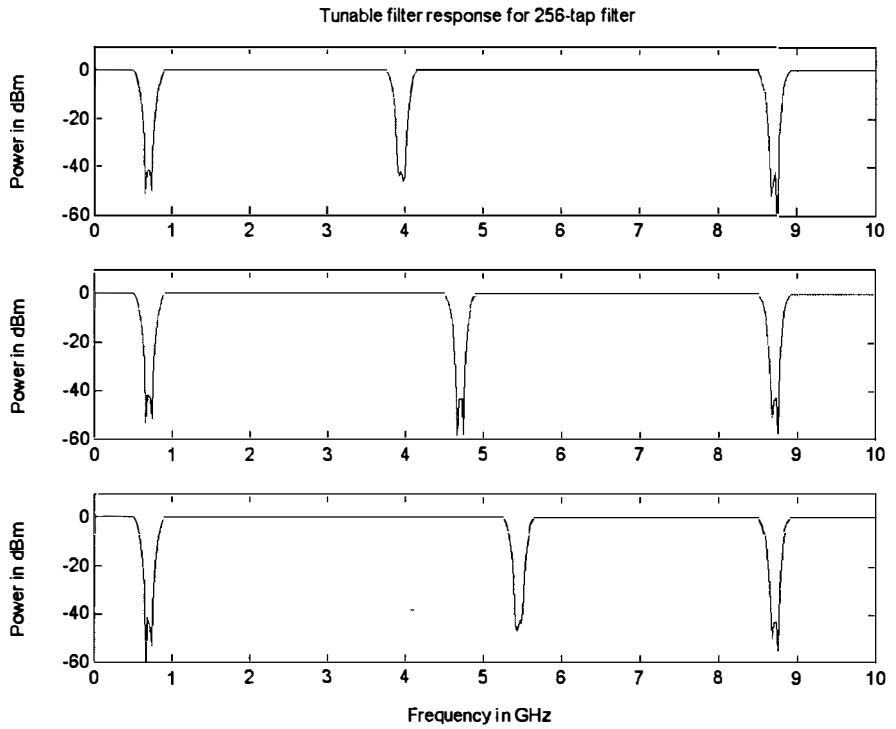

Figure 6.10: Three-band MicroPhotonic filter responses. Tuning around 4.75 GHz

Figure 6.10 shows the frequency responses for a 16-cavity MicroPhotonic filter employing a 16 × 16 photoreceiver array. The gain profiles were optimized to tune a notch response at center frequency around 4.75 GHz while synthesizing two fixed notches at 1.4 GHz and 8.75 GHz. The length of the shortest cavity was assumed to be 10 mm.

Figure 6.11 shows the frequency responses for a 16-cavity MicroPhotonic filter employing a 16 × 16 photoreceiver array. The gain profiles were optimized to generate three fixed notches at center frequencies of 0.7 GHz, 5.7 GHz and 8.2 GHz, and a tunable notch around 3.2 GHz. It is noted that the maximum passband ripples are less than 0.25 dB and a shape factor as low as 2 at -40 dB. This demonstrates the capability of the MicroPhotonic

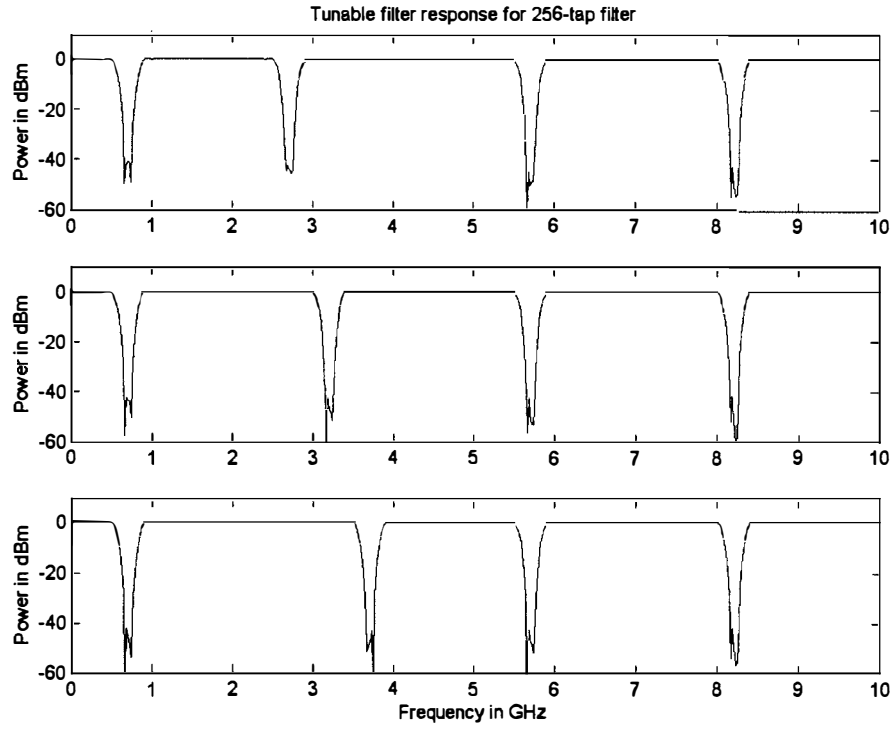

Figure 6.11: Four-band MicroPhotonic filter responses. Tuning around 3.2 GHz.

RF filter to synthesize adaptive notch responses over a wide frequency band.

BandPass filter

Figure 6.12 shows the responses of a multi-band bandpass filter of a 16-cavity MicroPhotonic filter employing a 16 × 16 photoreceiver array. The gain profiles were optimized to realize a double bandpass filter with the center frequencies of 2.5 GHz and 7.7 GHz. By tuning the weights of taps, one of the passbands can be tuned to 5.6 GHz. This demonstrates the capability of the MicroPhotonic RF filter to synthesize adaptive bandpass responses over a wide frequency band.

6.5.2 The impact of noises

It is important to note that the above simulation results do not include the noises generated by the VCSEL sources or the photoreceiver elements. To examine the impact

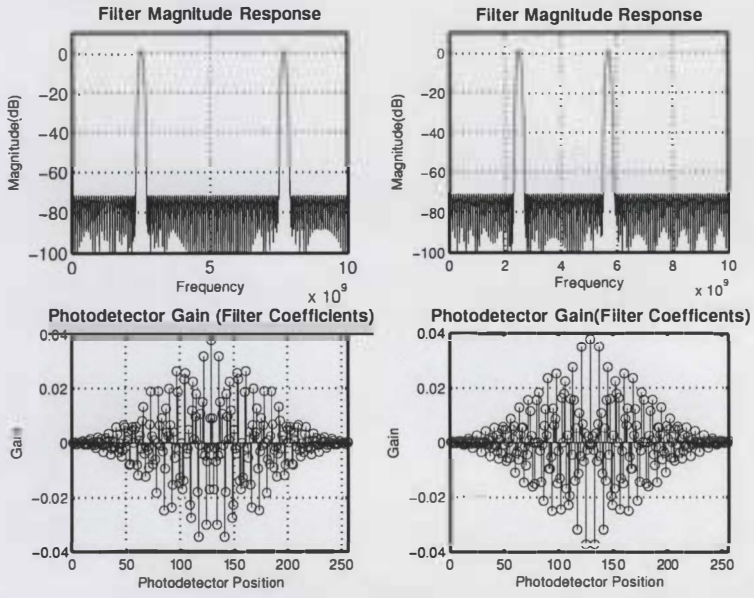

Figure 6.12: Microphotonic filter: (a) Magnitude response. (b) Filter coefficients.

of noise on the RF response of the MicroPhotonic RF filter, we have added uniformly distributed random fluctuations to the output photocurrent expressed by the maximum relative photocurrent current fluctuations. Figure 6.13 shows the RF frequency responses of the MicroPhotonic RF filter with maximum photocurrent fluctuations of 0%, 1% and 2.5%, respectively. It is obvious that for a photocurrent fluctuations of 1%, the notch depth drops from 40 dB to 30 dB, whereas for a photocurrent fluctuations of 2.5% the notch depth drops from 40 dB to 20 dB. Recent advances in low-noise photoreceiver arrays [105] and low intensity noise VCSEL arrays [106] will enable the implementation of a MicroPhotonic RF filter with photocurrent fluctuations well below 1%, making adaptive multi-band RF interference mitigation feasible.

6.5.3 Experimental results

To prove the principle of the MicroPhotonic filter, we built a 4-tap filter using 4 identical discrete Ortel 2601B photoreceivers of bandwidth 200 MHz and optical fibers as RF

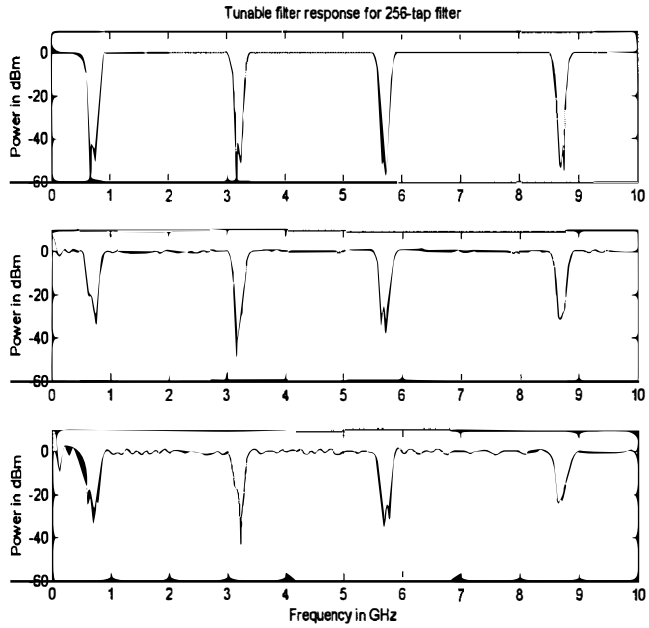

Figure 6.13: RF frequency responses of the MicroPhotonic RF filter for maximum photocurrent fluctuations of 0%, 1% and 2.5%, respectively.

true-time delay lines. To obtain a notch centre frequency around 200 MHz, the incremental optical fiber lengths were chosen to be 2 m, 4 m, and 6 m, as shown in Figure 6.14(a). Figure 6.14(b) shows the measured and predicted normalized responses of the 4-tap MicroPhotonic filter. The weights of the MicroPhotonic interference rejection filter were optimized to realize a notch depth of more than 35 dB. An excellent agreement between the measured and predicted frequency response for the MicroPhotonic interference rejection filter can be seen. Note that the slight discrepancy between the measured and predicted responses at high frequencies is due to the roll-off of the filter beyond 200 MHz.

Preliminary optical design has been carried out where one input beam generated a 4×6 spots array. Figure 6.15 shows the experiment setup where an input beam is firstly split by an optical fiber splitter, each beam is collimated through an optical fiber collimate array, then to a designed glass whose thickness is 20 mm and the reflective index is 95%. An optical beam array can be generated and detected by an infrad-CCD camera.

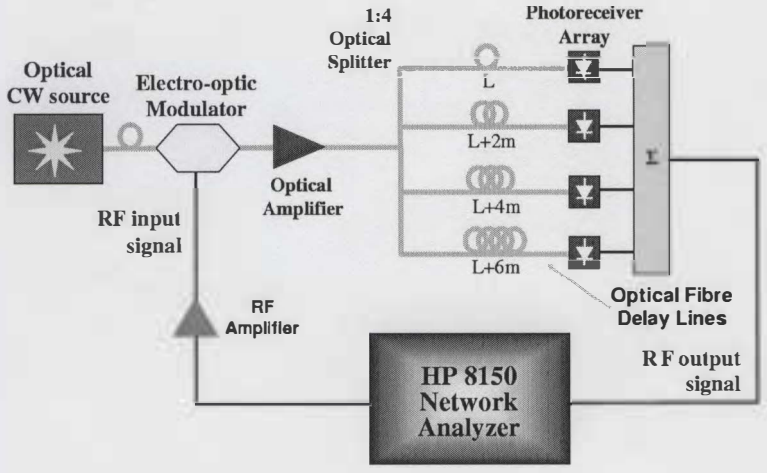

(a)

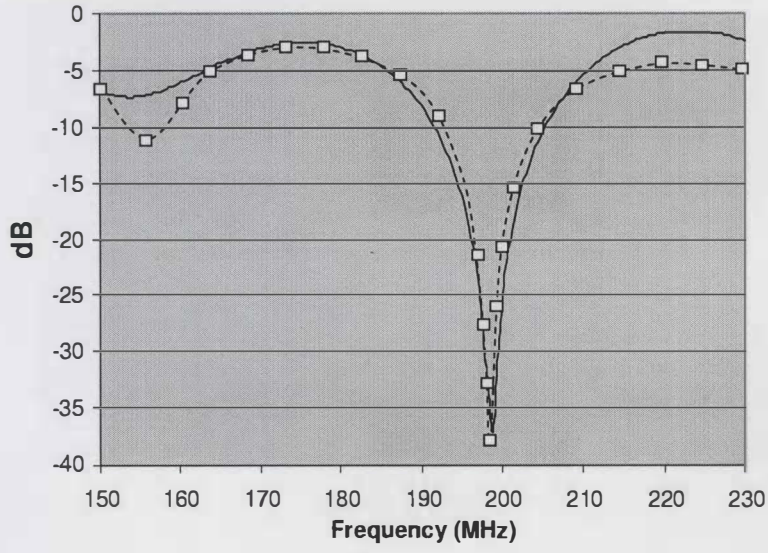

(b)

Figure 6.14: (a) 4-tap MicroPhotonic filter. (b) Measured (squares) and predicted (solid line) RF responses of a 4-tap proof-of- concept MicroPhotonic filter.

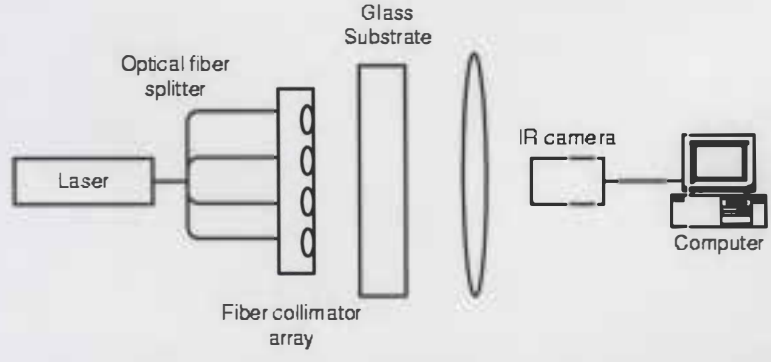

Figure 6.15: Preliminary optical filter setup with optical glass substrate

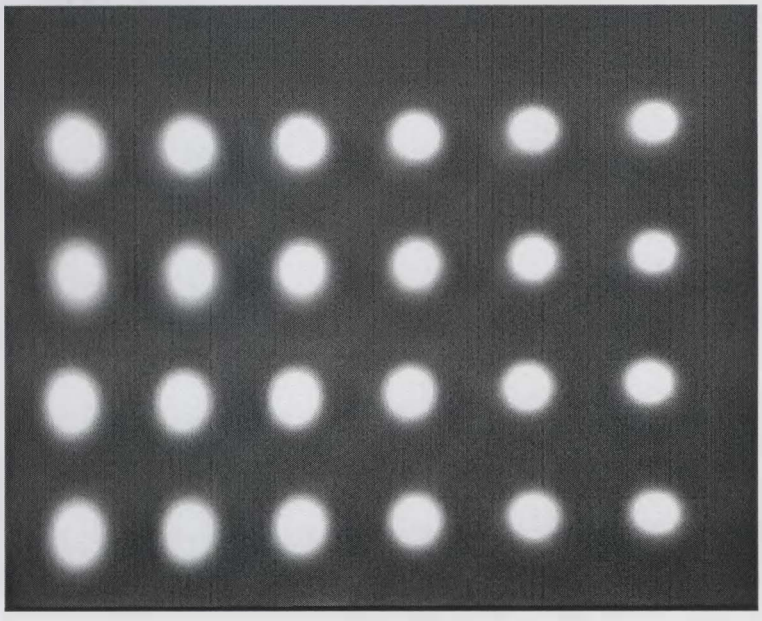

Figure 6.16: 4×6 Optical beam array

Figure 6.16 shows a spot array generated by launching four, 500 μm diameter collimated optical beams into a custom-made optical cavity of length 20 mm and mirrors of reflectivity 95% and 100%. This proves the capability of the MicroPhotonic RF filter to generate a spot array of delayed RF-modulated beams. It is obvious from Figure 6.16 that the beams diverge as they propagate within the cavity, and that a DOE film is critical for generating longer RF delays.

6.6 Conclusions

A MicroPhotonic broadband RF interference mitigation processor that generates true-time RF delays to perform finite impulse response transversal filtering, has been presented. The novel MicroPhotonic structure integrates a photoreceiver array, a Vertical Cavity Surface Emitting Laser (VCSEL) array, and a multi-cavity optical substrate to realize a low-cost adaptive wideband RF interference mitigation filter. The center frequency and passband or notch position of the filter can be reconfigured agilely. Simulation results

have demonstrated the capability of the MicroPhotonic structure to realize high-resolution, tunable interference mitigation filter with a shape factor as low as 2 and passband ripples less than 0.25 dB. We also discussed some design issues related to DOE film design.

Chapter 7

Conclusions and future work

In this Chapter, we discuss the technical approaches to realize the proposed integrated MicroPhotonic reconfigurable RF signal processor. Future work which may be initiated from this work will also be covered in this Chapter.

7.1 Technical approaches

Key enabling technologies for the integrated MicroPhotonic reconfigurable RF filter are a laser array, a DOE array attached to the optical substrate used as a wavefront correction for the beam expanding, a microlenslet used to focus the beams to the photodetector and a focal-plane photodetector array which can realize the high speed detection.

7.1.1 VESCEL array

In the proposed architecture, VESCEL array is used as the laser source. It is already a commercial product. The most recently reported electrically pumped tunable VCSELs [107] have a center wavelength of around 1550 nm and a tuning range of more than 30 nm, allowing flexible, reconfigurable implementations of high-speed optical networks.

This is the highest tuning range that has been published to date for electrically pumped long-wavelength VCSEL. The CW(continuous wave) output power at room temperature is higher than -10 dBm. The VCSELs show a single-mode spectrum with a side-mode suppression of more than 40 dB.

High-speed modulators are required for high speed signal encoding. Modulator and drivers working at 40 Gbit/s are now commercial available.

7.1.2 Photodetector array with diffractive optical element(DOE)

The reported photodetector can work at 40 GBit/s. A new generation of integrated circuits combining both electronic and optical devices is developed by HRL Laboratories where the opto-electro integrated circuit(OEIC) receiver array uses InGaAs/InAlAs/InP HBT technology.

Also several companies reported the product of 2-D integrated VESELs and detectors using different technical approaches such as monolithically integrate VCSELs and detectors depending on whether they have top or bottom emission and detection [108] or bump-bonding technology(TeraConnect).

7.1.3 2D array technology

Device designers are developing silica microlens that offer efficient coupling between optical fiber bundles and arrays of photodetectors, LEDs, or VCSELs.

Reports from Xanoptix show that the company commercializes a revolutionary new approach to semiconductor manufacturing: chip level direct die-to-die interconnection of integrated circuits. A highly manufacturable wafer scale micro-mechanical attachment processing to place multiple semiconductor die directly on top of silicon has been developed. The technique can be used to stack both silicon or compound semiconductors to

create Hybrid Integrated Circuits. The three dimensional stacking is possible. The process intimately combines large numbers of lasers, detectors and transistors with third-party silicon ICs fabricated in a conventional foundry. The resulting chips offer high integration density, low cost and reduced power consumption. Figure 7.1 is the schematic diagram of the integration.

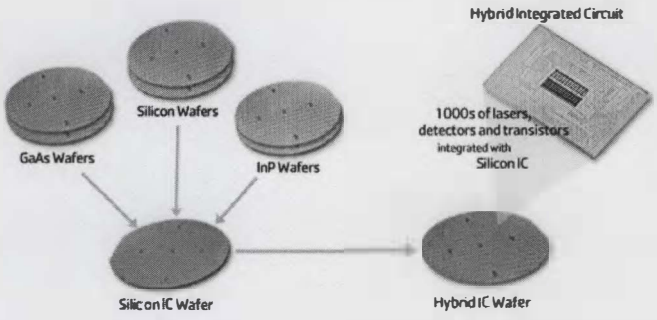

Figure 7.1: Integration of different wafer

Improvement of RF optoelectronic interfaces between the RF integrated circuit and optical discrete components will also improve the performance of optoelectronic devices for microwave applications, hence, it provides a more reliable and economical solution.

7.2 Future work

7.2.1 Implementation of the integrated MicroPhotonic wideband adaptive RF signal processing

We have designed several architectures for integrated MicroPhotonic wideband adaptive RF signal processors. The approaches to integrate discrete optical components were analyzed. To prove the concept of the proposed architectures, a small scale 2-D array of VCSELs and photodetector arrays are to be integrated with the optical substrate, therefore, more financial resources are required for full integration.

7.2.2 Algorithms of reconfigurable photonic RF signal processor

The algorithms for reconfigurable photonic RF signal processing have been developed. However, more user friendly algorithms need to be designed for commercial products.

7.2.3 Other applications

The architectures we discussed in this thesis are suitable for many applications such as optical header recognition in packet switched optical networking, however, this is beyond the scope of the thesis.

7.2.4 New methods for photonic RF signal processing

New techniques for photonic RF signal processing are emerging. Photonic crystals represent a new frontier in the field of optics, providing foundation for novel micro-photonic devices and avenues for tighter integration of these devices into a photonic chip. Photonic RF signal processing using photonic bandgap devices will be explored and investigated.

Bibliography

[1] A.E. Willner, D. Gurkan, A.B. Sahin, J.E. McGeehan, and M.C. Hauer. All-optical address recognition for optically-assisted routing in next-generation optical networks. *Communications Magazine, IEEE*, 41(5):S38–S44, 2003.

[2] P. Parolari, L. Marazzi, D. Rossetti, G. Maier, and M. Martinelli. Coherent-to-incoherent light conversion for optical correlators. *Lightwave Technology, Journal of*, 18(9):1284–1288, 2000.

[3] B. Moslehi. Fibre-optic filters employing optical amplifiers to provide design flexibility. *Electronics Letters, IEE*, 28(3):226–228, 1992.

[4] J. Capmany and J. Cascon. Discrete time fiber-optic signal processors using optical amplifiers. *Lightwave Technology, Journal of*, 12(1):106–117, 1994.

[5] D.B. Hunter, R.A. Minasian, and P.A. Krug. Tunable optical transversal filter based on chirped grating. *Electron.Lett.*, pages 2205–2207, 1995.

[6] D. Paster and J. Capmany. Fiber optic transversal filter using laser array and linearly chirped fiber grating. *Electron.Lett.*, pages 1684–1685, 1998.

[7] K. Sasayama, M. Okuno, and K. Habara. Coherent optical transversal filter using silica-based waveguides for high-speed signal processing. *Lightwave Technology, Journal of*, 9(10):1225–1230, 1991.

[8] N.A. Riza. 25-channel nematic liquid-crystal optical time-delay unit characterization. *Photonics Technology Letters, IEEE*, 7(11):1285–1287, 1995.

[9] Jong-Dug Shin, Seung-Hwan Paek, Hye-Young Kim, Kwangjoon Kim, and Cheoul-Shin Kang. Packet error analysis of an all-optical packet switching node using a fiber-optic delay line matched filter as an optical packet address processor. *Photonics Technology Letters, IEEE*, 9(12):1637–1639, 1997.

[10] Lin. Li, Stephen D. Scott, and Jitender S. Deogun. A novel fiber delay line buffering architecuture for optical packet switching. In *IEEE 2003 Global Communications Conference, GLOBECOM 2003*, San Francisco,USA, 2003.

[11] U. Gliese, T.N. Nielsen, M. Bruun, E. Lintz Christensen, K.E. Stubkjaer, S. Lindgren, and B. Broberg. A wideband heterodyne optical phase-locked loop for generation of 3-18 GHz microwave carriers. *Photonics Technology Letters, IEEE*, 4(8):936–938, 1992.

[12] W. Ng, A.A. Walston, G.L. Tangonan, J.J. Lee, I.L. Newberg, and N. Bernstein. The first demonstration of an optically steered microwave phased array antenna using true-time-delay. *Lightwave Technology, Journal of*, 9(9):1124–1131, 1991.

[13] A.C. Lindsay, G.A. Knight, and S.T. Winnall. Photonic mixers for wide bandwidth rf receiver applications. *Microwave Theory and Techniques, IEEE Transactions on*, 43(9):2311–2317, 1995.

[14] A.J. Seeds. Microwave photonics. *Microwave Theory and Techniques, IEEE Transactions on*, 50(3):877–887, 2002.

[15] A.C. Bordonalli, B. Cai, A.J. Seeds, and P.J. Williams. Generation of microwave signals by active mode locking in a gain bandwidth restricted laser structure. *Photonics Technology Letters, IEEE*, 8(1):151–153, 1996.

[16] L.N. Langley, M.D. Elkin, C. Edge, M.J. Wale, U. Gliese, X. Huang, and A.J. Seeds. Packaged semiconductor laser optical phase-locked loop (OPLL) for photonic generation, processing and transmission of microwave signals. *Microwave Theory and Techniques, IEEE Transactions on*, 47(7):1257–1264, 1999.

[17] D. Wake, D. Johansson, and D.G. Mopdie. Passive picocell-a new concept in wireless network infrastructure. *Electron.Lett.*, 33:404–406, 1997.

[18] H. Ogawa, D. Polifko, and S. Bamba. Millimeter-wave fiber optic systems for personal radio communication. *IEEE. Trans. Microwave Theory Tech.*, 40:2285–2292, 1992.

[19] H. Schmuck and R. Heidemann. High capacity hybrid fiber-radio field experiments at 60ghz. In *IEEE/IEICE Int. Microwave Photon.Topical Meeting*, pages 65–68, Kyoto, Japan, 1996.

[20] W.S. Birkmayer and M.J. Wale. Proof-of-concept model of a coherent optical beamforming network. *Optoelectronics [see also IEE Proceedings-Optoelectronics], IEE Proceedings J*, 139(4):301–304, 1992.

[21] R.A. Wilson, P. Sample, A. Johnstone, and M.F. Lewis. Phased array antenna beamforming using a micromachined silicon spatial light modulator. In *Microwave Photonics, 2000. MWP 2000. International Topical Meeting on*, pages 23–26, 2000.

[22] J. Stulemeijer, R. van Dijk, F.E. van Vliet, D.H.P. Maat, and M.K. Smit. Photonic chip for steering a four element phased array antenna. In *Microwave Photonics, 2000. MWP 2000. International Topical Meeting on*, pages 20–22, 2000.

[23] K.E. Alameh, E.H.W. Chan, and R.A. Minasian. High skirt selectivity photonics-based bandpass filters. In *International Topical Meeting on Microwave Photonics MWP'01*, pages 191–194, USA, 2002.

[24] R. A. Minasian and K.E. Alameh. Photonic signal processing. In *27th triennial General Assembly of the International Union of Radio Science*, page 192, The Netherlands, 2002.

[25] J. Capamany and J. Cascon. Discrete time fiber-optic signal processors using optical amplifier. *Lightwave Technology, Journal of*, pages 106–117, 1994.

[26] L. Benvenuti and L. Farina. The design of fiber-optic filters. *Lightwave Technology, Journal of*, 19(9):1366–1375, 2001.

[27] C.K. Madsen and J.H. Zhao. *Optical Filter Design and Analysis: A signal Processing Approach*. John Wiley & Sons., New York, USA, 1999.

[28] Fei Zeng, Jianping Yao, and Stephen J. Mihailov. Fiber bragg-grating-based all-optical microwave filter synthesis using genetic algorithm. *Opt. Eng.*, 42(8):2250–2256, 2003.

[29] K.P. Jackson, S.A. Newton, B. Moslehi, M. Tur, C.C. Cutler, J.W. Goodman, and H.J. Shaw. Optical fiber delay-line signal processing. *Microwave Theory and Techniques,IEEE Transactions on.*, MIT-33(2):193–210, 1985.

[30] D.M. Goodkin and M.H. Berry. Finite impulse response filter with large dynamic range and high smapling rate. *Appl. Opt.*, pages 1061–1062, 1990.

[31] M. Tur, J.W. Goodman, B. Moslehi, J.E. Bowers, and H.J. Shaw. Fiber-optic signal processor with applications to matrix-vector multiplication and lattice filtering. *Optics Letters, OSA*, 7(9):463–465, 1982.

[32] J.E. Bowers, S.A. Newton, W.V. Sorin, and H.J. Shaw. Filter response of single-mode fiber recirculating delay lines. *Electron. Lett.*, 18(3):110–111, 1982.

[33] S. Gweon, C.E. Lee, and H.F. Taylor. Wide-band fiber optic signal processor. *Photonics Technology Letters, IEEE*, 1(12):467–468, 1989.

[34] M.E. Frankel and R.D. Esman. Fiber-optic tunable microwave transversal filter. *Photonics Technology Letters, IEEE*, 7(2):191–193, 1995.

[35] T. Cusick, S. Iezekiel, R. Miles, S. Sales, and J. Capmany. Synthesis of all-optical microwave filters using mach-zehnder lattices. *Microwave Theory and Techniques, IEEE Transactions on*, 45:1458–1462, 1997.

[36] F. Coppinger, S. Yegnanarayanan, P.D. Trinh, B. Jalali, and I.L. Newberg. Nonrecursive tunable photonic filter using wavelength-selective true time delay. *Photonics Technology Letters, IEEE*, 8(9):1214–1216, 1996.

[37] D. B. Hunter and R. A. Minasian. Photonic signal processing of microwave signals using an active-fibre bragg-grating-pair structure. *Microwave Theory and Techniques, IEEE Transactions on*, 45(8):1463–1466, 1997.

[38] A. Molony, L. Zhang, J.A.R. William, I. Bennion, C. Edge, and J. Fells. Fiber bragg grating tru time delay systems:discrete-grating array 3-b delay lines and chirped-grating 6-b delay line. *Microwave Theory and Techniques, IEEE Transactions on*, page 1527, 1997.

[39] B. Moslehi, J.W. Goodman, M. Tur, and H.J. Shaw. Fiber-optic lattice signal processing. In *IEEE Proc.*, number 7, pages 909–930, 1984.

[40] B. Moslehi and J.W. Goodman. Novel amplified fiber-optic recirculating delay line processor. *Lightwave Technology, Journal of*, 10(8):1142–1147, 1992.

[41] K.K.Goel. New topologies of fiber-optic delay line filters. *Photonics Technology Letters, IEEE*, pages 1086–1088, 1993.

[42] S. Sales, D. Pastor, J. Capmany, and J. Marti. Fiber-optic delay-line filters employing fiber loops: signal and noise analysis and experimental characterization. *J.Opt.Soc.Am.A*, pages 2129–2135, 1995.

[43] J.E. Bower, S.A. Newton, W.V. Sorin, and H.J. Shaw. Filter response of sigle-mode fiber recirculating delay lines. *Electron. Lett.*, (3):110–111, 1982.

[44] R. You, N.and Minasian. High-Q optical microwave filter. *Electron.Lett.*, 35(24):2125–2126, 1997.

[45] Sungchui. Kim and Byoungho Lee. Recirculating fiber delay-line filter with a fiber bragg grating. *Appl.Opt.*, 37(23):5469–5471, 1998.

[46] D.B. Hunter and R.A. Minasian. Tunable microwave fiber-optic bandpass filters. *Photonics Technology Letters, IEEE*, 11(7):874–876, 1999.

[47] E.H.W. Chan, K.E. Alameh, and R.A. Minasian. Photonic bandpass filters with high skirt selectivity and stopband attenuation. *Lightwave Technology, Journal of*, 20(11):1962–1967, 2002.

[48] J. Capmany, D. Pastor, and B. Ortega. New and flexible fiber-optic delay-line filters using chirped bragg gratings and laser arrays. *Microwave Theory and Techniques, IEEE Transactions on*, 47(7):1321–1326, 1999.

[49] R. Minasian. Photonic signal processing of high-speed signals using fiber gratings. *Optical fiber technology*, 6(2):91–108, 2000.

[50] G. Yu, W. Zhang, and J.A.R. Williams. High-performance microwave transversal filter using fiber bragg grating arrays. *Photonics Technology Letters, IEEE*, 12(9):1183–1185, 2000.

[51] R.A. Minasian and K.E Alameh. Photonics-based interference mitigation filters. In *Microwave Conference, 2000 Asia-Pacific Meeting*, pages 544–547, Sydney, NSW ,Australia, 2000.

[52] B.A.Soref. Wavelength dependent, tunable, optical delay system for electrical signals. (4,670,604), 1987.

[53] G.A. Ball, W.H. Glenn, and W.W. Morey. Programmable fiber optic delay line. *Photonics Technology Letters, IEEE*, 6(6):741–743, 1994.

[54] D. Norton, S. Johns, C. Keefer, and R. Soref. Tunable microwave filtering using high dispersion fiber time delays. *Photonics Technology Letters, IEEE*, 6(7):831–832, 1994.

[55] N. You and R.A. Minasian. A novel high-Q optical microwave processor using hybrid delay-line filters. *Microwave Theory and Techniques, IEEE Transactions on*, 47(0018-9480):1304–1308, 1999.

[56] D. Hunter and R. Minasian. Programmable high-speed optical code recognition using fibre bragg grating arrays. *Electron. Lett., IEE*, 35:412–414, 1999.

[57] F. Ramos J. Marti, V. Polo and D. Moodie. Photonic tunable microwave filters employing electroabsorption modulators and wideband chirped fibre gratings. *Electronics Letters, IEE*, 35(4):305–306, 1999.

[58] Y. Yoffe, K.E. Alameh, and R. Minasian. Superposed wdm grating unit for short time delay processing of signals. *Microwave and Optical Technology Letters*, pages 390–391, 2000.

[59] K.P. Jackson, G. Xiao, and H.J. Shaw. Coherent optical fiber delay-line processor. *Electron. Lett.*, 22(25):1335–1337, 1986.

[60] W. Zhang, J. A. R. Williams, and I. Bennion. Optical fiber delay line filter free of limitation imposed by optical coherence. *Electron. Lett.*, 35(6):2133–2134, 1999.

[61] W. Zhang, J.A.R. Williams, and I. Bennion. Polarization synthesized optical transversal filter employing high birefringence fiber gratings. *Photonics Technology Letters, IEEE,*, 13(5):523–525, 2001.

[62] Xiaoke Yi, Chao Lu, Xiufeng Yang, Wen-De Zhong, Fang Wei, Lei Ding, and Yixin Wang. Continuously tunable microwave-photonic filter design using high-birefringence linear chirped grating. *Photonics Technology Letters, IEEE*, 15(5):754–756, 2003.

[63] J.X. Chen, Y. Wu, J. Hodiak, and P.K.L. Yu. A novel digitally tunable microwave-photonic notch filter using differential group-delay module. *Photonics Technology Letters, IEEE*, 15(2):284–286, 2003.

[64] F. Coppeinger, S. Yegnanarayanan, P.D. Trinh, and Jalali.B. All-optical incoherent negative taps for photonic signal processing. *Electronics Letters, IEE*, 33(11):973–975, 1997.

[65] D. Pastor, J. Capmany, S. Sales, P. Munoz, and B. Ortega. Reconfigurable fiber-optic-based RF filters using current injection in multimode lasers. *Photonics Technology Letters, IEEE*, 13(11):1224–1226, 2001.

[66] Jose. Azana and Lawrence R. Chen. Multiwavelength optical signal processing using multistage ring resonators. *IEEE Photon. Technol. Lett.*, page 654–655, 2002.

[67] V. Polo, B. Vidal, J.L. Corral, and J. Marti. Novel tunable photonic microwave filter based on laser arrays and $n \times n$ AWG-based delay lines. *Photonics Technology Letters, IEEE*, 15(4):584–586, 2003.

[68] T.H.Maiman. Stimulated optical radiation in ruby masters. *Nature*, 187:493–494, 1960.

[69] A. Javan, W.R. Bennett, and D.R. Herriott. Population inversion and continuous optical maser oscilliation in a gas discharge containing a He-Ne mixture. *Phys.Rev.Lett.*, 6(1):106–110, 1961.

[70] I. Hayashi, M.B. Panish, P.W. Foy, and S. Sumski. Junction lasers which operate contiunously at room temperature. *Appl.Phys.Lett.*, 17:109–111, 1970.

[71] Y. A. Akulova, C. Schow, A. Karim, S. Nakagawa, P. Kozodoy, G. Fish, A. J. DeFranco, A. Dahl, M. Larson, T. Wipiejewski, D. Pavinski, T. Butrie, and L. A. Coldren. Widely-tunable electroabsorption-modulated sampled grating dbr laser integrated with semiconductor optical amplifier. In *Proc. OFC*, pages 536–537, March 2002.

[72] K. Noguchi, O. Mitomi, and H. Miyazawa. Millimeter-wave $Ti : LiNBO_3$ optical modulators. *Lightwave Technology, Journal of*, page 615–619, 1998.

[73] R. G. Walker. Electro-optic modulation at mm-wave frequencies in gas/glass guided wave devices. In *in 8th IEEE LEOS Annu. Meeting*, page 118–119, San Francisco, CA, 1995.

[74] S. R. Sakamoto, R. Spickerman, and N. Dagli. Novel narrow gap coplanar slow wave electrode for travelling wave electro-optic modulators. *Electron. Lett.*, page 1183–1185, 1995.

[75] C. C. Teng. Travelling wave polymeric intensity modulator with more than 40 GHz 3 dB electrical bandwidth. *Appl. Phys. Lett.*, page 1538–1540, 1992.

[76] T. Ido, S. Tanaka, M. Suzuki, M. Koizumi, H. Sano, and H. Inoue. Ultra high-speed multiple quantum well electroabsorption optical modulators with integrated waveguides. *Lightwave Technology, Journal of*, page 2026–2034, 1996.

[77] D. Chen, H. Fetterman, A. Chen, W. H. Steier, L. R. Dalton, W. Wang, and Y. Shi. Demonstration of 110 GHz electro-optic polymer modulators. *Appl. Phys. Lett.*, page 3335–3337, 1997.

[78] H. Kawanishi, Y. Yamauchi, N. Mineo, Y. Shibuya, H. Murai, K. Yamada, and H. Wada. EAM-integrated DFB laser modules with more than 40 GHz bandwidth. *IEEE Photon. Technol. Lett.*, page 1471–1473, 2001.

[79] C. Cohen-Jonathan, L. Giraudet, A. Bonzo, and J. P. Praseuth. Waveguide alinas avalanche photodiode with a gain-bandwidth product of over 160 GHz. *Electron. Lett.*, 33:1492–1493, 1997.

[80] J. E. Bowers and C. A. Burrus. High-speed zero-bias waveguide photodetectors. *Electron. Lett.*, 22:905–906, 1986.

[81] K. Kato, A. Kozen, Y. Muramoto, Y. Itaya, T. Nagatsuma, and M. Yaita. 110 GHz 501.55 μm wavelength. *IEEE Photon. Technol. Lett.*, 6:719–721, 1994.

[82] et.al A. Umbach. Monolithic pin-hemt 1.55 μm photoreceiver on inp with 27 ghz bandwidth. *Electron. Lett.*, 32:2142–2143, 1996.

[83] Lei. LIN, Yujie. LIU, Chulchae CHOI, Xueping. ZHANG, and CHEN.Ray T. Hybrid integration of 1×12 metal–semiconductor–metal photodetector and polyimide waveguide array. *Optical Review*, 10(2):124–127, 2003.

[84] The MIT photonic crystal website. *http://ab-initio.mit.edu/photons/micropolis.html/*, 2004.

[85] P.J. Matthews and P.D. Biernacki. Photonic signal processing for microwave applications. In *Microwave Symposium Digest, 1999 IEEE MTT-S International Conference*, pages 877–880, Anaheim, CA , USA, 1999.

[86] S. Ahderom, M. Raisi, K. Lo, K.E. Alameh, and R. Mavaddat. Applications of liquid crystal spatial light modulators in optical communications. In *IEEE 5th International Conf. on High-speed Networks and Multimedia Communications, HSNMC'02*, pages 239–242, Korea, 2002.

[87] I.G. Manolis, T.D. Wilkinson, M.M. Redmond, and W.A. Crossland. Reconfigurable multilevel phase holograms for optical switches. *Photonics Technology Letters, IEEE*, 14(6):801–803, 2002.

[88] Y Yang, H Stark, and D Gurkan. High-diffraction-efficiency pseudorandom encoding. *Journal of Optical Society of America. A*, 17(2):285, 2000.

[89] M.R Feldman and C.C Guest. Iterative encoding of high-efficiency holograms for generation of spot arrays. *Optics Letters*, 14(10):479, 1989.

[90] M. Y. Frankel and R. Esman. Fiber optical tunable microwave transversal filter. *Photonics Technology Letter, IEEE*, pages 191–193, 1995.

[91] Moshe Tur., Behzad Mashi, and Joseph W.Goodman. Theory of laser phase noise in recirculating fiber optical delay lines. *Lightwave Technology, Journal of*, LT-3(1):20–31, 1985.

[92] James L.Gimlett and Nim K.Cheung. Effects of phase -to- intensity moise conversion by multiple reflections on gigabit-per-second DFB laser transmission systems. *Lightwave Technology, Journal of*, 7(6):885–895, 1989.

[93] Peter K. Pepeljugoski and Kam Y.Lau. Interfernce reduction in fiber optic links by superposition of high frequency modulation. *Lightwave Technology, Journal of*, 10(7):957–963, 1992.

[94] B. Moslehi. Analysis of optical phase noise in fiber-optic systems employing a laser source with arbitrary coherence time. *Lightwave Technology, Journal of*, 4(9):1334–1351, 1986.

[95] B. Moslehi. Noise power spectra of optical two-beam interferometers induced by the laser phase noise. *Lightwave Technology, Journal of*, 4(11):1704–1710, 1986.

[96] A.Yariv. *Optical Electronics in Modern Communication.* Fifth Edition. Oxford University Press, NewYork, USA, 1997.

[97] P.K. Pepeljugoski and K.Y. Lau. Interferometric noise reduction in fiber-optic links by superposition of high frequency modulation. *Lightwave Technology, Journal of*, 10(7):957–963, 1992.

[98] A. Yariv, H. Blauvelt, and S.-W. Wu. A reduction of interferometric phase-to-intensity conversion noise in fiber links by large index phase modulation of the optical beam. *Lightwave Technology, Journal of*, 10(7):978–981, 1992.

[99] A Yariv, Henry Blauvelt, David Huff, and HalZaren. An experimental and theoretical study of the suppression of interferometric noise and distortation in am optical links by phase dither. *Lightwave Technology, Journal of*, 15(3):437–443, 1997.

[100] San Blauvelt, Henry A.and Marino, John S.Frame. Terrance, and David B. Huff. Suppression of noise and distortion in fiber-optic systems. (5430569), Jul. 1995.

[101] T. Okoshi, K. Kikuchi, and A.Nakayma. Novel method for high resolution measurement of laser output spectrum. *Elec.Lett*, 6:630, 1980.

[102] C. Harder, K. Vahala, and A. Yariv. Measurement of the linewidth of enhancement factor α in semiconductor. *Appl.Phys.Lett.*, 42:328–330, 1983.

[103] E. Berglind. Linewidth of an externally modulated laser subjected to rayleigh backscattering from a fiber. *Photonics Technology Letters, IEEE*, 2(4):239–241, 1990.

[104] Yihong Chen and Ray T. Chen. A fully packaged true time delay module for a K-band phased array antenna system demonstration. *IEEE Photon. Technol. Lett.*, 14(8):?, 2002.

[105] J. Tang, B. Seshadri, K. N. Naughton, B. K. Lee, R. C. J. Chi, A. J. Steckl, and F. R. Beyette. Cmos-based photoreceiver arrays for page-oriented optical storage access. *IEEE Photon. Tech. Lett.*, pages 1234–1235, 2000.

[106] M. Stach, J. Broeng, A. Petersson, N.A. Mortensen, and R. Simonsen, H.R.and Michalzik. 10 GBit/s 850 nm vcsel based data transmission over 100 m-long multimode photonic crystal fibers. In *29th Europ. Conf. on Opt. Commun., ECOC'03*, pages 1024–1025, Rimini, Italy, 2003.

[107] http//:www.two-chip-photonics.com.

[108] http//:www.opticomp.com/opticomp/tech4.html.